11-1-2016 12:00 AM

Geochemical Constraints of the Gold Mineralization Sources from the South Mine Complex and the Main/'04 Breaks, Macassa Mine, Kirkland Lake, Ontario

Liana K.T. Stammers
The University of Western Ontario

Supervisor
Dr. Neil Banerjee
The University of Western Ontario

Graduate Program in Geology
A thesis submitted in partial fulfillment of the requirements for the degree in Master of Science

Abstract

Kirkland Lake Gold's Macassa Mine is a lode gold deposit in the Abitibi Greenstone Belt. It has two systems of mineralization: the Main/'04 Breaks, and the South Mine Complex (SMC). The objective of this work was to constrain mineralization sources between these systems using geochemical signatures. The SMC has different structure, mineralogy, alteration, trace- and major-elements composition, and $\delta^{18}O$ values. The Main/'04 is a series of faults with thin alteration dipping southeast 60-85º. The SMC is a series of structurally controlled zones dipping southeast 25-50° with wide alteration. It is interpreted to be a Riedel Shear between the '04 and Amalgamated Breaks. Significant findings include $\delta^{18}O$ values of quartz mineral separates of 10.1-12.9‰ (SMC) and 11.0-14.0‰ (Main/'04) and paired with chlorite mineral separate calculate temperatures between 134-616°C (SMC) and 128-434°C (Main/'04) within auriferous samples. This suggests higher temperatures and a greater magmatic component present in the mineralizing fluids within the SMC.

Keywords

Lode gold, Macassa Mine, oxygen isotopes, geochemistry, alteration, Abitibi Greenstone Belt.

Acknowledgments

I would like to thank my supervisors Dr. Neil Banerjee and Dr. Lisa van Loon for their guidance, support, and expertise in the writing of this thesis. Your feedback and encouragement made this thesis possible. Thank you to Stewart Carmichael, Rob Glover, Chris Evans, Sean Farrell, and Jaysen Johnson at Kirkland Lake Gold Inc. for their support and patience in teaching me about the Macassa Mine, and invaluable help in the collection of samples. Thanks to Erika Cayer for helping with the XRD collection and analysis, to Iffat Jabeen and Arshad Ali for helping me with the isotope data collection. I would also like to express my gratitude to Kathy Feick, who was always willing to help figure things out.

Thank you to my parents, Anthea and Mike, my partner, Spencer Reid, and all my friends who have supported and encouraged me throughout the researching and writing of this thesis. This would not have been possible without you. Finally, I must thank the swing and blues dancing scenes, for being a space to de-stress and maintain some semblance of sanity.

Table of Contents

Abstract i

Acknowledgments ii

Table of Contents iii

List of Tables vi

List of Figures vii

List of Appendices xi

Chapter 1 1

1 Introduction 1

1.1 Purpose of the Study 2

1.2 General Geology 2

1.2.1 Superior Province 2

1.2.2 Abitibi Subprovince 5

1.3 Kirkland Lake Geology 8

1.3.1 Camp Lithologies 9

1.3.2 Kirkland Lake Structures 10

1.4 Mineralized Zones 11

1.4.1 Main/'04 Break 12

1.4.2 South Mine Complex 13

1.5 Summary 13

Chapter 2 16

2 Methods 16

2.1 Objectives 16

2.2 Sample Collection 16

2.3 Optical Microscopy 19

2.4 X-Ray Diffraction 20
2.5 Scanning Electron Microscopy Analysis 20
2.6 Multi-Element Analysis 21
2.7 Stable Oxygen Isotopes Analysis 22
Chapter 3 24
3 Hand Sample and Photomicrographs 24
3.1 Regional Geological Setting 24
3.2 Mine Geology 24
3.2.1 Metavolcanic Tuffs 25
3.2.2 Intrusive Rocks 26
3.3 Zone Descriptions and Ore Mineralogy of the Gold Deposit 29
3.3.1 Main/'04 Break 30
3.3.2 South Mine Complex 34
3.4 Summary 43
Chapter 4 46
4 Multi-Element Analysis 46
4.1 Lithology 46
4.2 Alteration Geochemistry 48
4.3 Geochemistry of Mineralization 50
4.4 Discussion 55
4.4.1 Lithological Influences 55
4.4.2 Alteration Geochemistry 58
4.4.3 Mineralization Geochemistry 61
4.5 Conclusions 73
Chapter 5 74
5 Oxygen Isotope Analysis 74

5.1 Whole Rock Analysis 74
5.2 Quartz-Chlorite Mineral Separates 76
5.3 Discussion 79
5.3.1 Whole Rock Oxygen Isotopes 79
5.3.2 Mineral Separates Oxygen Isotopes 84
5.4 Conclusions 90
Chapter 6 92
6 Summary and Conclusions 92
6.1 Summary 92
6.2 Mineralization Sources 97
6.3 Other Orogenic Deposits 102
6.4 Further Work 105
References 106
Appendices 112
Curriculum Vitae 125

List of Tables

Table 1: Resources for the Main/'04 Breaks and SMC for Kirkland Lake Gold Inc., as of January 2014. 29

Table 2 – Comparison of the SMC zones: the New South Zone, Barchetta, Lower D, Limelight, #7 Break, Lower D North, and ’08 Break 44

Table 3: Major and Trace Elements in Fresh (<10% Altered) Host Rock Lithologies at the Macassa Mine. 47

Table 4: Major and Trace Elements of 10-25% Altered Rock in Macassa Mine Ore Zones. 48

Table 5: Major and Trace Elements in Mineralized Zones and Alteration >25% at the Macassa Mine 52

Table 6: Oxygen isotope compositions of quartz and chlorite separates and calculated $\delta^{18}O_{qtz\text{-}chl}$, and fluid temperatures. 85

Table 7 - Comparison of the differences between the SMC and the Main/'04 Breaks for alteration, mineralogy, mineralization textures, and geochemistry. 99

List of Figures

Figure 1 - Location of the Abitibi Subprovince highlighted in grey within the Superior Province of Canada. 3

Figure 2 - Lithotectonic assemblages, intrusions, and major structures in the Kirkland Lake area. 9

Figure 3 - Longsection of the Kirkland Lake Deposit from the Macassa Mine to the historical Wright-Hargreaves property looking north showing the location of the SMC with respect to the Main/'04 Breaks. 12

Figure 4 - Cross Section looking east of the locations of the 2013 and 2014 sampling program 17

Figure 5 - Plan View at the 5300 Level of the locations of the 2013 and 2014 sampling program 18

Figure 6 - Cross section of geology and mineralization at Macassa Mine looking northeast 25

Figure 7 - Metavolcanic Lithologies at the Macassa Mine: (A) bedded volcanic tuff, (B) volcanic tuff with lapilli. 26

Figure 8- Intrusive Lithologies at the Macassa Mine: (A) augite (mafic) syenite, (B) syenite porphyry with feldspar phenocrysts, (C) type II syenite porphyry with reabsorbed feldspar phenocrysts, (D) mafic xenoliths as found in a type II syenite porphyry. 27

Figure 9 – Narrow cataclastic zone of the Main Break as observed on surface within the Lakeshore outcrop 31

Figure 10 - Typical alteration found in the Main and ’04 Breaks with (A) olive green sericite + carbonate ± pyrite found shallow on the Main break at Lakeshore in sample LSKGI119, (B) brick red K-feldspar + hematite + sericite + carbonate found at depth on the ’04 Break at Stope 3827 in sample LSKGI115 32

Figure 11 – Thin section of alteration typically seen in the Main/’04 Breaks from LSKGI119 in (A) polarized, and (B) cross-polarized light. 32

Figure 12 – Scanning Electron Microscope (SEM) back-scatter electron (BSE) images of gold and tellurides found within the ’04 Break in thin section. 33

Figure 13 - Typical mineralized quartz vein along the ’04 Break. 34

Figure 14 - 5300 level geological plan of the Macassa Mine showing variation of the alteration assemblages, as well as the mineralized zones of the SMC and slip surfaces..... 36

Figure 15 - Hand samples showing mineralization within the NSZ as (A) molybdenite matrix supported breccias, (B) quartz-molybdenite flooding, (C) quartz veining, and (D) quartz supported breccias. 37

Figure 16 - Gold mineralization in thin section by Scanning Electron Microscope (SEM) back-scatter electron (BSE) images as (A) gold tellurides, (B) gold inclusions within pyrite, and (C) free gold within the SMC. 38

Figure 17 - Photomicrographs of Lower D Mineralization in (A) Cross-Polarized Light and in (B) Reflected Light.. 40

Figure 18 - Hand samples taken from (A) Limelight, (B) the #7 Break, and (C) Lower D North showing typical shearing fabrics and narrow associated quartz veins.. 41

Figure 19 - Series of petrographic images from the Lower D North footwall in plane polarized light (A), in cross polarized light (B) and reflected light (C) mineralization within quartz-molybdenite veining. 45

Figure 20 – Select box plots of elements showing variability as a result of different lithologies where (A) TiO_2 (wt %), (B) P_2O_5 (wt %), (C) U (ppm), (D) Sr (ppm), (E) Zr (ppm), (F) Ba (ppm), (G) Y (ppm), (H) Th (ppm), (I) Rb (ppm), and (J) Nb (ppm)..... 56

Figure 21 – Box plot showing the total SiO_2 wt.% between tuff, augite syenite, and syenite porphyry in fresh samples with minimal alteration and veining..... 57

Figure 22 - Chondrite Normalized REE of Augite Syenite, Syenite Porphyry, and Tuff in fresh, altered, and mineralized samples. 57

Figure 23 - Relationship between K_2O representing alteration, and (A) Na_2O, (B) Fe_2O_3, (C) CaO, and (D) Al_2O_3 found within samples of varying degrees of alteration within the Main/'04 Breaks, the Narrow Shear SMC Zones, and the Wide Flooding SMC Zones. 60

Figure 24 - Box plots showing variation of mobile elements (A) Cs (ppm), (B) Pb (ppm), and Eu (ppm) for all fresh, altered and mineralized samples. 62

Figure 25 – Fe_2O_3 (wt%) shown plot against S (wt. %) between the Main/'04 Breaks, the SMC Narrow Shear Zones, and the SMC Wide Flooding Zones. 63

Figure 26 - Box Plot showing the relative abundance of Au within mineralized and heavily (>25%) altered samples 64

Figure 27 - Box Plots showing the relative abundances between the wide flooding SMC zones, the Main/'04 Break, and the narrow shear SMC zones of Mo, Pb, and SiO_2 within mineralized and heavily (>25%) altered samples. 65

Figure 28 - Box Plots showing the relative abundances between the narrow shear SMC zones and the Main/'04 Break, and the wide flooding SMC zones. Cu, CaO, Fe_2O_3, and MgO within mineralized and heavily (>25%) altered samples are considered..... 67

Figure 29 - Box Plots showing the relative abundances between the Main/'04 Break, the narrow shear SMC zones, and the wide flooding SMC zones of Ga, Cs, and Th within mineralized and heavily (>25%) altered samples 68

Figure 30 - Correlation between Au Mineralization and (A) Pb, (B) Ag, and (C) Cu in the Main/'04 Breaks, SMC Narrow Shear Zones, and SMC Wide Flooding Zones for all samples..... 69

Figure 31 – Photomicrographs showing opaque pyrite, gold, and molybdenite mineralization in shear zone cutting original syenite porphyry host rock in (A) plane polarized light, (B) cross polarized light, and (C) reflected light optical microscopy. 66

Figure 32 - Correlation between Au mineralization with (A) Mo and (B) As in the Main/'04 Breaks, SMC Narrow Shear Zones, and SMC Wide Flooding Zones for all samples 70

Figure 33 - Correlation of Au Mineralization with (A) SiO_2 and (B) Sb in the Main/'04 Breaks, SMC Narrow Shear Zones, and SMC Wide Flooding Zones for all samples 71

Figure 34 - Correlations of Au Mineralization with (A) S and (B) Ga in the Main/'04 Breaks, SMC Narrow Shear Zones, and SMC Wide Flooding Zones for all samples 72

Figure 35 - Bulk Rock $\delta^{18}O_{V\text{-}SMOW}$ for the SMC and the Main/'04 Breaks. 75

Figure 36 - Bulk rock $\delta^{18}O_{V\text{-}SMOW}$ for wide flooding SMC zones, narrow shear SMC zones, and the Main/'04 Breaks 76

Figure 37 –Photomicrographs of quartz – chlorite veining showing examples of poor equilibrium textures in (A) plane and (B) cross polarized light, and of good equilibrium textures in (C) plane and (B) cross polarized light 77

Figure 38 - $\delta^{18}O_{VSMOW}$ values in the SMC and Main/'04 Breaks for (A) quartz and (B) chlorite mineral separates 78

Figure 39 - $\delta^{18}O_{VSMOW}$ of (A) quartz and (B) chlorite mineral separates for wide flooding SMC zones, narrow shear SMC zones, and the Main/'04 Breaks 78

Figure 40 - Bulk Rock $\delta^{18}O_{VSMOW}$ for the SMC and the Main/'04 Breaks showing lithological influence of augite syenite, syenite porphyry, and tuff 79

Figure 41 - Whole rock $\delta^{18}O_{VSMOW}$ compared to mineralization, represented by Au, within all samples, including fresh, altered, and mineralized samples from all lithologies 80

Figure 42 - Whole rock $\delta^{18}O_{VSMOW}$ compared to alteration, represented by the total Al_2O_3, Fe_2O_3, CaO, and K_2O within within all samples, including fresh, altered, and mineralized samples from all lithologies 81

Figure 43 - Whole rock $\delta^{18}O_{VSMOW}$ compared to (A) Mo and (B) SiO_2 within all samples within wide flooding SMC zones, narrow shear SMC zones, and the Main/'04 Breaks 82

Figure 44 - Whole rock $\delta^{18}O_{VSMOW}$ compared to mobile elements (A) Rb and (B) Sr within all samples within wide flooding SMC zones, narrow shear SMC zones, and the Main/'04 Breaks 84

Figure 45 - Box plots of mineralizing fluid temperatures of the SMC and Main/'04 Breaks calculated from oxygen isotope compositions of quartz-chlorite pairs 87

Figure 47 - Box plots of the mineralizing fluid temperatures of the wide flooding SMC, the narrow shear SMC, and Main/'04 Breaks calculated from oxygen isotope compositions of quartz-chlorite pairs 90

Figure 48 - Diagram of the continuum model. This is over a 20-25 km vertical profile with conditions ranging between granulite to sub-greenschist facies..... 104

List of Appendices

Appendix A : Sample Overview and Associated Studies..... 112

Appendix B : Hand Sample and Thin Section Descriptions..... 120

Appendix C : X-Ray Diffraction Results..... 121

Appendix D : Multi-Element Data..... 122

Appendix E : Stable Oxygen Isotope Analysis..... 123

Appendix F : Scanning Electron Microscopy..... 124

Chapter 1

1 Introduction

Canada is host to some of the most extensive and profitable gold deposits in the world, making it a leader in the global gold market. One prominent region of gold mineralization is the Kirkland Lake gold camp, located within the Southern Abitibi Greenstone Belt. Kirkland Lake represents a prolific gold mining camp that gained momentum following the discovery of gold in 1906. Production in the camp was continuous for 90 years, until 2000 when the Macassa Mine was closed. The Macassa Mine and 6 other past producers contributed over 25 million ounces of gold production in the camp. Kirkland Lake Gold Inc. owns 5 of these former producers that have produced about 22 million ounces of gold since 1917 to 1999, and accounts for about 90% of the historical production from the camp (Kirkland Lake Gold Inc., 2013). Mining occurred along a strike length of 21,000’ and to a depth of 8,100’ along the Kirkland Lake fault system, which includes the Main and ’04 Breaks (Ispolatov et al., 2008; Kirkland Lake Gold Inc., 2013). In 2002, Kirkland Lake Gold Inc. re-opened the Macassa Mine and the mine is currently producing gold at a rate of ~100,000 oz./year (Kirkland Lake Gold Inc. 2013). The Kirkland Lake camp currently ranks second in Canada, after Timmins, with respect to total ounces of gold produced.

The majority of that gold is being mined from the South Mine Complex (SMC), a new system discovered in 2003 through a drilling program run by Kirkland Lake Gold (KLG) to the south of the ’04 Break. The SMC represents an entirely new mineralized system in the Kirkland Lake camp. It is generally characterized by shallowly dipping (25° - 50°) structurally controlled zones of finely disseminated pyrite, visible gold, and tellurides, in contrast to the steeply dipping (70° - 80°) quartz vein hosted gold of the Main and ’04 Break (Kirkland Lake Gold Inc., 2013; Rhys, 2006; Rhys and Ross, 2008; Clark, 2013; Clark, 2014). Since the discovery of the SMC in 2003 by Kirkland Lake Gold, a full characterization of the mineralization has yet to be completed. Here, the SMC and the Main/’04 Break will be compared and contrasted to give a better understanding of the potential sources to improve upon exploration models of the deposit.

1.1 Purpose of the Study

This project stemmed from questions posed by Kirkland Lake Gold to advance exploration at the Macassa Mine using techniques which are not readily available to the industry. The objective of this study was to provide a comprehensive comparison of mineralization in the South Mine Complex (SMC) and the Main/'04 Breaks, the two main systems of mineralization at Macassa Mine, using characteristic mineralogical, structural, and geochemical signatures. This has been done primarily by comparing the alteration mineral assemblages, ore mineral assemblages, and fluid characteristics between the SMC and the Main/'04 Breaks. Petrography, XRD, oxygen isotope analysis of whole rock and mineral separates, and multi-element analysis were used to help define similarities and differences within zones of the SMC and Main/'04 Breaks. This knowledge can then be used by Kirkland Lake Gold to further enhance exploration.

1.2 General Geology

1.2.1 Superior Province

The Superior Province is the largest uncovered Archean craton in the world at 1 572 000 km^2 (Jackson and Fyon, 1991). It is located in the north-central portion of the North American continent, and forms part of the Canadian Shield (Figure 1). It is surrounded and truncated by Early Proterozoic orogens, thought to be collision zones between Archean provinces (Card, 1990; Hoffman, 1988; Gibb, 1983). The western, northern, and southeastern boundaries of the Superior Province are in contact with the Trans-Hudson and Grenville orogens with thrust and transcurrent faulting. The southern and eastern contacts with the Penokean and New Québec orogens represent Early Proterozoic supracrustal sequences unconformably overlaying and thrust upon the Superior Province (Card, 1990; Card and Ciesielski, 1986; Jackson and Fyon, 1991).

The Superior Province is comprised of east-west trending Neoarchean sedimentary and granite-greenstone subprovinces which surround a central Mesoarchean gneissic unit with minor greenstone belts (Jackson and Fyon, 1991; Percival and Card, 1983; 1985). The Superior Province stabilized in the Late Archean, except Proterozoic mafic dyke swarms, alkali rock-carbonatite complexes, and scattered Proterozoic and Phanerozoic

sedimentary cover (Card, 1990). The subprovinces are generally fault-bounded by linear structures (Card and Ciesielski, 1986; Jackson and Fyon, 1991).

Figure 1 - Location of the Abitibi Subprovince highlighted in grey within the Superior Province of Canada with the location of the Kirkland Lake mining camp starred (modified from Jackson and Fyon, 1991). The Superior Province is located mainly in Ontario, but also Manitoba, Quebec, Minnesota, North Dakota, and South Dakota.

1.2.1.1 Tectonic Setting

The Superior Province is host to a multitude of tectonic settings spread through this Archean terrane. It comprises of platformal or foredeep, mafic plain or oceanic volcanic, magmatic arc, pull-apart basin, and back arc basin environments (Corfu et al., 1991; Jackson and Fyon, 1991; Thurston and Chivers, 1990).

Komatiitic to tholeiitic volcanism in a marginal basin setting first occurred in the area prior to 2700 Ma. This was followed by tholeiitic to calc-alkalic arc sequence. The arc then collided with another arc, or a stabilized continental landmass leading to a suite of

tonalitic to granodiorite, calc-alkalic plutons and porphyries. The formation of the Timiskaming Group, as well as a large area of the southern Abitibi greenstone belt, by platformal or foredeep alluvial-fluvial sedimentation and calc-alkalic to alkalic magmatism occurred between 2686 Ma and 2677 Ma, during the last stage of this arc environment (Corfu et al., 1991). After the platform sequence, the mafic-ultramafic sequence, and arc volcanism, there was rift-related volcanism in the Superior province orogeny (Thurston and Chivers, 1990). Thurston and Chivers (1990) suggest that there may have been either one or two cycles of platform to mafic plain to arc to rift pull apart within the Superior Province.

1.2.1.2 Geology and Subprovinces

The volcanic and plutonic rocks in the Superior Province range from 3.1 – 2.6 Ga, and have had several major magmatic intrusive episodes of tholeiitic, calc-alkalic, komatiitic and alkali composition. Plutons include gneissic tonalite, foliated tonalite suites, diorite-monzonite-granodioride suites, muscovite-bearing granites, and massive granodiorite-granite suites (Jackson and Fyon, 1991). Sediments mostly consist of volcanogenic clastic, chemical sediments, and turbidites (Card, 1990).

The terrane is subdivided into volcano-plutonic, metasedimentary, plutonic, and high-grade gneiss subprovinces on basis of lithology, structure, metamorphic grade, geophysical and metallogenetic characteristics, and the ages of rock units and tectonic events. The subprovinces are typically bounded by zones of structural and/or metamorphic transition (Jackson and Fyon, 1991; Card and Ciesielski, 1986).

Subprovinces in the Superior Province include the Thompson Belt, Pikwitonci, Sachigo, Berens River, Uchi, Bird River, English River, Winnipeg River, Wabigoon, Quetico, Wawa, Minnesota River Valley, Abitibi, Opatica, Pontiac, Nemiseau River, Opatica River, La Grande River, Bienville, Minto, Cape Smith Belt, Sugluk, and Ashuanipi (Jackson and Fyon, 1991; Card and Ciesielski, 1986). The northern and southern subprovinces are high-grade gneiss, while alternating volcano-plutonic and metasedimentary subprovinces dominate a broad central region. The high-grade gneiss subprovinces are upper amphibolite- and granulite-facies gneisses of a supracrustal and

plutonic origin. The central region is a low-grade metavolcanic and metasedimentary greenstone belt. This is surrounded and intruded by granitoid batholiths. The majority of the metasedimentary terranes are deformed and metamorphosed turbidites and anatectic granites (Card, 1990; Jackson and Fyon, 1991; Card and Ciesielski, 1986).

1.2.2 Abitibi Subprovince

The 85,000 km^2 Abitibi greenstone belt is comprised of the komatiitic, tholeiitic, and calc-alkaline volcanic rocks of the Tisdale (2710 - 2704 Ma), Upper Blake River (2701 – 2696 Ma), and Lower Blake River (2704 - 2701 Ma) assemblages (Ayer et al., 2005). It is bound to the west by the Kapuskasing Structural Zone, to the east by the Grenville Front, to the north with the Opatica Subprovince paragneiss and orthogneiss, to the southeast by a fault separating the Pontiac Subprovince, and to the southwest the Abitibi is unconformably overlain by sediments in the Huronian supergroup and the Keweenawan volcanics and sediments (Card, 1990).

1.2.2.1 Tectonic Setting

The Abitibi is comprised of discrete oceanic and arc-related assemblages accreted by 2700 Ma by southward-migrating, north-dipping subduction. Volcanism was terminated due to the collision of a large continental mass to the south between 2700 Ma and 2688 Ma (Corfu et al., 1991; Thurston et Chivers, 1990; Wilkinson et al., 1999). This leads to the tectonic thickening and the turbidite-dominated sediments that are present within the Abitibi (Dimroth et al., 1983; Jackson and Fyon, 1991; Wilkinson et al., 1999). Like a modern island arc, it is hypothesized that there were submarine eruptions of komatiites and low-K tholeiites as submarine lava plains. Later calc-alkalic and tholeiitic lavas and pyroclastic eruptions within the central volcanic complexes built up to sea level. As the island arcs matured through continued volcanism, plutonism, and crustal thickening, the erosion and pyroclastic eruptions formed aprons of volcaniclastics and turbidites. Deposition of the coarse clastic sediments found in some areas of the Abitibi are due to extension, which led to the package’s rifting, uplift, erosion and subsequent deposition (Card, 1990).

1.2.2.2 Lithologies

The Abitibi subprovince contains volcanic rocks, clastic, and chemical sedimentary rocks intruded by multiple phases of tonalite-trondhjemite-granodiorite suites (Houle, 2008). The volcanic and sedimentary strata are typically separated by east-west trending faults. The subprovince is 40% supracrustal rocks and 60% granitoid rocks of which the supracrustal rocks have a composition of komatiitic to tholeiitic, and calc-alkalic to alkalic (Corfu, 1993).

The Abitibi Greenstone belt, where the Macassa Mine is located, is part of this subprovince. The greenstone belt is 80% volcanics/intrusions (70% tholeiitic, 25% calc-alkalic, with minor komatiitic and alkalic packages), and 20% metasediments (Card, 1990).

1.2.2.2.1 Sediments

The majority of the Abitibi subprovince sediments consist of east-west trending bands of turbiditic greywackes deposited between 2700 and 2680 Ma (Ayer et al., 2005). They are located in volcanic synclinal troughs and are mostly postvolcanic, but with some pre- or syn-volcanic (Corfu, 1993; Dimroth et al., 1973; Jolly, 1978). In the Kirkland Lake area, there are also later alluvial-fluvial metasediments deposited between 2680 and 2670 Ma, thought to form past the last stages of island arc formation (Ayer et al., 2005).

1.2.2.2.2 Volcanics and Intrusives

The volcanics within the Abitibi subprovince range from felsic rhyolite to ultramafic komatiite (Card, 1990; Goodwin, 1977). Intrusive rocks within the terrane form large batholiths to plutons and stocks of mafic to felsic composition. Intervening domes are cored by synvolcanic or syntectonic plutonic rocks of gabbro-diorite, tonalite, and granite composition (Card, 1990; Goodwin, 1977; Jackson and Fyon, 1991).

There are thought to be several major volcanic cycles throughout the formation of the Abitibi: a lower ultramafic-mafic, a middle tholeiitic basalt, and an upper tholeiitic and calc-alkalic mafic-intermediate-felsic assemblage. The lower ultramafic-mafic cycle is a komatiitic sequence of flows and intrusions with minor felsic tuffs and chert. The thick

tholeiitic sequences of the lower and middle parts of volcanic cycles are mostly pillow and massive basalt flows and in the north of the Abitibi are intruded by layered gabbro-anorthosite complexes (Card 1990; Corfu, 1993; Goodwin, 1977; Jackson and Fyon, 1991).

Timiskaming volcanics hosting the Kirkland Lake deposit are chemically similar to modern alkali volcanics of mature island arcs, and therefore the Timiskaming assemblage is thought to be associated with the last stage of island arc volcanism (2680 – 2707 Ma). This is because their REE patterns are highly fractionated with LREE enrichment because of its derivation from mantle sources which have been enriched (Basu et al., 1984; Capdevila et al., 1982; Card, 1990; Ujike, 1985). This assemblage is associated with the Larder Lake – Cadillac deformation zone (Card, 1990).

1.2.2.3 Major Structures (Faults and Folds)

The earliest stage of deformation (D1) in the Abitibi is folding. This led to upright east-west trending anticlines and synclines with no axial planar cleavage throughout the subprovince, for example, the Blake River synclinorium (Corfu, 1993; Dimroth et al., 1983; Jackson, 1991; Wilkinson et al., 1999). Following D1, the most evident and important deformation event for the lode gold deposits occurred and resulted in two major east-west striking deformation zones: the Larder Lake-Cadillac deformation zone in the south and the Porcupine-Destor deformation zone in the north. This occurred between 2681 – 2676 Ma and was associated with the Timiskaming alluvial-fluvial sedimentation and alkali magmatism along these systems (Corfu et al., 1991; Jackson, 1991; Wilkinson et al., 1999). Following this was regional folding and thrusting (D3) which led to the development of the foliation and greenschist facies metamorphism observed in the subprovince (2676 – 2643 Ma) (Jackson, 1991; Wilkinson et al., 1991).The Abitibi is sub-greenschist to greenschist facies, except for around large pluton contact aureoles, where locally the facies is amphibolite or higher (Corfu, 1993). Finally, late hydrothermal activity occurred along the two major deformation zones between 2630 – 2580 Ma (Wilkinson et al., 1999).

1.2.2.4 Mineralization Typical of the Abitibi Greenstone Belt

Mineralization within the Abitibi contains a diverse suite of economic commodities. Deposit types include orogenic lode gold, such as the Kirkland Lake deposits, volcanic-associated Cu-Zn-(Pb) massive sulphide (VMS), such as the Kidd Creek deposit, and magmatic Ni-Cu-(PGE), such as the Shaw Dome (Houle, 2008; Jackson and Fyon, 1991).

Within the Abitibi Greenstone Belt, the VMS deposits are formed in volcanic-dominated assemblages. Gold rich VMS deposits are only associated with the youngest of these assemblages. The Ni-Cu-(PGE) deposits are only found in the younger volcanic dominated assemblages of the Abitibi. Orogenic lode gold deposits occur across multiple assemblages within the Abitibi Greenstone Belt, but are spatially and genetically related to the Porcupine – Destor or the Larder Lake – Cadillac Deformation Zones (Ayer et al., 2005; Houle, 2008). A more complete review of deposits within the Abitibi Greenstone Belt is discussed by Ayer et al. (2005), Houle (2008), and Jackson and Fyon (1991).

1.3 Kirkland Lake Geology

Kirkland Lake is located in Teck Township along a tertiary splay of the Larder Lake – Cadillac deformation zone in the southern Abitibi subprovince (Figure 2). Bound to the south by the Larder Lake – Cadillac deformation zone, this 3 – 5 km wide area is comprised of the Kirkland Lake fault, or the Main and ’04 Breaks, and of the 2700 Ma Timiskaming assemblage of sedimentary, volcanic, and intrusive rocks forming an east-plunging synclinorium (Thomson, 1948). The Timiskaming assemblage unconformably overlies the Blake River assemblage and is intruded by a composite syenite stock and late intermediate shoots and dykes (Hyde, 1980).

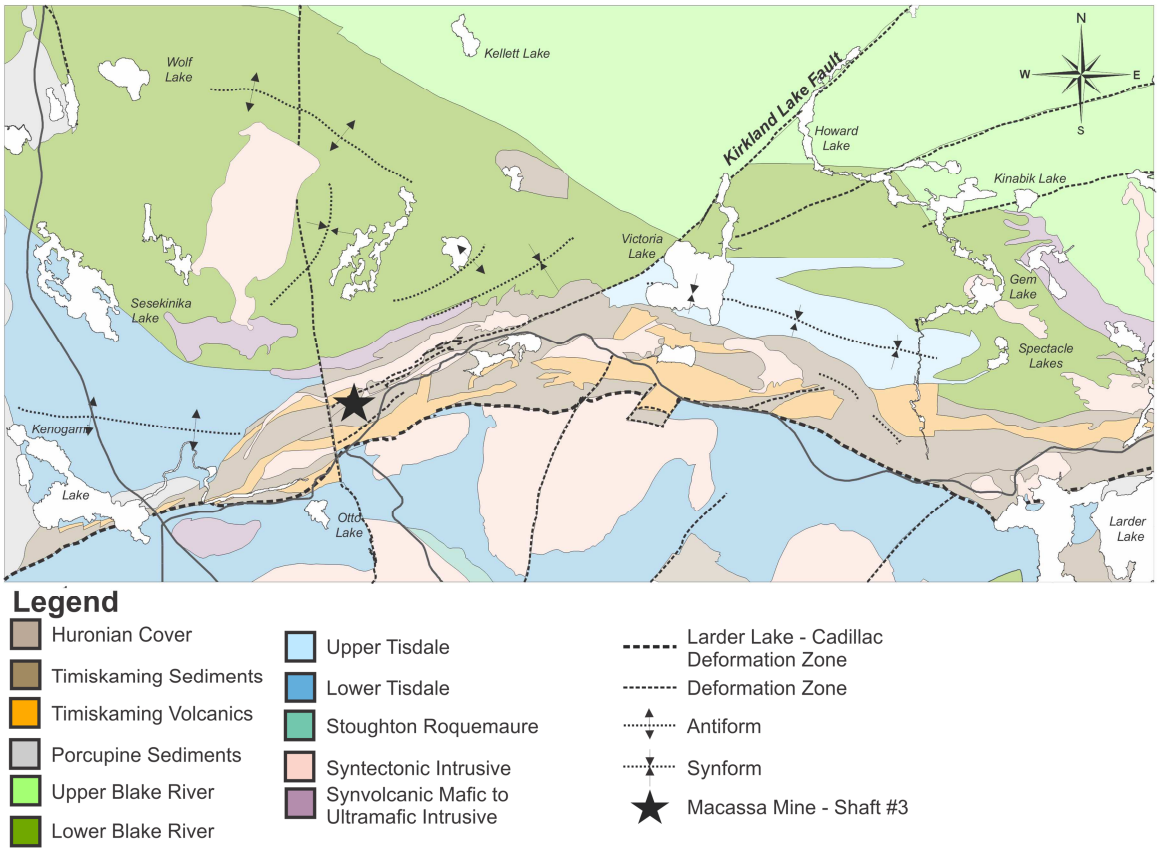

Figure 2 - Lithotectonic assemblages, intrusions, and major structures in the Kirkland Lake area (Adapted from Ayer et al., 2005 and Rhys, 2005). Macassa Mine #3 Shaft is denoted by the star.

1.3.1 Camp Lithologies

1.3.1.1 Measedimentary and Metavolcanic Rocks

The Timiskaming assemblage is comprised of alluvial- fluvial facies metasediments and alkali metavolcanic rocks resting unconformably on the older mafic metavolcanic rocks of the Blake River assemblages. Metasediments and metavolcanics include conglomerate, sandstone, siltstone, argillite, chert, trachytic and phonolitic flows, agglomerate, and tuff (Hyde, 1980). The sedimentary sequence dips moderately to steeply to the south and is south facing.

1.3.1.2 Intrusives

Near Kirkland Lake, there are thought to be two cycles of volcanism, separated by sedimentary rocks. (Hyde, 1980; Thurston and Chivers, 1990) Each is komatiitic at the

base, and is overlain by tholeiitic and calc-alkaline rocks. The later cycle is capped by an additional upper alkaline sequence, in which the Timiskaming volcanics are found. The Timiskaming volcanics are composed of pyroclastic and massive trachytic flows (Hyde, 1980). The Timiskaming volcanic center is thought to be in the central Lebel Township, where trachyte flows and tuffs are present on a large scale (Hyde, 1980).

Late syntectonic intrusions, formed between 2680-2672 Ma, are broadly coeval with the Timiskaming assemblage (Ayer et al., 2005; Corfu, 1993; Wilkinson et al., 1999). These relatively small intrusions occur in close proximity to the Larder Lake – Cadillac deformation zone. These are alkalic, and consist of monzonite, syenite, albitite, diorite, gabbro, clinopyroxenite, hornblendite, and lamprophyre (Ayer et al., 2005). There are large syenitic plutons exposed south of the Larder Lake – Cadillac deformation zone into the Boston and Larder Lake assemblages and could be a potential source for the smaller syenitic stocks within Kirkland Lake. There are multiple phases of syenitic intrusions within Kirkland Lake with an early stage of augite syenite and later stages of syenite porphyry intrusions. Intermediate lamprophyric dykes are the last phase coeval with the syenitic intrusions. Most of these dykes are post-mineralization, but there have been a few which have been mineralized. The Matachewan diabase dykes are post-tectonic intrusions and are unmineralized. These will be further described in subsequent Chapter 3.2.

1.3.2 Kirkland Lake Structures

1.3.2.1 Fault Structures

The main structure within the Kirkland Lake area is the Larder Lake – Cadillac deformation zone. It follows the contact between the mafic metavolcanic rocks of the Boston and Larder Lake assemblages to the south and the metasediments of the Hearst and Timiskaming assemblages to the north. At the Macassa Mine area, it is E-W striking, a 10-500m wide zone with intense carbonate and chlorite alteration extending to depth at least 15 km. Quartz-carbonate veins splay off the structure as intrusions and the fault zone has strong steep foliation and lineation (Wilkinson et al., 1999).

The Main and ’04 Breaks are part of the Kirkland Lake fault, a tertiary splay 2 km north of the Larder Lake – Cadillac deformation zone. This brittle fault is also northeast striking and dips steeply to the south. In addition to the series of NE striking faults are a set of N-S cross faults which offset mineralization. These are late Proterozoic faults which are steeply dipping and brittle, and have chloritic clay filled gouge. These include the Q, Tegren, and Amikougami Faults in the west portion of the camp and the Lake Shore, Sylvanite, and Murdock Creek Faults in the east portion of the camp (Rhys, 2005).

1.3.2.2 Folds and Deformation Events

Post-Timiskaming deformation events (D2 to D4) occurred between 2675-2665 Ma and overprinted the pre-Timiskaming D1 folds and thrusts. The earliest measurable deformation event, D2, is observed as steeply south dipping S2 foliation trending east-northeast and is concentrated on the Larder Lake – Cadillac deformation zone. D3 formed S3 foliation which strikes several degrees counter-clockwise to D2, but is still steeply south dipping. The low strain S4 foliation (D4) is locally developed in the Kirkland Lake area and is northerly trending and east dipping (Ispolatov et al., 2005; Rhys, 2005; Wilkinson et al., 1999).

1.4 Mineralized Zones

The Kirkland Lake camp is a greenstone-hosted quartz-carbonate vein deposit, which is a subtype of Archean lode gold deposits (Dubé and Gosselin, 2007; Poulsen et al., 2000; Thomson et al., 1950; Todd, 1928). These types of deposits are generally sulphide-poor and associated with the occurrence of tellurides. These deposits are mesothermal and orogenic (Dubé and Gosselin, 2007), and the gold deposit at the Macassa Mine is thought to have formed during major fracturing and subsequent ductile deformation during the emplacement of granitic batholiths (Kerrich, 1983; Kerrich and Watson, 1984). The Macassa Mine has two main systems of mineralized zones. Both are associated with mineralized faults, known as breaks. The first system is related to the Main/’04 Break and the second is the South Mine Complex (Figure 3). Further alteration mineral assemblages and ore mineralogy characterization will be discussed in Chapter 3.

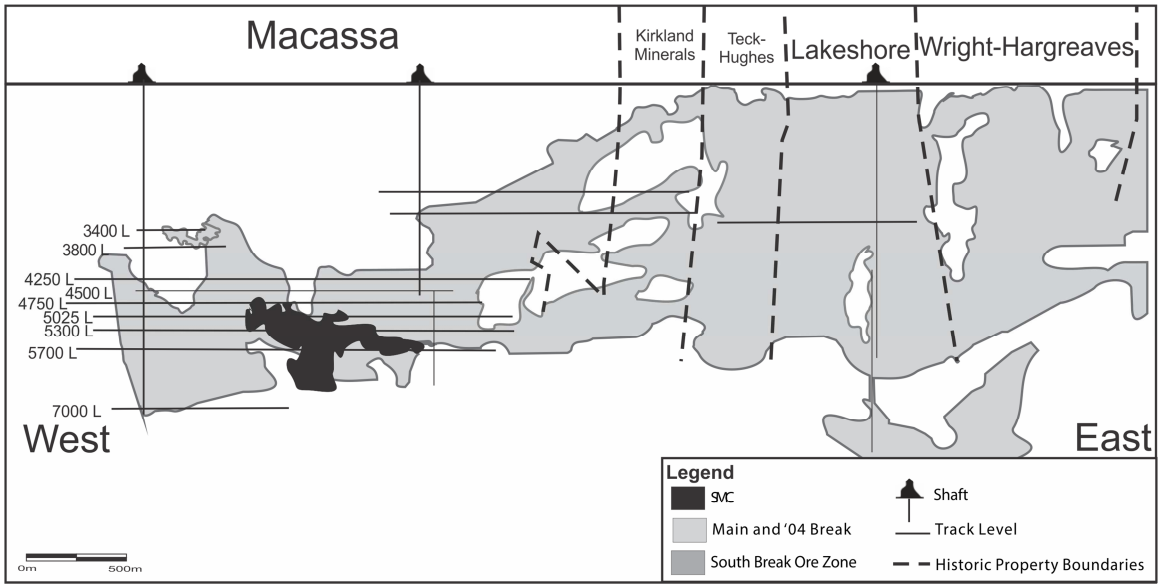

Figure 3 - Longsection of the Kirkland Lake Deposit from the Macassa Mine to the historical Wright-Hargreaves property looking north showing the location of the SMC (black) with respect to the Main/'04 Breaks (light grey). Historic property boundaries are dashed, shafts are marked by vertical lines below a shaft silhouette, and track levels are vertical lines with levels marked accordingly.

1.4.1 Main/'04 Break

The Main Break and '04 Break are the main components of a steeply southeast dipping, semi-brittle reverse-fault system. These, together with other breaks and associated structures, comprise the Kirkland Lake fault system (Rhys, 2005), a tertiary splay off the Larder Lake-Cadillac deformation zone. Mineralization of the Kirkland Lake fault system (Figure 3) stretches 7 km along strike and from surface to 2460m depth at Wright-Hargreaves 8100' level workings (Stills, 2001; Thomson et al., 1950). Mines from west to east are Macassa, Kirkland Lake Gold, Teck-Hughes, Lake Shore, Wright-Hargreaves, Sylvanite, and Toburn (Figure 3).

The system dips south at 60° to 85° and strikes northeast between 060° to 080°. There is no distinct change in strike and dip from east to west. Mineralization occurs within and adjacent to quartz veins associated with early displacement. The breaks are hosted within syenite porphyry, augite syenite, tuff, trachyte, and sometimes metasedimentary rocks such as conglomerate, sandstone, and siltstone (Kirkland Lake Gold Inc., 2013).

1.4.2 South Mine Complex

The South Mine Complex (SMC) is a newly discovered (2003) system to the south of the ’04 Break. It is comprised of a series of veins-faults which dip for the most part more shallowly to the south-east than the ’04 Break at 25° to 50°, with the ’08 Break dipping up to 75° at depth in the southern SMC (Kirkland Lake Gold Inc., 2013; Rhys, 2008). It is just less than 1 km in strike length and is found between 1447m to 2135m depth within the Macassa Mine. The SMC is open to the east and at depth (Kirkland Lake Gold Inc., 2013). The SMC is mostly hosted within syenite porphyry, augite syenite, and tuff (Kirkland Lake Gold Inc., 2013; Rhys 2008).

The zone is thought to be formed as a Riedel shear between the Main/’04 Break and a break to the south, possible the Amalgamated Break (Figure 6). Another hypothesis (Rhys, 2013) is that the SMC could be a step or a continuation of the Main Break as a gradual rotation of the structural zone, dissipating it into a broadening zone of smaller structures that could be the SMC.

1.5 Summary

The Abitibi greenstone belt is the largest and most economically important Archean granite-greenstone terrane of the Canadian Shield. It extends from west of Timmins, Ontario to east of Chibougama, Quebec (Hodgson et al., 1991). The belt is part of the Abitibi Subprovince, a smaller division of the Superior Province, the largest Archean craton of the Canadian Shield. It is primarily composed of metamorphosed sedimentary and volcanic rocks and associated intrusive rocks that trend east-west and extends over 1500 km in length (Calvert and Ludden, 1999). The southwestern part of the belt is host to some of the most well-known copper-zinc and gold deposits in the world (Ayer et al., 2005). The vast majority of large gold deposits in the southern Abitibi Greenstone Belt occur within a few kilometers of two east-west trending fault zones, the northern Porcupine-Destor Deformation Zone (PDDZ) and the lower Larder-Lake Cadillac Deformation Zone (LLCDZ) (Ayer et al., 2005; Jackson and Fyon, 1991).

The Kirkland Lake region is underlain by a succession of Archean supracrustal rock assemblages. Two cycles of volcanism are represented in the Tisdale and Blake River

assemblages. The Tisdale assemblage is comprised of a variety of volcanic to volcaniclastic rocks, including komatiitic, tholeiitic, and calc-alkaline rocks. Succeeding the Tisdale assemblage is the Blake River assemblage, which includes calc-alkaline basalts, tholeiitic mafic volcanics, and rhyolite. Lying unconformably over the volcanic units are the Timiskaming rocks, which consist mainly of clastic sedimentary units, and some intercalated alkaline volcanic rocks. Lastly, syenitic intrusions of Timiskaming age are observed to crosscut the local assemblages (Ayer et al., 2005).

The Kirkland Lake region occurs on the southern limb of the Blake River synclinorium, which is truncated in the north by the Destor-Porcupine Break, and in the south by the Cadillac-Larder Lake Deformation Zone and its associated deformation corridor (Ewert et al., 2011). The Larder Lake-Cadillac Deformation Zone is considered to have been a major east-west thrust fault that later experienced expansion, creating a basin that was then filled with calc-alkaline volcanic and clastic sedimentary rocks of the Timiskaming Group. Later compression of this area created parallel and splay faults in the Timiskaming and Lower Tisdale group rocks, along which many of the gold deposits of the Kirkland Lake Gold Camp was formed (Corfu et al., 1991; Ewert et al., 2011; Thurston and Chivers, 1990).

The majority of gold deposits in the Kirkland Lake gold camp are described as lode-gold deposits, where gold mineralization is hosted in laminated quartz-carbonate fault fill veins. The veins are structurally controlled and distributed along crustal scale fault zones with multiple generations of strain, allowing for the migration of mineralizing fluids (Ispolatov et al., 2005; Dubé and Gosselin, 2007; Poulsen et al., 2000). Syenitic, calc-alkaline intrusives, and Timiskaming-aged sediments within proximity to the east-west trending Cadillac-Larder Lake deformation zone and smaller, syn-genetic fault zones are host to the majority of these gold bearing quartz-carbonate veins.

The Macassa Mine, part of the Kirkland Lake camp, has two main systems of mineralized zones. The first system is related to the Main/’04 Break and the second is the South Mine Complex (Figure 3). Both are associated with the mineralized faults systems, locally known as breaks. The Main Break and ’04 Break are the main components of a steeply

southeast dipping, semi-brittle reverse-fault system which is 7 km along strike and goes to a depth of 2460 m. The Kirkland Lake fault system is a tertiary splay off the Larder Lake-Cadillac deformation zone. It dips south at 60° to 85° and strikes northeast between 060° to 080°. The Main/’04 Breaks show characteristics of a typical lode-gold deposit: it is epigenetic, is structurally controlled, has associated narrow quartz-carbonate veining, and is hosted in greenstone. The South Mine Complex (SMC) is a series of veins-faults that strike northeast 060° to 080° and dips 25° to 50°. The zone is thought to be formed as a Riedel shear between the Main/’04 Break and a break to the south, known as the Amalgamated Break. The SMC is comprised of approximately 15 different zones with similar characteristics. Major zones include the New South Zone and Barchetta with characteristic quartz-molybdenum flooding, and Lower D, Limelight, #7 Break, Lower D North, and ‘08 Break displaying cataclasite with narrow veins.

Chapter 2

2 Methods

2.1 Objectives

The objective of this work is to constrain mineralization between the SMC and Main/'04 Breaks, and between zones of the SMC, using geochemical signatures. This has been done by comparing the alteration mineral assemblages, ore mineral assemblages, and fluid characteristics. Petrography, XRD, multi-element analysis, and oxygen isotope analysis of whole rock and mineral separates were used to define the SMC and to contrast the varying zones of the SMC and Main/'04 Breaks. New South Zone data from Horvath (2010) and Main/'04 Break data from Kerrich and Watson (1984) were used to supplement results.

2.2 Sample Collection

Samples used from Horvath (2010) were collected in 2010 and include drill core samples encompassing the main lithologies observed in the SMC portion of the Macassa Mine. These were taken within the New South Zone (NSZ). Lithologies include basic syenite, tuff, bimodal porphyry, syenite porphyry and trachyte. Samples were also taken from drill core for different mineralization styles, including multiple stages of quartz veins, breccias, and quartz-molybdenite flooding. Horvath (2010) collected thirty-two (32) samples were taken at 30 m intervals from a single drill hole (53-1562). Extra samples were taken at 2 – 3 m spacing above, within, and below mineralization for better characterization of the mineralized zones. Select samples were chosen for their large quartz veins with associated chlorite.

The twenty-seven (27) samples from Kerrich and Watson (1984) were collected from across the strike of the Kirkland Lake Fault system from Macassa to Wright-Hargreaves, and at from levels 2475' – 7200'. They encompassed unaltered rocks of augite syenite, syenite porphyry, trachyte, and tuff. Samples from altered rock and mineralization were also taken.

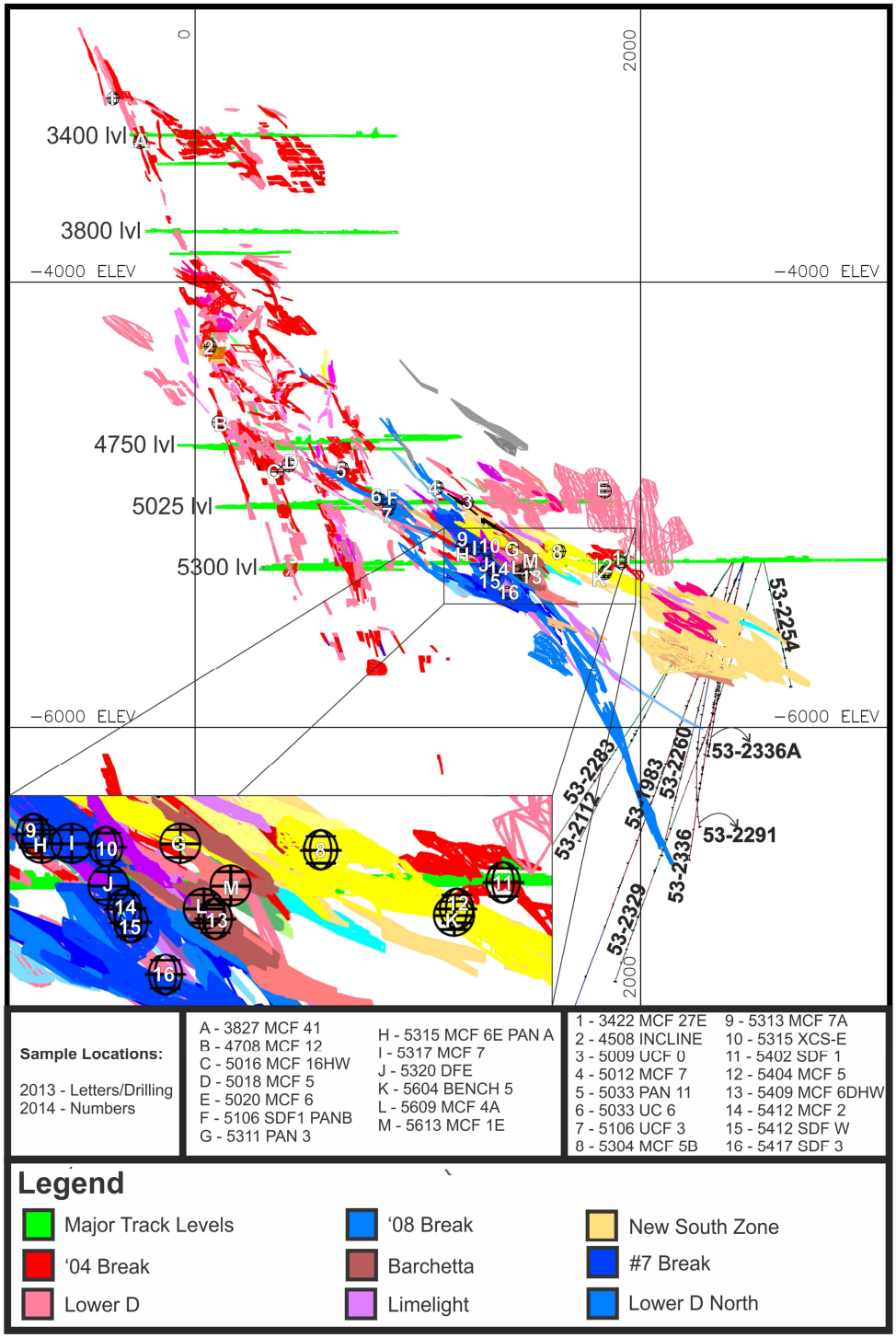

Figure 4 - Cross Section looking east of the locations of the 2013 and 2014 sampling program where spheres represent hand samples from underground grab samples and intersections of drillholes with zones represent core samples. Green represents major track levels in the mine while zones are represented by the other various colours (red - '04 Break, pink - Lower D, beige/yellow - NSZ, dark blue - #7 Break, medium blue - Lower D North, light blue -'08 Break, brown - Barchetta, and purple – Limelight).

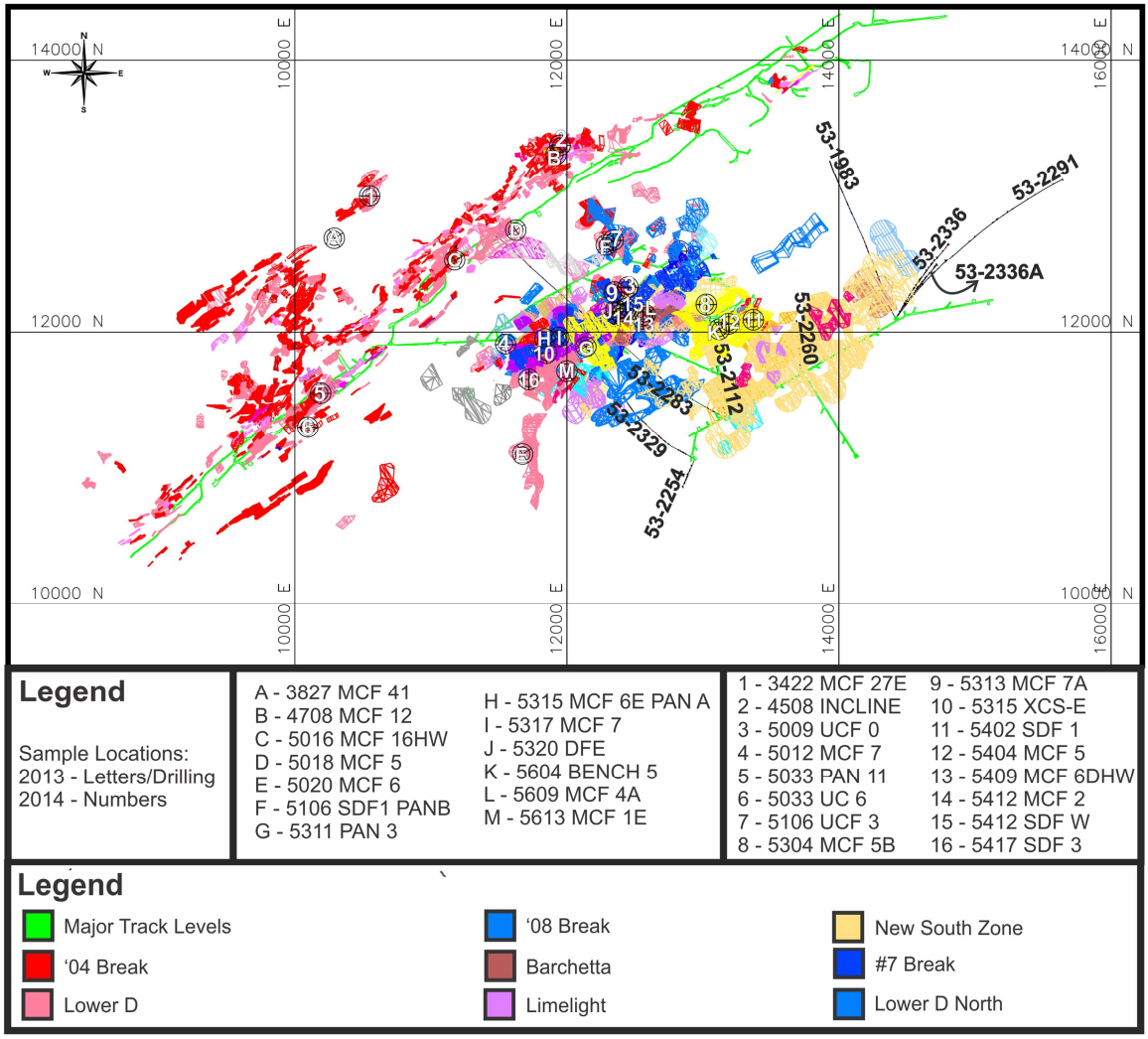

Figure 5 - Plan View at the 5300 Level of the locations of the 2013 and 2014 sampling program where spheres represent hand samples from underground grab samples and intersections of drillholes with zones represent core samples. Green represents major track levels in the mine while zones are represented by the other various colours (red - '04 Break, pink - Lower D, beige/yellow - NSZ, dark blue - #7 Break, medium blue - Lower D North, light blue -'08 Break, brown - Barchetta, and purple – Limelight).

Within this study, in the 2013-2014 sampling program, 165 samples (Appendix A) were taken as hand samples from underground grab samples as well as from core (Figure 4 and 5). Samples in the SMC were collected from the New South Zone (91), #7 Break (12), Barchetta (8), Lower D North (15), Limelight (5), and Lower D (5). There were 29 samples taken from the '04 Break and its hangingwall veins. Samples were collected in

each area as follows: one to three (1 – 3) samples showing characteristic mineralization of the zone, one (1) sample on in the hangingwall and footwall alteration zone, and were possible, one (1) sample in fresh to weakly altered rock in the hangingwall and footwall. Areas were chosen to demonstrate typical mineralization types of the before mentioned zones within different lithologies. Samples locations were limited based on accessibility and therefore introduced some sampling bias. However, this was minimized by collecting samples which were spatially distributed as possible throughout Macassa Mine (Figures 4 and 5) as well as collecting samples with a variety of mineralization textures.

Samples from SMC drill core and underground workings were collected for comparison of the SMC with the Main/'04 Breaks. Samples were selected based on alteration intensities (both unaltered and altered), mineralization, and location in the SMC. Samples typified different ore types within each selected zone. Mineralized samples not only included quartz veins, but also break and sheared materials, molybdenite breccias, and high pyrite (5-10%) concentrations in heavily altered host rock. A few samples containing high-grade gold were specifically collected to characterize the gold-bearing ore geochemically. Underground samples were collected for ore characterization and comparison with wall rocks as well as to have a good distribution of samples throughout the different zones in the SMC and the '04 Break. These samples were collected mostly from the 5300 Level of the Macassa Mine, but also from 5600, 5100, 5025, 4750, and 3800 Levels (Figures 4 and 5).

2.3 Optical Microscopy

A total of 58 samples taken from the SMC and the Main/'04 Breaks were made into polished thin sections in the Rock Preparation Laboratory at the Western University, the University of Alberta Thin Section Laboratory, and Spectrum Petrographics. Out of these 58 thin sections, 44 were from various zones in the SMC, and 14 were from the Main/'04 Breaks.

Thin Sections were studied in reflected, and plane and cross polarized transmitted light with a Nikon Eclipse LV100 POL microscope in the Earth and Planetary Materials Imaging and Analysis Laboratory at Western University. A 10X optical eyepiece and five

attached optical lenses at 2.5X, 10X, 20X, 40X and 100X on the microscope were used to make petrographic descriptions (Appendices B). Photographs were taken with a Nikon Digital Sight DS-Ri1 high resolution digital camera attached to the microscope and were then manipulated using NIS-Element software.

2.4 X-Ray Diffraction

X-Ray Diffraction (XRD) analysis is used to identify the crystalline components of samples. Of the samples collected, 77 samples representative of various stages of mineralization from multiple zones of both the SMC and the ’04 Break, as well as samples representative of unaltered tuff, augite syenite, and syenite porphyry were analyzed for bulk rock mineralogy using XRD (Appendix C). XRD was performed in the Laboratory for Stable Isotope Sciences at Western University. Powdered samples X-Ray Diffraction (XRD) analyses were used to identify the crystalline components of samples.

Powdered samples (~200 mg) were packed into the back window of aluminum plates and mounted to glass slides. This ensures random orientation of the crystals and minimizes strain that can offset peak positions. A Rikagu Rotaflex Diffractometer collected diffractions from 2º to 82° 2θ, with a step size of 0.02° and scanning speed of 10°/min. This was operated at 45kV and 160mA with a Cobalt rotating anode source (Co Kα, λ=1.7902Å). Diffractograms were analyzed using Bruker DIFFRAC plus EVA software package. Data is shown graphically as scattered patterns which are correlated to mineral phases in the International Center for Diffraction Data (ICDD) PDF4 database.

2.5 Scanning Electron Microscopy Analysis

Twelve (12) samples from the ’04 Break (3), the #7 Break (2), Barchetta (1), Lower D North (2), Limelight (1), and New South Zone (3) were analyzed at Surface Science Western by Scanning Electron Microscopy (SEM). Samples were chosen based on ore mineralogy such as tellurides, gold, pyrites, and molybdenite seen in optical microscopy as well as to encompass a representative selection of different zones. Carbon coated thin sections were analyzed by Scanning Electron Microscopy (SEM) with Back-Scatter Electron (BSE) imaging using a Hitachi SU3500 Variable Pressure SEM combined with

an Oxford AZtec X-Max50 SDD X-ray analyzer. Point probe analysis was conducted with Energy Dispersive X-Ray Spectroscopy (EDS) from 0 keV to 5 keV to determine elemental ratios to identify ore mineralogy. . Elemental weight percent from EDS was used to determine mineralogy of the spot samples. Appendix F contains SEM BSE images for mineralized grains for these samples as well as EDS analysis results.

2.6 Multi-Element Analysis

Forty (40) samples from the SMC and the Main/'04 Breaks collected as part of Kirkland Lake Gold's 2013 exploration program in drillcore of the NSZ and collected hand samples throughout different levels and zones of the mine from the 2013-2014 sampling program were selected for multi-element analysis. Representative samples were chosen based on zone, mineralization type, and lithology. These samples expand on the samples collected by Horvath (2010), and Kerrich and Watson (1984).

Samples were sent to Swastika Labratories to be pulverized to >90% minus 150 mesh and assayed for gold by Fire Assay with an Atomic Absorption Spectroscopy finish (FA-AAS) at low concentrations (detection at 5ppb), and Fire Assay with a Gravimetric finish (FA-GRAV) at higher concentrations (detection at 0.30ppm).

Pulverized samples were then sent to The Laboratory for Geochemical Analysis at Western University, Ontario to be analyzed for SiO_2, TiO_2, Al_2O_3, Fe_2O_3, MnO, MgO, CaO, K_2O, Na_2O, P_2O_5, Cr_2O_3, BaO, and SrO by X-Ray Fluorescence (XRF) fusion. Twenty (20) of these samples were analyzed for Mo, Nb, Zr, Y, Sr, Rb, Th, U, Pb, Ga, As, Zn, Cu, Ni, Co, Cr, V, Mn, Sc, Ba, La, Ce, Pr, Nd, Sm, Eu, Gd, Tb, Dy, Ho, Er, Tm, Yb, Lu, Hf, Ta, Cs, Sb, Sn, and Ag by borate fusion Inductively Coupled Plasma Mass Spectrometry (ICP-MS) analysis, and for S by LECO TruMac CNS. Bi, Br, Hg, Se, Te, and W were omitted from reporting due to poor accuracy within the borate fusion-ICP-MS analysis. In Fusion XRF for major elements 3 standards were run 3 times for every run of 40 samples: SY-2, JA-1, and JG-2. Duplicate runs of the standards were used to measure precision. XRF for trace elements used 3 standards for every run of 40 samples: AN-G, JB-2, and JG-3. LECO S analysis used 2 standards for every run of 20 samples: Ore 4005, and Ore 4022. One sample was duplicated to verify precision. Standard results

and values are included in Appendix D along with sample results. Results were analyzed using ioGAS-64, an advanced geochemistry exploratory data analysis program (http://reflexnow.com/iogas/).

2.7 Stable Oxygen Isotopes Analysis

Forty-one (41) SMC samples collected as part of Kirkland Lake Gold's 2010 exploration program in drillcore of the NSZ and in hand sample on the 5300 level of Macassa Mine were selected for oxygen isotope analysis. These were run for whole rock (41 samples), quartz separate (9 samples), and chlorite separate (4 samples) analysis. Samples focused on comparing the mineralization within different lithologies.

$\delta^{18}O_{V\text{-}SMOW}$ values of silicate rocks and minerals were measured with one of two gas source isotope ratio mass spectrometers at the Laboratory for Stable Isotope Science (LSIS) at the University of Western Ontario, with the same instrumentation and methods used by Watson and Kerrich (1984). Procedures for determination of oxygen stable isotope values used techniques similar to the pioneers of stable isotopes, Clayton and Mayeda (1963) and Taylor and Epstein (1962). For use on a silicate line, one replicate of eight to ten milligrams of powdered rock or mineral separates were weighed and samples were heated for 12 hours in a dry box. They were then placed in nickel tubes to be reacted with ClF_3 at 150°C for 18 hours, then at 300°C for 2 hours. This causes the bonds in the silicates to break and produce O_2:

$$4ClF_3 + 3SiO_2 \rightarrow 3SiF_4 + 3O_2 + 2Cl_2 \text{ (Eq. 1)}$$

The oxygen then reacts with a hot carbon rod to produce CO_2, which was then extracted on one of the VG Optima dual-inlet stable isotope mass-spectrometer, or the Micromass PRISM II dual inlet mode stable isotope ratio spectrometer. Samples in each run of 10 were compared to at least two lab standards. Duplicate analyses of oxygen in standards showed error less than ±0.2‰.The expected $\delta^{18}O$ values of the standards used were: +11.5 ± 0.2 ‰ for ORX (internal laboratory standard quartz sand), and +7.5 ± 0.2 ‰ for BAS-206 (internal laboratory standard basalt).

Samples with quartz and chlorite were selected for temperature estimates. Samples selected were seen to be in equilibrium in thin section. The temperature estimates allow a calculation of the temperature of the fluid, and therefore will give an estimate of the mineralizing fluid temperature. These minerals were removed from the samples by separately crushing the quartz, and scraping the chlorite off. Each of the quartz and chlorite samples was crushed into small grains using a mortar and pestle. A binocular microscope was used to separate out grains of quartz and chlorite. XRD analysis identified pure quartz samples for stable isotope analysis. Chlorite separates showed minor contamination (<5%) of other minerals which would affect temperature estimates. Further XRD analyses showed pure samples or small amounts of contamination with quartz due to the fine nature of the intergrowths. In a method similar to Watson (1984), the relative proportions for each of the quartz and chlorite were determined using the relative intensities of the peaks on the XRD patterns.

Chapter 3

3 Hand Sample and Photomicrographs

3.1 Regional Geological Setting

The Macassa Mine is located along a tertiary splay of the Larder Lake – Cadillac deformation zone within the southern Abitibi subprovince in Ontario, Canada. The package of rocks within the district (Figure 2) is bound to the south by the Larder Lake – Cadillac deformation zone, and is comprised of the Timiskaming assemblage of sedimentary, volcanic, and intrusive rocks forming an east-plunging synclinorium (Thomson, 1948). This is intruded by a composite syenite stock and late intermediate shoots and dykes similar in age to the Timiskaming assemblage (Hyde, 1980). A more complete description of the regional geology is found within Chapter 1.

3.2 Mine Geology

The mineralization observed in this study of the Macassa Mine is hosted in metavolcanic tuffs of the Timiskaming assemblage, and late syntectonic intrusions coeval with the Timiskaming assemblage including augite syenite, and syenite porphyry (Ayer et al., 2005; Ispolatov et al. 2005). The Timiskaming assemblage is dated at 2680-2707 Ma during what is thought to be the last stage of island arc volcanism. The syenitic syntectonic intrusions formed between 2680-2672 Ma and are broadly coeval with the Timiskaming assemblage. These have intruded (Figure 6) into Timiskaming conglomerates, sandstones, and siltstones, which were not part of this study.

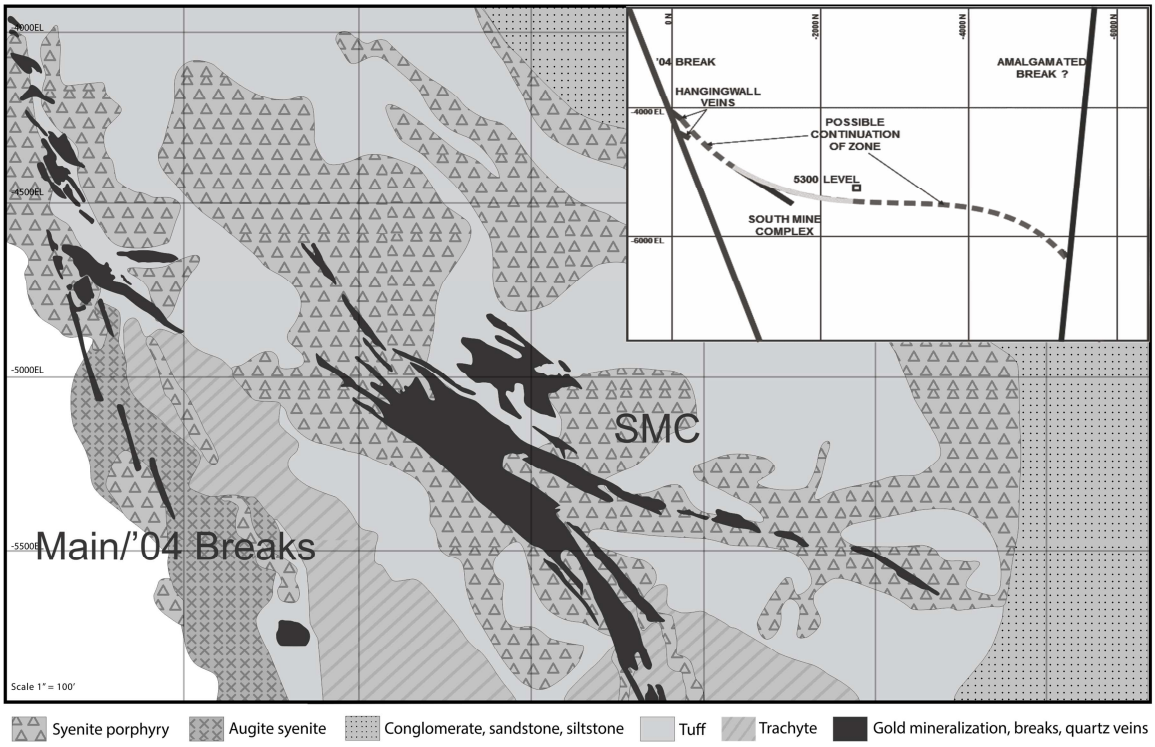

Figure 6 - Cross section of geology and mineralization at Macassa Mine, looking northeast at 567922.6543E (-1200E) from 5331863.2716N to 5332912.4686N (S 0 to 3250) in UTM Coordinates. Main/'04 Breaks is the mineralization in black dipping steeply in the north of the cross section and the SMC is the mineralization in black dipping more shallowly to the south of the Main/'04 Breaks. Host lithologies are shown by medium grey with syenite porphyry as triangles, augite syenite as x, sediments as dots, tuff as solid grey, and trachyte as lines. Inset shows possible interpretation of SMC as Riedel shear between the '04 Break to the north and the Amalgamated Break to the south.

3.2.1 Metavolcanic Tuffs

Within the Macassa Mine, two types of tuff are observed within samples. The first tuff is fine to medium grained tuff with pronounced layering (Figure 7A) 1 mm to 2 m thick. It ranges in colour from dark maroon to brown. In photomicrographs, a representative modal mineralogy has 50% alkali feldspars, 20% plagioclase feldspars, and 10% quartz primary minerals. Feldspars were distinguished using twinning seen within the plagioclase, with albite being considered as part of the plagioclase series. Alteration minerals include 15% very fine grained white micas and 5% chlorite altered from mafic minerals. Green layers contain more chlorite while brown layers contain more feldspars. XRD reveals feldspars as orthoclase (alkali feldspar), microcline (alkali feldspar), and albite (potassium feldspar). Accessory minerals include magnetite (<0.5%), pyrite (2-

3%), biotite (1-2%), and carbonate (5%). The second tuff (Figure 7B) is massive with 0.5 cm to 2 cm spherical red to orange to pink lapilli. This is in a dark brown to black groundmass. Modal mineralogy is found to be similar to the layered tuffs. Differential textures include a lack of layers and the addition of lapilli, which contain remnant textures of mafic minerals which have been completely altered to clays and chlorite.

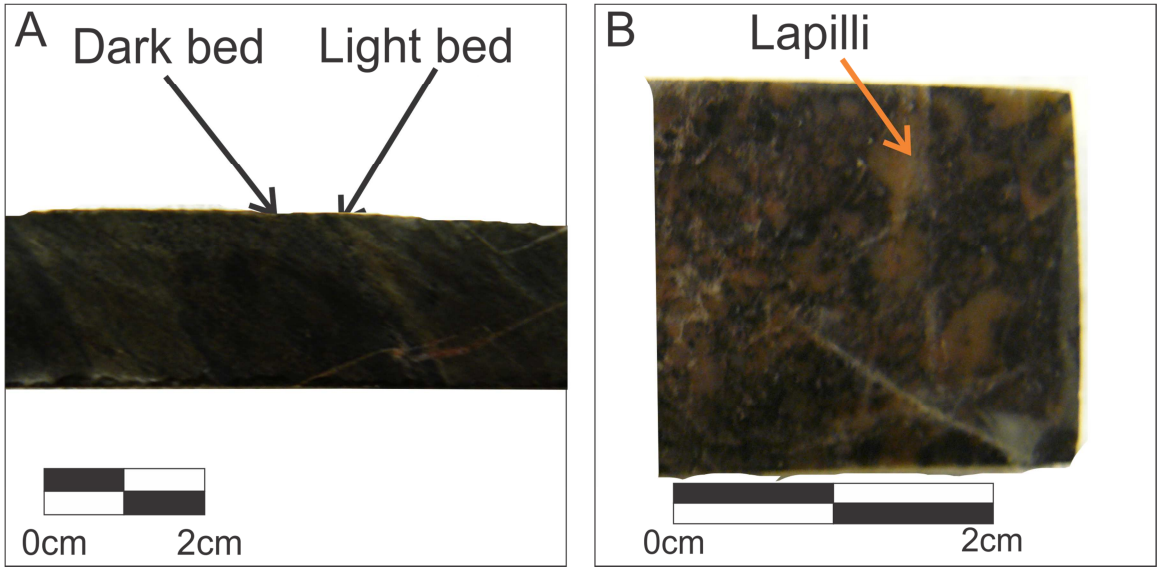

Figure 7 - Metavolcanic Lithologies at the Macassa Mine: (A) bedded volcanic tuff, (B) volcanic tuff with lapilli. Beds in (A) alternate between thicker olive green coloured layers which contain abundant chlorite in thin section, and thinner black-brown layer which contain more K-feldspars in thin section. Lapilli highlighted in (B) are thought to be mafic clasts, but are completely altered to clays and chlorite in thin section.

3.2.2 Intrusive Rocks

There are several different types of intrusive bodes found at the Macassa Mine, ranging from the felsic composite syenite stock to the late intermediate shoots and dykes. Mineralization is hosted within the different phases of the composite syenite stock: augite syenite and syenite porphyry.

There is a rock type known at Macassa Mine as basic syenite, which is augite syenite. It is a massive dark grey-green medium to coarse grain, equigranular, crystalline intrusive (Figure 8A). The augite syenite has well-developed pyroxene (augite) crystals (30-60%) observed in thin section (Appendix B) have a light green cast to them, due to replacement by chlorite and carbonate. Potassium feldspars (40-70%) with minor plagioclase (0-10%)

comprise the remainder of the rock. Accessory minerals include magnetite (<0.5%), apatite (<0.5%), and minor titanite (<0.5%). There are leucocratic inclusions within the augite syenite, but they are not observed within the samples within this study. They are thought to be bands of fractionation of felsic syenite within the augite syenite. They are parallel to the intrusive body near the edge of the intrusion and more randomly oriented further within the body. The wider the inclusions, the coarser the crystals can become. These have the same granitic texture, but are instead orange-red and have a more felsic composition of potassium feldspar.

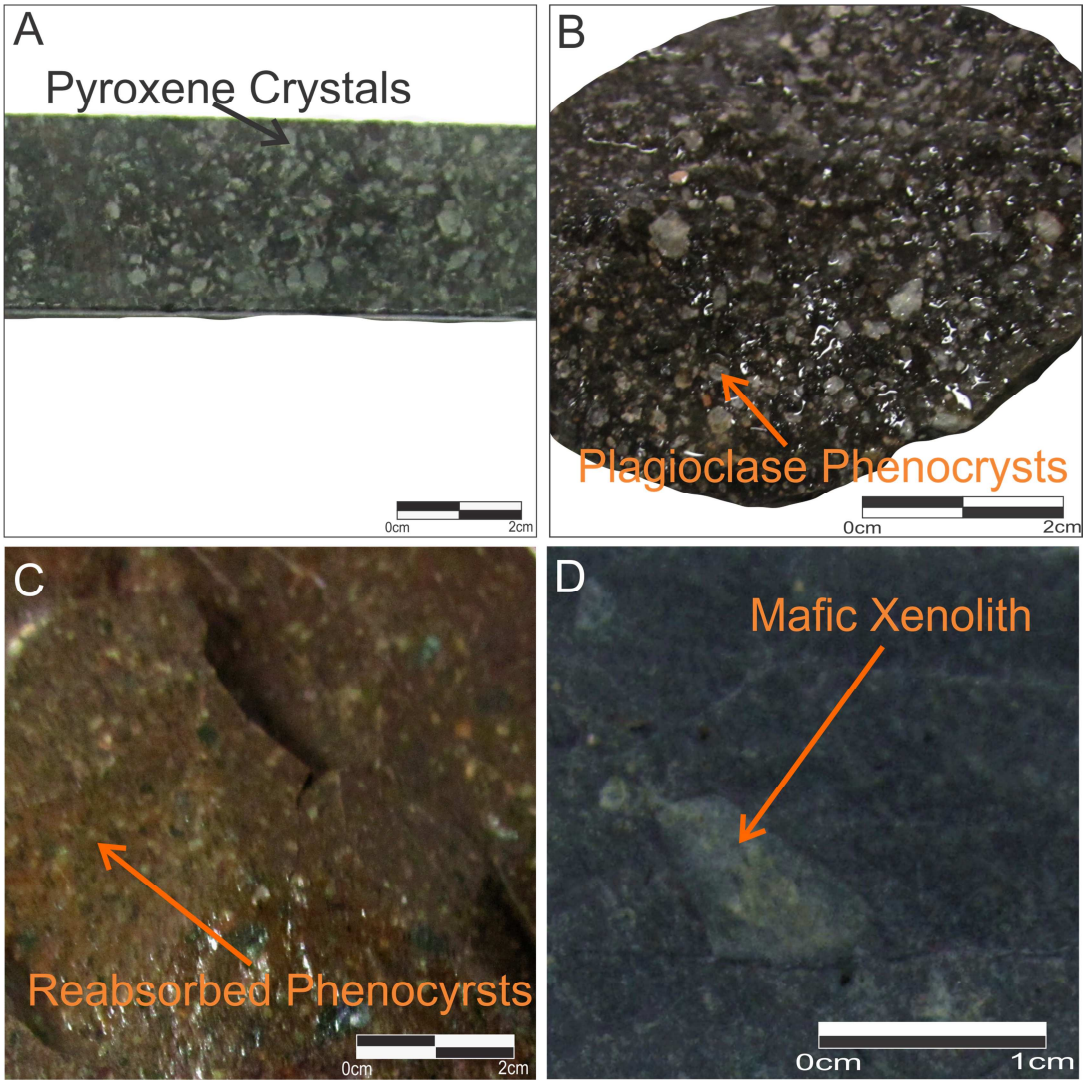

Figure 8- Intrusive Lithologies at the Macassa Mine: (A) augite (mafic) syenite, (B) syenite porphyry with feldspar phenocrysts, (C) type II syenite porphyry with reabsorbed feldspar phenocrysts, (D) mafic xenoliths as found in a type II syenite porphyry.

Syenite porphyry (Figure 8B) is the second type of intrusive lithology. It hosts the majority of the newly found SMC and a significant portion of mineralization related to the Main/'04 Break structures as well. The fine grained groundmass is a maroon to grey-black and has opaque white tabular felspathic phenocrysts. Optical microscopy (Appendix B) shows that the feldspar phenocrysts are well developed and are anywhere between 1-3mm long and 0.25-1mm wide, and can comprise anywhere between 30-50% of the sample. The groundmass is composed of 75-80% alkali feldspars and 15-20% plagioclase feldspars with 5% ferromagnesian minerals including biotite, hornblende, and chlorite and accessory minerals (<0.5%) include apatite, magnetite, and ilmenite. The phenocrysts are found by XRD most commonly as microcline (60%), an alkali feldspar, but can also be present as albite (40%), a plagioclase feldspar (Appendix B). Mafic xenoliths comprising up to 3% of the rock are also found within the porphyries (Figure 8D). The xenoliths are between 3-15mm in diameter and are typically chloritized basalts.

A second type of porphyry locally known as bi-modal porphyry has an additional phenocryst phase to the syenite porphyry. The modal mineralogy is the same as the syenite porphyry: the groundmass contains 75-80% potassium feldspars and 15-20% plagioclase feldspars with 5% ferromagnesian minerals including biotite, hornblende, and chlorite. The second phase phenocryst is albititic, like the first phase, except the phenocrysts are significantly larger than the first phase and up to 2-5mm long. Albite is known due to the albite twinning seen in thin section. The third distinctive porphyry is known locally as type-II porphyry (Figure 8C). This is a texturally different variety from the syenitic porphyry. The type-II porphyry therefore has the same modal mineralogy of the syenite porphyry described above, but the white albitic phenocrysts are being reabsorbed back into the matrix. The phenocrysts are rounded, fade into the matrix, and only compose 10-20% of the unit. Both the bi-modal porphyry and the type-II porphyry comprise <5% of the total intrusives within Macassa Mine, and only one sample of each was collected.

Fine grained dioritic dykes are the last phase coeval with the syenitic intrusions and are locally referred to as intermediate dykes. Most of these dykes are unmineralized (post-mineralization), but there have been a few which have been mineralized within Macassa

Mine. These dioritic dykes are fine to medium grained with chilled contacts, massive, and are pale green. These are moderately to strongly sericitized and locally chloritized throughout. No optical petrography has been done on this rock type within this study, as no samples were collected.

Mesozoic diabase dykes are post-tectonic intrusions and are unmineralized. The dark grey to green diabase dykes has fine to medium grained crystals and the dykes have chilled contacts. No optical petrography has been done on this rock type within this study, as no samples were collected.

3.3 Zone Descriptions and Ore Mineralogy of the Gold Deposit

The Kirkland Lake camp is an Archean lode gold deposit. The Macassa Mine has two main systems of mineralized zones. The first system is related to the Main/'04 Break and the second is the South Mine Complex (SMC) (Figure 3). Both are associated with mineralized faults, locally known as breaks. Reserves and resources are as in Table 1. Most of the observations and descriptions within this section were personal observations, but much of the information and interpretations were provided by or were put into context and confirmed in discussions with and contributions by Kirkland Lake Gold geologists.

Table 1: Resources for the Main/'04 Breaks and SMC for Kirkland Lake Gold Inc., as of January 2014.

Main/'04 Breaks	**tons**	**oz./t**	**Au oz.**
Probable & Proven	1,292,269	0.44	571,941
Measured & Indicated	2,119,230	0.39	826,073
Inferred	571,698	0.33	189,972

SMC	**tons**	**oz./t**	**Au oz.**
Probable & Proven	1,491,693	0.54	812,683
Measured & Indicated	1,464,535	0.69	1,012,091
Inferred	1,205,203	0.67	808.047

Previous works done by Ispolatov (2005, 2008), Kerrich and Watson (1984), Stills (2001), and Watson (1984) have described the Main and ’04 Breaks. This project is a continuation and elaboration on work done by Horvath (2010), and seeks to detail and more clearly define the newly discovered SMC. Chapter 3.2 describes the mineralized zones and their associated alteration found within both the Main/’04 Break and the SMC. Full descriptions of hand samples and thin sections are found within Appendix B. Appendix C lists XRD results.

3.3.1 Main/’04 Break

The Main Break and ’04 Break are the main components of a steeply southeast dipping, semi-brittle reverse-fault system. These, together with other breaks and associated structures, comprise the Kirkland Lake fault system (Rhys, 2005), a tertiary splay off the Larder Lake-Cadillac deformation zone. The system dips south at 60° to 85° and strikes northeast between 060° to 080°. Mineralization occurs within and adjacent to quartz veins associated with early displacement.

3.3.1.1 Main Break, and Hangingwall Structures

The steeply dipping Main break is present in the eastern edges of the Kirkland Lake camp and continues eastwards through to the Toburn mine (Figure 3). The break is the main structure within this area of the camp. The Main Break dips south at 60° to 85° and strikes northeast between 060° to 080°. Mineralization occurs within and adjacent to quartz veins associated with early displacement on this reverse fault.

The break typically is immediately surrounded by up to 0.5m of cataclasite on either side. Late movement on the fault is observed with the presence of gouge, which can be weakly healed and chloritized. This is observed within the surface expression of the Main Break at an outcrop at Lakeshore Mine (Figure 9). The mineralization is mainly found as visible gold and tellurides within quartz veins which either pinch and swell along the break or splay off into the hangingwall, and some into the footwall.

Figure 9 – Narrow cataclastic zone of the Main Break as observed on surface within the Lakeshore outcrop. Textures are similar within all of the Main/'04 Break, although many areas have larger cataclasite zones (5-20cm veins paralleling the break). The break is highlighted by the dashed line with shear textures aligning parallel and up to 3cm on either side of the break. The footwall is below and the hangingwall is above the dashed line in this figure. Note the green sericitic alteration proximal to the break, and the red hematite alteration distally. Quartz veining is seen trending parallel to the break in the footwall. The ruler as scale is in decimal feet, where 0.1' = 3.05cm.

Strong hematite, carbonate, sericitic, and K-feldspar alteration (Figure 10), observed within hand sample, thin section, and XRD patterns (Appendices B and C), is present in proximity to the break and the K-feldspar alteration can continue in samples 5–10m past the structure. Up to 5% fine grained euhedral to subehedral disseminated pyrite is found within the strong alteration surrounding the break.

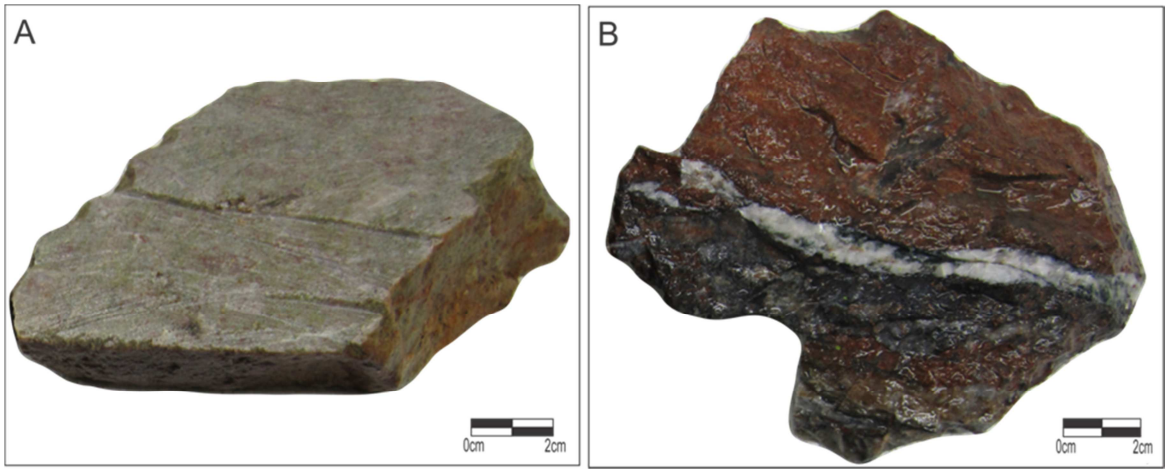

Figure 10 - Typical alteration found in the Main and '04 Breaks with (A) olive green sericite + carbonate ± pyrite found shallow on the Main break at Lakeshore in sample LSKGI119, (B) brick red K-feldspar + hematite + sericite + carbonate found at depth on the '04 Break at Stope 3827 in sample LSKGI115 with a narrow quartz veinlet paralleling the break. Alteration assemblages were verified with optical microscopy.

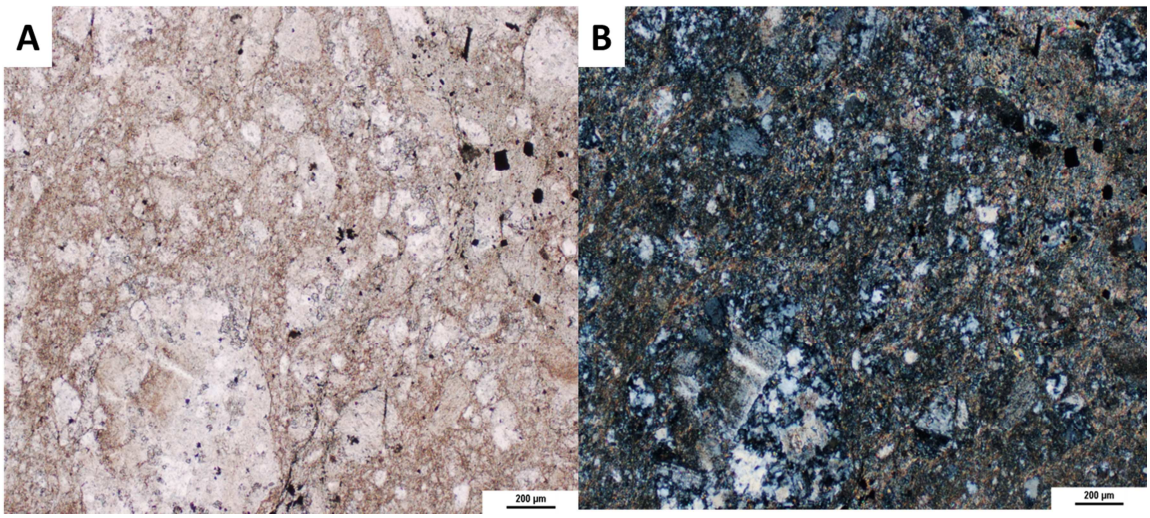

Figure 11 – Photomicrographs of alteration typically seen in the Main/'04 Breaks from LSKGI119 in (A) polarized, and (B) cross-polarized light. In polarized light, hematite is seen as a light red dusting over the entire sample, while sericite, carbonate, and K-feldspar replace the groundmass in cross-polarized light. Fine grain sericite replaces feldspar phenocrysts.

In thin section, the hematite is observed staining silicate minerals, and no microscopically distinct grains are observed. Carbonate and sericite minerals overprint the fine grained groundmass with a higher concentration around fractures/shearing (Figure 11). Altaite (PbTe) followed by calaverite ($AuTe_2$) are the most common tellurides found in the Main

Break as anhedral disseminations and blebs identified with XRD (Appendix C). Gold is found as pyrite fracture fill, inclusions, and rims as well as small blebs (Figure 12) (Watson, 1984).

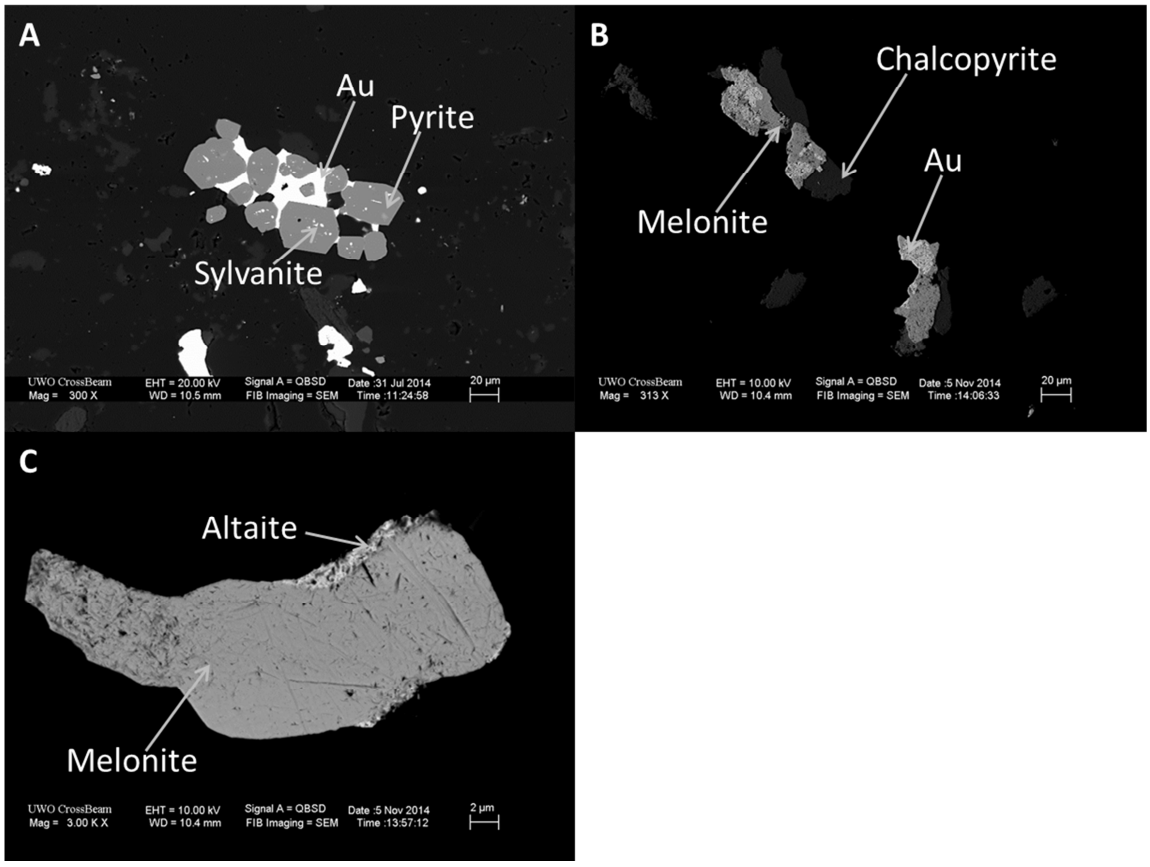

Figure 12 – Scanning Electron Microscope (SEM) back-scatter electron (BSE) images of gold and tellurides found within the '04 Break in thin section. (A) shows sample LSKGI098 with sylvanite ($AuAgTe_2$) inclusions within subhedral partially reabsorbed pyrites with free gold between the pyrite grains. (B) is sample LSKGI142 with multiple stages of mineralization: a first pulse of gold, which is nearly later encased by melonite (NiTe), and has late chalcopyrite. (C) shows an early melonite grain with partial rims of altaite (PbTe). Mineral identification was done using Energy Dispersive X-Ray Spectroscopy (EDS).

3.3.1.2 '04 Break and Hangingwall Structures

The '04 Break is in the western portion of the Kirkland Lake camp and is similar to the Main Break but stepped 125m north of the Main Break, to which it is linked with a series of en echelon structures (Rhys, 2005). The '04 Break is a steeply south dipping structure composed of a mineralized fault structure with late movement. The fault structure is surrounded by cataclasite. As with the Main Break, weakly healed to un-healed

chloritized or mud gouge represent late movement along this structure. The structure has associated quartz veining (Figure 13) which pinches and swells up to 1m wide. Mineralization is observed as visible gold, tellurides, <5% pyrite, and very fine grained molybdenite. More shallowly dipping hangingwall veins splay off the main ’04 structure to the south, displaying a similar style.

Surrounding the break and quartz veins is 0.5–1m of strong K-feldspar, carbonate, hematite, sericite, and minor pyritic alteration (Figure 10, 11). Weak K-feldspar alteration, and in some areas hematite alteration, continues into the wall rock for up to 6–10m. Alteration and mineralization textures observed in photomicrograph are reminiscent of the Main Break described in section 3.2.1.1.

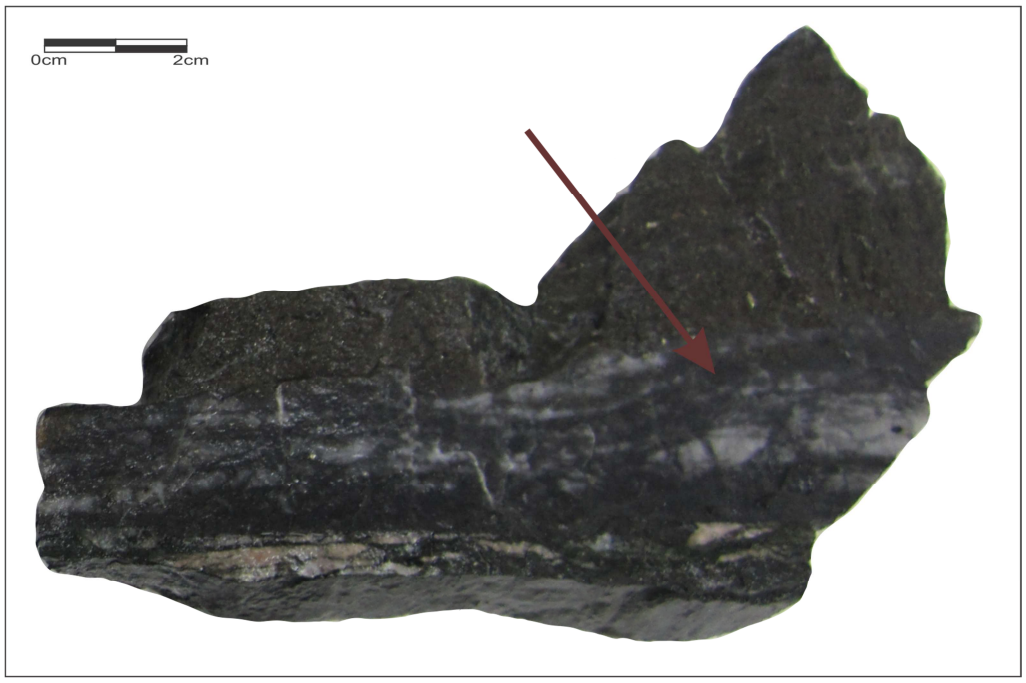

Figure 13 - Typical mineralized quartz vein along the ’04 Break from the 5018 stope in the Macassa Mine in sample LSKGI098. Vein structures can be up to 0.5m thick. Note the dark purple-grey strands of molybdenite within the white-light grey quartz vein shown by the arrow. Below the vein is more competent part of the fault with aligned shear textures.

3.3.2 South Mine Complex

The South Mine Complex (SMC) is a newly discovered (2003) system to the south of the ’04 Break. It is comprised of a series of vein hosted in faults, known locally as breaks,

which dip more shallowly to the south-east than the ’04 Break at 25° to 50°, except for the ’08 Break which dips up to 75°. The SMC is comprised of approximately 15 different zones with similar characteristics. Major zones include the New South Zone and Barchetta with characteristic wide diffuse quartz-molybdenite veining, known locally as quartz-moly flooding, and Lower D, Limelight, #7 Break, Lower D North, and ‘08 Break displaying cataclasite with narrow veins (Figure 4 and 5). In the sections below, each individual zone is described in detail. All of the SMC is characterized by a wide (> 20m) zone of alteration surrounding the breaks (Figure 14). Alteration can consist of a combination of K-feldspar, sericite, pyrite, carbonate, and hematite (XRD and optical microscopy, Appendices B and C).

The SMC mineralization is characterized in the south-eastern portion by zones of quartz-molybdenite flooding that is typically over 2m wide in the hangingwall or footwall of well-healed breaks, and its western and northern portions by zones of cataclasite that are 20cm wide surrounding breaks with associated narrow quartz veins. Mineralization commonly splays within the SMC, and pinches and swells in intensity along its length. Mineralization is found as visible gold, gold associated with 10-15% pyrite or non-auriferous tellurides, or as gold tellurides (XRD analysis, Appendix C).

It should be noted that Re-Os dating on the molybdenite found within the samples was not successful, as there were no molybdenite crystals that were amenable to dating. The molybdenite found within the Macassa Mine is very fine grained and is usually found in thin strands within shear zones. In addition, there have been many periods of reactivation on the breaks, and most of the molybdenite is deformed by post mineralization movement on the fault systems.

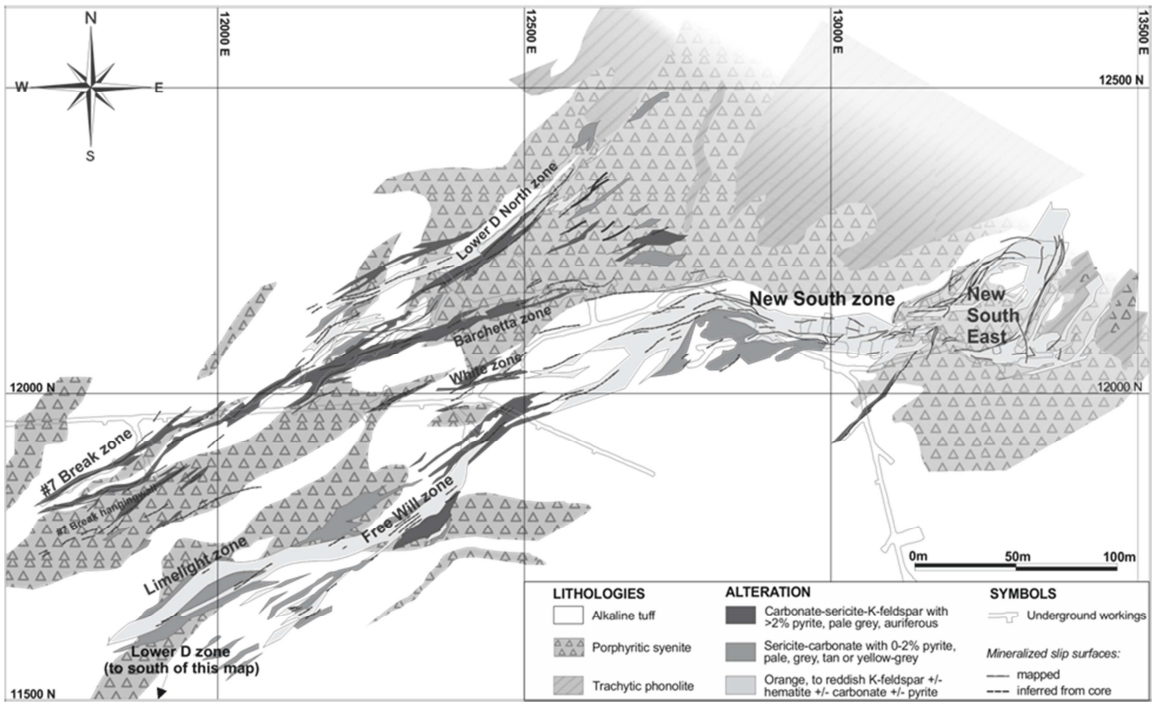

Figure 14 - 5300 level geological plan of the Macassa Mine showing variation of the alteration assemblages, as well as the mineralized zones of the SMC and slip surfaces (Adapted from Rhys and Ross, 2008).

3.3.2.1 New South Zone

The New South Zone (NSZ) is located in the south-east portion of the SMC and is mostly hosted in syenite porphyry, but is also found within tuff, trachyte, and basic syenite close to contacts with the syenite porphyry. It has an average strike of 055° and a dip of 25° SE (Figure 14).

Alteration surrounds this mineralization structure and decreases in intensity further away from the mineralized zone. Proximal alteration encompasses the entire rock for up to 3m on each side of the break while distal alteration surrounds quartz stringers by less than 1cm. The main form of alteration is strong K-feldspar, pyrite, and sericite alteration, but weak to moderate hematite alteration is also present in some samples down dip towards the south. This alteration is locally known as bleaching, sericitization, and hematization. Pyrite associated within the alteration euhedral to subhedral in thin sections. Sericite replaces the fine-grained groundmass, and K-feldspar overprints original textures within the groundmass. Like the Main/’04 Breaks, hematite is observed as a dusting over the entire section, and clearly overprints silicate minerals (Figure 11).

There are multiple stages of mineralized veining both in the main veins and within their hangingwall and footwall veins present associated with the fault system. This includes a molybdenite matrix supported breccia, quartz-molybdenite flooding, and quartz-veining and brecciation (Figure 15A-D). The molybdenite matrix supported breccia and quartz-molybdenite flooding are the earlier phases of mineralization, and can be cut and brecciated by later quartz veining (Figure 15C-D). The paragenetic relationship between the molybdenite matrix supported breccia and quartz-molybdenite flooding is not observed within the samples collected.

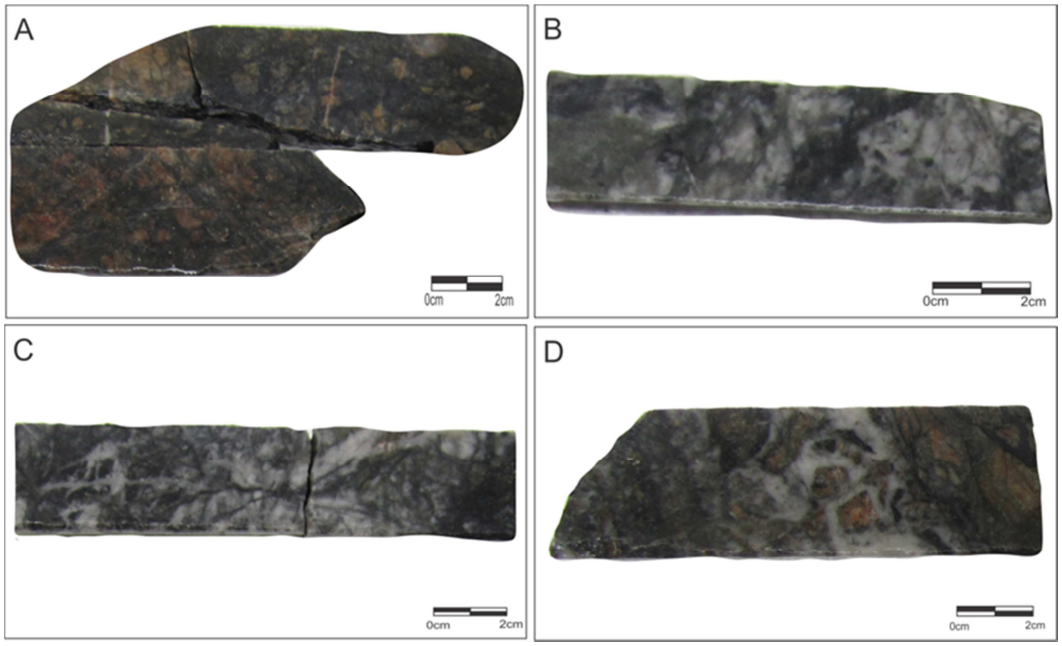

Figure 15 - Hand samples showing mineralization within the NSZ as (A) molybdenite matrix supported breccias from sample LSKGI038, (B) quartz-molybdenite flooding from LSKGI032, (C) quartz veining from LSKGI046, and (D) quartz supported breccias from sample LSKGI050. (A) demonstrates clasts of original host rock which have been altered to hematite and K-feldspar within a very fine grain matrix, which, within thin section is found to contain molybdenite. (B) demonstrates a quartz vein with abundant strands of purple-grey molybdenite with a clast of heavily sericite altered host rock on the left side. (C) demonstrates a quartz vein which has clasts of previous quartz-molybdenite veining. (D) is a quartz vein with clasts of K-feldspar altered host rock, with some clasts of dark purple-grey molybdenite.

In all of these mineralization stages, the mineralogy remains similar. Tellurides and visible gold are typically associated with the quartz ± molybdenite vein systems (Figure 16B) and abundant pyrite is observed within the veins and the proximal alteration. Within thin sections it is observed that gold is associated with very fine grained subhedral

reabsorbed pyrites and fine grained anhedral tellurides within fractures, inclusions and on the rims (Figure 16B). Free anhedral gold is also observed (Figure 16C). Molybdenite is commonly found within micro-fractures with anhedral grains aligned with shear direction or less frequently as inclusions within pyrite grains. XRD (Appendix C) analyses identify tellurides as calaverite ($AuTe_2$), petzite (Ag_3AuTe_2), and altaite (PbTe). A brief Scanning Electron Microscope (SEM) study of Energy Dispersive X-Ray Spectroscopy (EDS) on select individual grains (Appendix F) confirms these tellurides and also demonstrates the presence of some layers of melonite ($NiTe_2$) within some tellurides (Figure 16A).

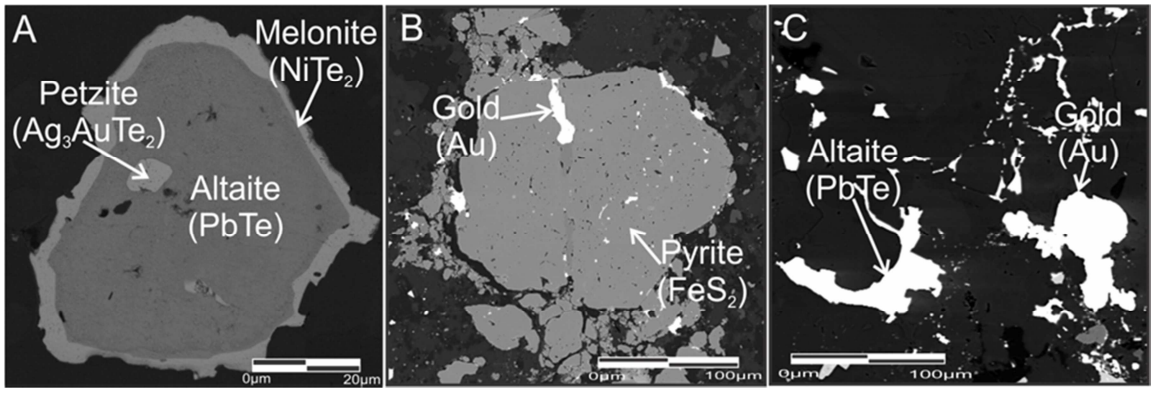

Figure 16 - Gold mineralization in thin section by Scanning Electron Microscope (SEM) back-scatter electron (BSE) images as (A) gold tellurides in LSKGI090 from the NSZ, (B) gold inclusions within pyrite in LSKGI092 from the #7 HW, and (C) free gold within the SMC in LSKGI111 from the NSZ. Mineral identification was done using Energy Dispersive X-Ray Spectroscopy (EDS).

3.3.2.2 Barchetta

The Barchetta zone is hosted within syenite porphyry directly north of the NSZ and is associated with a break striking 060° and dipping 40° SE that hosts both hangingwall and footwall veins. As with the NSZ, Barchetta has strong quartz-molybdenite diffuse veining associated with the fault, as opposed to narrow veining observed within the western and northern areas of the SMC. There is typically less molybdenite found within the Barchetta veining than observed in the NSZ.

Strong disseminated pyrite alteration continues 2m out from the break, as well as K-feldspar, carbonate, and sericite alteration. K-feldspar alteration permeates further (>10m) from the break. Alteration textures are similar to those found within the NSZ:

pyrite alteration is euhedral to subhedral, sericite replaces the fine-grained groundmass, and K-feldspar overprints original textures within the groundmass.

Visible gold and tellurides are associated with the veining, as well as 10-15% very fine grained pyrite, which is typically more abundant than the NSZ. Textures mimic those found within the NSZ (Chapter 3.3.2.1). Tellurides, visible gold, and abundant pyrite are typically associated with the quartz ± molybdenite vein systems. Within thin section it is observed that gold, tellurides are associated with very fine grained euhedral partially reabsorbed pyrites and with each other within fractures, inclusions and on the rims (Figure 16B). Free anhedral gold is also observed (Figure 16C). Molybdenite is commonly found within micro-fractures with anhedral grains aligned with shear direction or less frequently as inclusions within pyrite grains.

3.3.2.3 Lower D

The Lower D is a steeply dipping (70° E), north striking (000) set of strong sericitization and K-feldspar bands 0.2-1m wide that impart a distinctly lighter colour on the hosts rocks and is locally known as bleaching. It is hosted mainly within lapilli tuff. The tuff between the lighter colour bands is typically dark brown to maroon as it is fresh to weakly altered, and contains no mineralization.

The lighter colour bands of alteration contain 7-10% very fine grained to fine grained disseminated pyrite. Thin pinching quartz-moly veinlets within the alteration contain visible gold. Microshears aligned with thin quartz veinlets are observed in thin section that contains minor subhedral molybdenite. Pyrite found within the shearing and veining is subhedral and partially reabsorbed, while pyrite grains within the main alteration are euhedral-subhedral (Figure 17A-B).

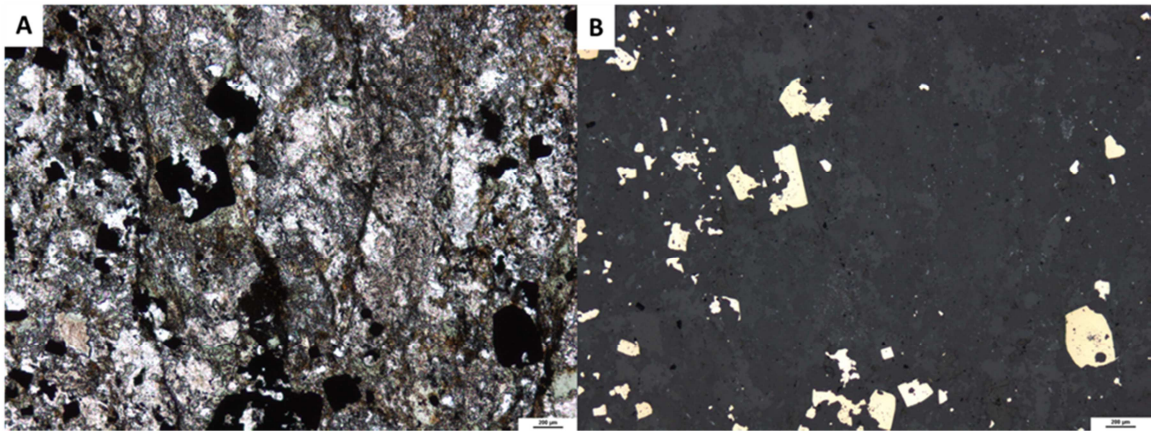

Figure 17 - Photomicrographs of Lower D Mineralization in (A) Cross-Polarized Light and in (B) Reflected Light. Note the euhedral partially corroded texture of the pyrites. Scale bar is 200µm. Tuff is heavily altered by chlorite and carbonate overprinting the sheared groundmass. Cataclastic shears and fractures (angular fragments) all align in one direction with pinching quartz veinlets which are also aligned. Pyrite and associate molybdenite is found within shear fractures with clays and chlorite. Original textures have been completely overprinted by the shearing and alteration.

3.3.2.4 Limelight

The Limelight zone is hosted within syenite porphyry and tuff close to the syenite porphyry contact strikes 070° and dips 22° S and is thought to be a western limb of the NSZ (Carmichael, pers.comm, 2016). Limelight is characterized by a weakly to moderately healed narrow chloritized cataclastic shear zone with narrow hangingwall and footwall quartz veins.

The shear zone is surrounded by proximal moderate K-feldspar alteration with chloritized stringers and slips, and distal (>3m) alteration of host tuff and syenite porphyry to patchy but moderate pyrite, sericite, carbonate and K-feldspar alteration.

Limelight has one main vein in the hangingwall, and the footwall of the break has mineralized stringers. The hangingwall veins have visible gold and weak molybdenite mineralization. The footwall has stringers of quartz with 5-7% disseminated fine grained pyrite (Figure 18A). In thin section, pyrite is euhedral-subhedral and weakly sieved, and has molybdenite as inclusions and rims. This pyrite is found within micro-shear zones and within narrow quartz veinlets paralleling these shears. Gold was not observed within the thin sections collected for this study.

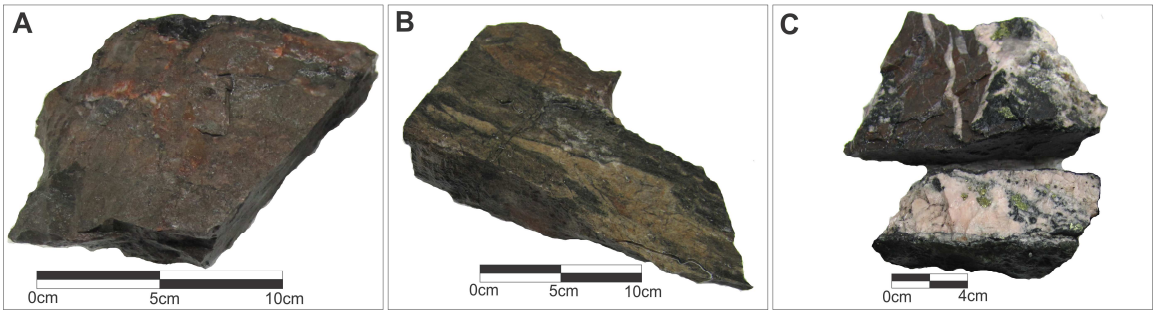

Figure 18 - Hand samples taken from (A) LSKGI126 in Limelight, (B) LSKGI091 in the #7 Break, and (C) LSKGI158 in Lower D North showing typical shearing fabrics and narrow associated quartz veins. This shows examples of the cataclasite with narrow quartz veins in a variety of zones. A) shows very narrow veining and pyrite mineralization, B) shows a good example of some of the shear textures that can be seen proximal to the break, C) shows typical quartz veining.

3.3.2.5 #7 Break

The #7 Break and hangingwall are healed faults (breaks) striking 057° and dipping 45° SE in the north-western area of the SMC (Figure 14). The system is hosted by both tuff and syenite porphyry. There is cataclasite with chlorite within 20cm of the fault. Narrow (<5cm thick) quartz veins running parallel to the fault's slip surfaces occur in most areas (Figure 18B).

These faults have strong alteration comprised of sericite, pyrite, K-feldspar, and carbonate decreasing in intensity within 0.5–1m from the structures. Sericite, pyrite, and K-feldspar alteration textures are the same as elsewhere in Macassa Mine: sericite replaces the fine-grained groundmass, pyrite alteration is euhedral to subhedral, and K-feldspar overprints original textures within the groundmass. Carbonate alteration is predominantly overprinting the groundmass in association with sericite.

Mineralization is generally observed as fine grained disseminated pyrite (7-10%) and tellurides, visible gold, and gold bearing pyrite within the thin quartz veins. Texturally, the pyrite within the stronger sericite-carbonate alteration and shearing are subhedral, partially reabsorbed, and fractured. Gold and molybdenite are associated with the pyrites as inclusions, within fractures, and as rims. Molybdenite is found as anhedral grains within the shear zone with fabric paralleling the shear direction. Tellurides are observed

as blebs associated with the molybdenite in both the shear zones and in proximity to gold and partially reabsorbed pyrites in veinlets.

3.3.2.6 Lower D North

The Lower D North (LDN) is located in the north-east section of the SMC within the syenite porphyry (Figure 14). It is typically characterized by a strong break with chloritic gouge and cataclasite which is surrounded by brittle fractures and chloritic slips perpendicular and parallel to the main structure. The break strikes from 055° to 025° and dips from 30° to 35° SE. A narrow (5-10cm wide) quartz-molybdenite vein is observed to run parallel to the fault.

The structure is surrounded by 0.5–1m of moderate to strong sericite-carbonate-pyrite-k-feldspar alteration. Outside of this area, K-feldspar alteration is only present in weak to moderate patches and surrounding quartz stringers (<5cm) (Figure 18C). Alteration textures are similar to those within other zones: sericite replaces fine-grained groundmass, pyrite alteration is euhedral to subhedral, K-feldspar overprints original textures within the groundmass, and carbonate alteration is overprinting the groundmass in association with sericite.

Mineralization is observed as 5-7% fine grained disseminated pyrite and as visible gold, tellurides, and gold associated with pyrite within the narrow quartz-molybdenite veins. Pyrite within stronger sericite-carbonate alteration and shearing is subhedral, partially reabsorbed, and fractured. Gold and molybdenite are associated with the partially reabsorbed pyrites as inclusions, within fractures, and as rims. Molybdenite is found as anhedral grains within the shear zone with fabric paralleling the shear direction. Tellurides are observed as blebs associated with the molybdenite in both the shear zones and in proximity to gold and reabsorbed pyrites in veinlets. These textures are similar to those of the #7 Break, although quartz veins and veinlets have ~5% more molybdenite, and there are more tellurides found within the veins. There is also a younger quartz-carbonate vein set which contains euhedral-subhedral coarse grained chalcopyrite, very fine grain tellurides, and fine grain partially reabsorbed pyrite with molybdenite within these sieves.

3.3.2.7 ’08 Break

The ’08 Break is thought to be a steepening portion of the Lower D North, and eventually parallels the ‘04 break and extends down to -2133m (Carmichael, pers. comm., 2014). It dips 55° down to 75°, and strikes 057°. Generally the break is found within syenite porphyry between 2 lenses of trachyte. The break associated with the zone is usually parallel to the upper trachyte-porphyry contact.

The host rock is typically altered with a sericite-carbonate-K-feldspar-pyrite assemblage. Mineralization is found as 3-6cm white to dark grey quartz-molybdenite veins paralleling the break. Pyrite, gold, and tellurides are all found within the veining.

3.4 Summary

Work done within the Main/’04 Breaks confirms previous work done the most recently by Kerrich and Watson (1984), Watson (1984), Stills (2001), and Ispolatov et al. (2008). These studies built off of early studies done on the Kirkland Lake mineralization completed by Tyrell and Hore (1926), Todd (1928), Thomson (1950), Thomson et al. (1950), and Charlewood (1964). This semi-brittle reverse fault system has an orientation of 060-080°/60-85°, and mineralization occurs within and directly adjacent to quartz veins associated with early displacement. Some post-mineral faults displace mineralization. Alteration of K-feldspar, carbonate, hematite, sericite, and minor pyrite is within 0.5-1m of the break and quartz veins. Mineralization is observed as gold, tellurides, minor molybdenite, and up to 5% pyrite. The most common tellurides are altaite (PbTe) and calaverite ($AuTe_2$).

The SMC differentiates from the Main/’04 Breaks in a few ways. The SMC is structurally different and dips much more shallowly than the Main/’04 Breaks at 25°-50°. The alteration halo surrounding the breaks in the SMC is much wider than the Main/’04 Breaks as it continues up to 10m on past the break, as opposed to 1m. The alteration mineralogy is also slightly different: the SMC has more sericite and pyrite, and less hematite than the Main/’04 Break. While the mineralogy of the mineralization remains similar, quantities vary between the two zones. The SMC has 5-10% pyrite on average, while the Main/’04 Break has <5%. There are also more gold and tellurides present in the

SMC. Proven and probably resources is 14.7g/t for the Main/'04 Breaks and 17.5g/t for the SMC (Kirkland Lake Gold, 2014).

The different zones in the SMC are the New South Zone (NSZ), Barchetta, the Lower D, Limelight, #7 Break, Lower D North (LDN), and '08 Break. These are compared in Table 2 according to their orientation, mineralization, and alteration. There are two varieties of zones within the SMC: those which have cataclasite with narrow quartz veins, and those which have wide diffuse quartz-molybdenite veining. The Lower D, Limelight, #7 Break, Lower D North, '08 Break are part of the former, and NSZ and Barchetta are part of the latter.

Table 2 – Comparison of the SMC zones: the New South Zone, Barchetta, Lower D, Limelight, #7 Break, Lower D North, and '08 Break. Comparison focuses on orientation of the break, mineralization (styles and mineralogy), and alteration.

	Orientation	Mineralization	Alteration
New South Zone	055°/25°	Wide diffuse veining with molybdenite breccias, quartz-molybdenite veining, and brecciating quartz veining. Tellurides, visible gold, pyrite (8-10%)	Strong up to 3m, weak up to 10m of K-feldspar, pyrite, sericite ± hematite
Barchetta	060°/40°	Wide diffuse veining with quartz-molybdenite veining, and brecciating quartz veining. 10-15% pyrite, tellurides, and visible gold.	Strong pyrite, K-feldspar, carbonate, and sericite 2m from the break. K-feldspar up to 10m from the break.
Lower D	000°/70°	7-10% pyrite. Visible gold within thin pinching quartz-molybdenite veinlets within alteration.	Sericite and K-feldspar in 0.2-1m wide bands.
Limelight	070°/22°	Chloritized cataclasitic with narrow hangingwall and footwall veins. Veins have visible gold, molybdenite in veins/stringers, and 5-7% pyrite.	Strong K-feldspar <3m. Moderate patchy pyrite, sericite, carbonate, and K-feldspar 3-10m
#7 Break	057°/45°	Chloritized cataclasite with parallel narrow quartz veins. Veins have 7-10% pyrite, tellurides, and visible gold. Molybdenite within shear.	Sericite-pyrite-K-feldspar-carbonate decreasing in intensity w/in 0.5-1m from structure
Lower D North	055°/30°-024°/35°	Chloritized cataclasite with parallel quartz-molybdenite vein. Veins have 5-7% pyrite, visible gold, and tellurides.	0.5-1m moderate to strong sericite-carbonate-pyrite-K-feldspar. 1-5m K-feldspar in patches
'08 Break	057°/55°-75°	Narrow quartz-molybdenite veins paralleling cataclasite. Veins contain pyrite, gold, and tellurides.	Sericite-carbonate-K-feldspar-pyrite

Lower D is distinctly different from any other zone in the SMC and within the Main/'04 Breaks. Although it is physically located in proximity to the SMC (Figure 14), it is

different in a variety of ways and it is possible that this zone belongs to a different system. There is no distinct break is observed within some areas, it strikes almost north, compared to the rest of the SMC, which strikes east-south-east, and mineralization is found within thin pinching quartz veinlets as opposed to veins at least 5cm thick. Further study is recommended to better define this zone and its relationship to the SMC and Main/'04 Breaks.

Gold is found within all zones as free gold, as rims, inclusions, and fracture fill within euhedral partially corroded pyrite (Figure 16B), in association with tellurides (Figure 16A), and as gold tellurides. Tellurides are present mostly as altaite (PbTe) and calaverite ($AuTe_2$), but also as sylvanite ($AgAuTe_2$), melonite ($NiTe_2$), and petzite (Ag_3AuTe). These are found as inclusions, rims, and fracture fill on sieved pyrites, as well in association with gold. There can be zonation of different tellurides (Figure 16A), as well as tellurides and gold (Figure 19). The different zones of minerals entail that there are separate stages or pulses of mineralization.

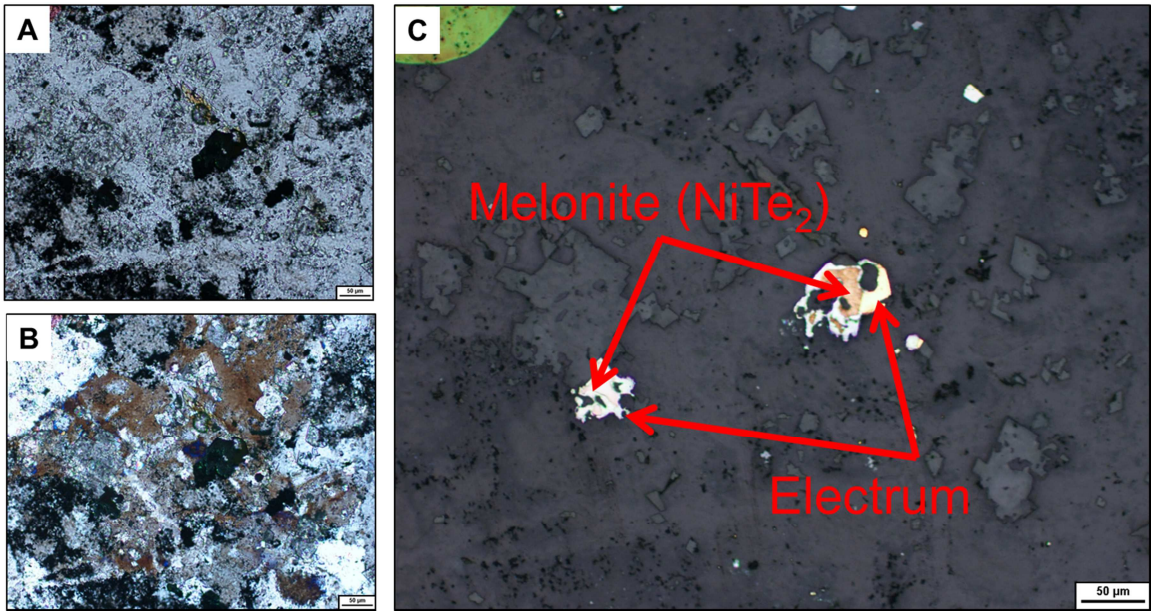

Figure 19 - Series of petrographic images of sample LSKGI105 from the Lower D North footwall in plane polarized light (A), in cross polarized light (B) and reflected light (C) mineralization within quartz-molybdenite veining. Within the vein, free gold is observed, as well as gold encasing earlier melonite ($NiTe_2$). Melonite and electrum were identified using EDS with SEM BSE.

Chapter 4

4 Multi-Element Analysis

Representative samples of zones, mineralization types, alteration styles, and lithology were chosen for multi-element analysis. These samples expand on the samples collected by Horvath (2010), and Kerrich and Watson (1984). Kerrich and Watson (1984) provides a detailed multi-element analysis along strike and at different depths on the Main/'04 Break. Horvath's (2010) study details the geochemistry within four (4) drillholes intersecting and one underground heading in the New South Zone at different locations. The goals of this study are to expand the geochemical database of the SMC, to compare the SMC to the Main/'04 Breaks, to compare different zones within the SMC, and to define alteration geochemistry.

Representative samples were collected as from the New South Zone (NSZ), #7 Break, Barchetta, Lower D North, Limelight, Lower D, Main, and '04 Break, concentrating on the SMC. Samples were pulverized to >90% minus 150 mesh and assayed for a wide selection of elements (see Chapter 2). Results were analyzed using ioGAS-64, an advanced geochemistry exploratory data analysis program.

4.1 Lithology

Fresh samples of augite syenite, syenite porphyry, and tuff from a variety of locations were taken. These samples have no mineralization or alteration. Au, Ag, S, and Sn fall below detection limits for unmineralized samples. These include samples collected in proximity to the NSZ within drillcore, and '04 Break underground headings, as well as supporting samples from the NSZ drillcore collected by Horvath (2010) and Main/'04 Break underground headings from Kerrich and Watson (1984).

The average major and trace element geochemistry of the lithology of the host rock is as in Table 3. For a comprehensive list of results, consult Appendix D. For a description of the different lithologies, refer to Chapter 3. A comparison of the tuff, syenite porphyry, and augite syenite lithological units are found within the Discussion in Section 4.4.1.

Table 3: Major and Trace Elements in Fresh (<10% Altered) Host Rock Lithologies at the Macassa Mine.

Host Rock	Augite Syenite			Syenite Porphyry			Tuff		
	Mean	Min	Max	Mean	Min	Max	Mean	Min	Max
SiO_2 (%)	54.7	48.9	66.2	62.4	46.2	68.2	49.4	42.4	55.9
TiO_2 (%)	1.00	0.44	1.90	0.52	0.31	1.02	0.94	0.41	1.70
Al_2O_3 (%)	15.2	11.9	19.2	14.7	12.1	18.8	14.3	10.6	19.9
Fe_2O_3 (%)	3.6	1.0	9.8	4.1	1.3	9.6	7.6	3.8	11.6
MnO (%)	0.11	0.05	0.17	0.07	0.03	0.15	0.18	0.09	0.27
MgO (%)	3.8	0.8	7.9	2.2	1.2	7.2	3.0	0.8	6.1
CaO (%)	4.7	1.4	11.6	3.2	1.7	9.0	6.5	2.7	10.6
K_2O (%)	5.5	2.6	7.8	4.2	2.4	10.9	7.0	2.6	10.4
Na_2O (%)	3.5	2.3	4.9	4.8	0.1	6.6	2.2	0.4	4.4
P_2O_5 (%)	0.39	0.10	0.60	0.22	0.04	0.60	0.53	0.15	0.99
Nb (ppm)	15	6	28	6	1	16	20	11	32
Zr (ppm)	223	145	320	171	140	440	464	278	784
Y (ppm)	22	18	23	16	10	40	37	24	52
Sr (ppm)	788	430	1622	1966	650	5100	2151	1275	3058
Rb (ppm)	228	190	312	108	50	334	244	69	333
Th (ppm)	16	6	31	8	5	29	53	52	54
Pb (ppm)	22	10	41	24	11	55	52	36	77
Ga (ppm)				20	8	33			
As (ppm)	7	2	12	2	<1	10	16	6	36
Zn (ppm)	93	38	136	57	22	161	113	50	173
Cu (ppm)	55	8	106	39	7	297	26	15	37
Ni (ppm)	53	16	121	35	1	106	35	19	54
Co (ppm)	26	6	53	16	4	54	12	1	49
Cr (ppm)	197	53	380	138	6	279	112	49	176
V (ppm)	203	77	390	98	33	377	391	125	508
Sc (ppm)	12	5	23	14	14	14	35	35	35
Ba (ppm)	1827	732	3480	2412	780	6590	4639	2076	8386
La (ppm)				42	14	158			
Ce (ppm)				84	30	314			
Pr (ppm)				10	4	36			
Nd (ppm)				38	15	128			
Sm (ppm)				7	4	21			
Eu (ppm)				2	1	5			
Gd (ppm)				5	3	14			
Tb (ppm)				1	<1	2			
Dy (ppm)				3	2	7			
Ho (ppm)				1	0	1			
Er (ppm)				2	1	3			
Tm (ppm)				<1	<1	<1			

Host Rock	Augite Syenite			Syenite Porphyry			Tuff		
	Mean	Min	Max	Mean	Min	Max	Mean	Min	Max
Yb (ppm)				2	1	3			
Lu (ppm)				<1	<1	<1			
Hf (ppm)				5	4	10			
Cs (ppm)				4	1	28			
Sb (ppm)	3	2	4	1	<1	5	11	1	34
Sn (ppm)				1	1	2			
Ag (ppm)	0.6	0.5	1	4.17	0.50	33.0	0.5	0.5	0.5
Au (ppm)	0.02	<0.01	0.05	0.03	0.01	0.11	0.05	0.01	0.14
S (wt. %)	0.4	<0.1	2.4	0.8	0.1	2.0	0.3	0.1	1.3

4.2 Alteration Geochemistry

Altered samples from a variety of different zones (Figure 4 and 5, Chapter 2) and their respective alteration styles were taken. These samples have low (<ppm Au) mineralization. Results are shown in Table 4 for major and trace elements of total alteration between 10-25%. The degree of alteration was determined by thin section. For a description of alteration styles in the different zones, refer to appropriate subsections in Chapter 3.These alteration styles include K-feldspar, carbonate, hematite, sericite, and minor pyritic alteration in the Main/'04 Breaks and strong K-feldspar, pyrite, sericite, and some hematite alteration in the SMC.

Compared to all lithologies of fresh rock, there is an increase in K_2O, Fe_2O_3, and CaO and a decrease in Na_2O within the major elements. Other notable differences within the minor and trace elements include an increase in Mo and Light Rare Earth Elements (LREEs) such as La, Ce, Pr, Nd, Sm, Eu, and Gd. The SMC has a higher concentration of SiO_2, Na_2O, SrO, and Mo and lower concentrations of Fe_2O_3, MgO, CaO, Th, As, Zn, Cu, Co, V, and LREE than the Main/'04 Break in its alteration.

Table 4: Major and Trace Elements of 10-25% Altered Rock in Macassa Mine Ore Zones.

Zone	Main/'04			SMC		
	Average	Min	Max	Average	Min	Max
SiO_2 (%)	49.4	43.2	59.6	59.95	40.58	71.60
TiO_2 (%)	0.74	0.44	0.80	0.45	0.23	1.39
Al_2O_3 (%)	13.0	10.2	16.4	13.68	11.70	15.50
Fe_2O_3 (%)	7.8	4.9	9.9	4.42	2.70	13.11

Zone	Main/'04			SMC		
	Average	Min	Max	Average	Min	Max
MnO (%)	0.13	0.10	0.17	0.09	0.01	0.18
MgO (%)	5.1	2.8	6.9	2.14	0.03	5.48
CaO (%)	6.3	4.3	8.2	3.78	1.22	8.88
K_2O (%)	5.3	3.6	7.1	4.94	3.01	12.53
Na2O (%)	2.6	0.3	4.1	4.06	0.26	5.70
P_2O_5 (%)	0.46	0.16	0.60	0.28	0.12	1.21
Cr_2O_3 (%)	0.04	0.04	0.04	0.02	0.01	0.04
BaO (%)	0.10	0.10	0.10	0.27	0.22	0.33
SrO (%)	0.07	0.05	0.09	0.19	0.13	0.29
Mo (ppm)	14	14	14	57	2	312
Nb (ppm)	14	6	26			
Zr (ppm)	174	139	206	142	110	160
Y (ppm)	23	17	30	15	10	20
Sr (ppm)	904	444	1622	1180	750	1690
Rb (ppm)	189	92	312	80	70	100
Th (ppm)	30	15	34	5	4	8
U (ppm)	8	8	8	2	1	3
Pb (ppm)	38	21	94			
Ga (ppm)	16	16	16	17	14	19
As (ppm)	10	4	26	1	1	2
Zn (ppm)	91	55	136	31	17	56
Cu (ppm)	20	10	49	13	8	17
Ni (ppm)	83	38	121	34	22	55
Co (ppm)	55	29	79	9	5	16
Cr (ppm)	259	118	333			
V (ppm)	320	198	406	40	14	51
Mn (ppm)	1408	1408	1408			
Sc (ppm)	19	10	23			
Ba (ppm)	1404	847	2610	1803	1020	2950
La (ppm)	57	57	57	33	28	42
Ce (ppm)	116	116	116	64	51	81
Pr (ppm)	14	14	14	8	6	10
Nd (ppm)	53	53	53	29	22	37
Sm (ppm)	10	10	10	5	4	7
Eu (ppm)	3	3	3	1	1	2
Gd (ppm)	8	8	8	4	3	5
Tb (ppm)	1	1	1	1	<1	1
Dy (ppm)	4	4	4	3	2	3
Ho (ppm)	1	1	1	1	<1	1
Er (ppm)	2	2	2	1	1	2

Zone	Main/'04			SMC		
	Average	Min	Max	Average	Min	Max
Tm (ppm)						
Yb (ppm)	1	1	1	1	1	2
Lu (ppm)						
Hf (ppm)	5	5	5	4	3	5
Ta (ppm)						
Cs (ppm)	2	2	2	1	1	2
Sb (ppm)	8	2	23			
Sn (ppm)	1	1	1			
Ag (ppm)	0.7	0.5	1.4			
Au (ppm)	0.3	<0.1	2.6	1.2	<0.1	5.2
S (wt. %)	0.3	<0.1	1.1			

4.3 Geochemistry of Mineralization

Major and trace element geochemistry of different mineralized zones are reported in Table 5, which represent a variety of different mineralization styles. Barchetta and NSZ have wide diffuse molybdenite-quartz veining with tellurides, visible gold, and abundant pyrite. Lower D has bands of K-feldspar alteration in which there are thin pinching quartz-molybdenite veinlets with visible gold and abundant pyrite. Limelight, #7 Break, Lower D North, and ’08 Break have narrow cataclasite faults with parallel quartz-molybdenite veins with pyrite, visible gold and tellurides. The Main/’04 Break has narrow cataclasite faults with quartz veins with visible gold, tellurides, and minor pyrite. For a full description of mineralized zones, see Chapter 3.

Below is a table of averaged geochemistry results of mineralized samples from different zones with anomalous values highlighted. These results include work done by Kerrich and Watson (1984) and Horvath (2010) in addition to this study. Compared to the samples that exhibit 10-25% alteration, these heavily altered (>25%) and mineralized samples have increased Fe_2O_3, CaO, and K_2O and decreased Na_2O. The Main/’04 Breaks have an increase in SiO_2 compared to moderately altered samples, while the SMC typically has less SiO_2. Other notable differences within the minor and trace elements include an increase in Mo, Nb, Sr, Cu, Ni, Sb, Sn, Ag, Au, S, and Light Rare Earth

Elements (LREEs) such as La, Ce, Pr, Nd, Sm, Eu, Gd, Tb, and Dy in the mineralized samples compared to the altered samples.

In Table 5 below, bold indicates higher values, while italics indicate lower values. Note that there are many anomalous values associated with Limelight and the NSZ. In the NSZ, TiO_2, MnO, BaO, SrO, Nb, Zr, Y, Th, Pb, As, Ni, Co, Cr, Sb, Sn, Ag, and Au are higher while Al_2O_3, Fe_2O_3, CaO, K_2O, Sr, and Rb are lower compared to other zones. In Limelight, K_2O, BaO, Nb, Zr, Sr, Zn, Cu, V, and S are higher concentrations while Na_2O, Rb, Ba, the Light Rare Earth Elements (La, Ce, Pr, Nd, Sm, Eu, Gd, Tb, Dy), and Sb are lower.

Table 5: Major and Trace Elements in Mineralized Zones and Alteration >25% at the Macassa Mine. Bold indicates higher values while italics indicate lower values relative to other zones.

	Main/'04			#7			Barchetta			LDN			Limelight			NSZ		
	Avg	Min	Max	Avg	Min	Max	Avg	Min	Max	Avg	Min	Max	Avg	Min	Max	Avg	Min	Max
SiO_2 (%)	61.5	44.6	91.4	44.5	36.7	63.4	48.4	41.9	54.8	56.0	27.2	88.3	49.5	42.7	56.2	39.7	5.6	83.9
TiO_2 (%)	0.53	0.13	1.20	0.98	0.30	1.19	0.51	0.24	0.78	0.52	0.09	0.94	0.82	0.38	1.25	**2.29**	**0.16**	**10.20**
Al_2O_3 (%)	10.9	3.8	20.0	11.9	11.1	12.9	10.6	10.0	11.3	9.7	3.3	13.6	13.6	12.3	15.0	*6.3*	*<0.1*	*16.4*
Fe_2O_3 (%)	6.1	1.5	11.5	9.6	3.1	12.2	5.3	2.8	7.8	6.6	1.5	12.7	7.3	3.8	10.8	*2.9*	*0.4*	*10.2*
MnO (%)	0.10	0.01	0.17	0.16	0.07	0.20	0.22	0.19	0.24	0.16	0.05	0.34	0.11	0.09	0.12	**1.64**	**0.02**	**8.77**
MgO (%)	3.1	0.2	9.0	4.2	1.4	5.4	4.5	2.5	6.4	3.2	0.7	7.5	3.1	1.5	4.7	3.4	0.4	13.3
CaO (%)	4.8	0.5	8.1	7.8	2.8	9.6	7.5	4.9	10.1	6.4	1.3	12.4	4.6	3.3	5.9	3.0	0.1	8.8
K_2O (%)	4.8	1.2	10.8	6.2	4.6	8.6	7.1	6.7	7.5	5.4	2.7	8.2	9.4	6.9	11.9	3.0	0.1	13.3
Na_2O (%)	1.6	0.1	5.4	1.4	0.8	1.9	0.4	0.1	0.7	1.6	0.2	4.6	0.1	0.1	0.1	1.5	<0.1	7.1
P_2O_5 (%)	0.30	0.01	0.89	1.05	0.20	1.36	0.40	0.32	0.48	0.45	0.05	0.82	0.77	0.24	1.30	0.26	0.06	1.12
Cr_2O_3 (%)	0.03	0.01	0.05	0.03	<0.01	0.09	0.01	0.01	0.01	0.02	0.01	0.04	0.01	<0.01	0.02	0.08	0.01	0.58
BaO (%)	0.27	0.05	0.51	0.38	0.20	0.58	0.73	0.23	1.24	0.27	0.07	0.43	1.03	0.33	1.74	2.61	0.06	7.32
SrO (%)	0.11	0.04	0.16	0.18	0.11	0.24	0.52	0.21	0.82	0.16	0.03	0.22	0.56	0.15	0.98	15.30	0.03	48.32
Mo (ppm)	169	27	356	157	34	281	486	486	486	**812**	**1**	**2699**	75	75	75	489	3	2290
Nb (ppm)	12	<1	69	11	5	16	17	17	17	11	9	13	**22**	**22**	**22**	**16**	**6**	**60**
Zr (ppm)	174	49	492	339	236	442	818	818	818	226	40	380	**897**	**897**	**897**	**677**	**38**	**3365**
Y (ppm)	20	5	57	28	11	45	30	30	30	31	3	48	16	16	16	**67**	**9**	**247**
Sr (ppm)	1023	154	2670	1530	1082	1978	6692	6692	6692	1146	231	1900	**8830**	**8830**	**8830**	*588*	*3*	*3365*
Rb (ppm)	152	27	401	159	142	176	59	59	59	106	59	188	*20*	*20*	*20*	*64*	*2*	*247*
Th (ppm)	19	5	42	14	10	17				9	5	16				**150**	**3**	**1916**

	Main/'04			#7			Barchetta			LDN			Limelight			NSZ		
	Avg	Min	Max	Avg	Min	Max	Avg	Min	Max	Avg	Min	Max	Avg	Min	Max	Avg	Min	Max
Pb (ppm)	65	16	113	10	10	10	27	27	27	99	18	234				155	1	1916
Ga (ppm)	8	4	16	18	14	22	9	9	9	11	4	16	11	11	11	25	2	83
As (ppm)	7	1	19	7	5	10	9	9	9	13	3	26	2	2	2	57	1	298
Zn (ppm)	71	18	135	82	30	135	82	82	82	61	14	124	**131**	**131**	**131**	31	6	83
Cu (ppm)	41	10	219	24	20	28	107	107	107	**1449**	**8**	**5689**	**826**	**826**	**826**	65	6	298
Ni (ppm)	36	12	85	23	17	28	11	11	11	20	13	29	35	35	35	**85**	**6**	**290**
Co (ppm)	26	<1	72	23	6	40	12	12	12	28	4	38	7	7	7	**65**	**6**	**267**
Cr (ppm)	237	63	331	216	121	311	278	278	278	196	90	258	353	353	353	**490**	**143**	**1255**
V (ppm)	358	49	1716	193	64	323	320	320	320	165	29	353	**504**	**504**	**504**	**93**	**4**	**267**
Mn (ppm)	1133	735	1336	1158	521	1795	1857	1857	1857	1336	369	2239	**1215**	**1215**	**1215**	**1556**	**323**	**4625**
Sc (ppm)	16	<1	56	17	7	26	6	6	6	6	3	10	**30**	**30**	**30**	**38**	**4**	**176**
Ba (ppm)	1941	268	5209	2327	2023	2630	12172	12172	12172	1935	598	3648	**17979**	**17979**	**17979**	**1008**	**26**	**4625**
La (ppm)	47	11	97	68	26	110	193	193	193	93	8	142	**32**	**32**	**32**	**33**	**3**	**176**
Ce (ppm)	97	21	201	142	53	230	369	369	369	191	17	294	**68**	**68**	**68**	**78**	**11**	**359**
Pr (ppm)	12	2	24	17	6	28	41	41	41	23	2	36	**8**	**8**	**8**	**11**	**2**	**44**
Nd (ppm)	46	10	96	68	23	113	147	147	147	92	7	147	**32**	**32**	**32**	**26**	**1**	**166**
Sm (ppm)	8	2	18	13	4	21	22	22	22	18	1	28	*6*	*6*	*6*	8	1	31
Eu (ppm)	2	1	4	3	1	5	6	6	6	5	<1	9	*2*	*2*	*2*	**2**	**<1**	**8**
Gd (ppm)	7	2	14	11	4	18	17	17	17	14	1	22	*5*	*5*	*5*	**5**	**1**	**22**
Tb (ppm)	1	<1	1	1	<1	2	2	2	2	2	1	2	<1	<1	<1	1	<1	3
Dy (ppm)	4	1	6	6	2	9	7	7	7	7	1	10	*3*	*3*	*3*	**3**	**1**	**13**
Ho (ppm)	1	<1	1	1	<1	2	1	1	1	1	<1	2	1	1	1	<1	<1	2
Er (ppm)	2	1	3	3	1	4	3	3	3	3	<1	5	2	2	2	2	1	5

	Main/'04			#7			Barchetta			LDN			Limelight			NSZ		
	Avg	Min	Max	Avg	Min	Max	Avg	Min	Max	Avg	Min	Max	Avg	Min	Max	Avg	Min	Max
Yb (ppm)	1	<1	2	2	1	3	2	2	2	2	<1	3	1	1	1	3	1	12
Hf (ppm)	4	1	7	6	3	8	11	11	11	6	1	8	*4*	*4*	*4*	**4**	**1**	**12**
Cs (ppm)	5	<1	12	2	1	4	2	2	2	3	<1	6	*3*	*3*	*3*	**2**	**1**	**8**
Sb (ppm)	4	1	9	6	2	10	5	5	5	4	1	11	*1*	*1*	*1*	**9**	**<1**	**116**
Sn (ppm)	1	1	2	1	1	2	2	2	2	2	<1	3	1	1	1	101	<1	1547
Ag (ppm)	5.4	0.5	15.2	14.2	5.4	23.0	8.0	8.0	8.0	9.2	4.7	15.3	6.3	6.3	6.3	12.1	0.6	115.9
Au (ppm)	14.5	<0.1	86.4	152.0	9.2	645.9	54.5	11.3	97.8	54.3	4.4	148.9	3.5	2.1	4.8	182.6	0.3	1547.1
S (wt. %)	2.5	0.1	9.3	1.2	1.0	1.3	5.5	5.5	5.5	3.5	0.7	7.1	**4.4**	**4.4**	**4.4**	2.1	0.3	3.7

4.4 Discussion

4.4.1 Lithological Influences

Some of the trace and major element geochemistry of the mineralization is dependent on the lithology of the host rock. Kerrich and Watson (1984) found several trends within the local unaltered lithologies. Overall, they found that the different members of the alkalic igneous suite in the Kirkland Lake Camp might have a common parentage which has undergone several processes to form the compositional differences found within the different lithologies.

First, tuff tends to be higher in incompatible elements, including Ti, P, U, Th, Rb, Sr, Y, Zr, Nb, and Ba, compared to the augite syenite, and the syenitic porphyries. This is also observed within the Rare Earth Elements (REEs) of Kerrich and Watson's samples. These large ion lithophiles (LILs) are common elements in the volcanic rocks of plutonic-extrusive complexes due to the preferential distribution of LILs and volatiles in extrusive phases (Taylor et al., 1979). Within the confines of this study, several of these features are observed within the mineralization. As shown in Figure 20A-F, tuff shows an abundance of TiO_2, P_2O_5, U, Sr, Zr, and Ba compared to the concentrations measured within augite syenite or syenite porphyry. However, Y is present in high concentrations in both tuff and augite syenite, and augite syenite typically has greater amounts of Th, Rb, and Nb (Figure 20G-J). The chondrite normalized plot confirms the influence of lithology on mineralization in terms of REEs (Figure 22). Tuff has more REEs than the augite syenite and most syenitic porphyries, even within mineralization.

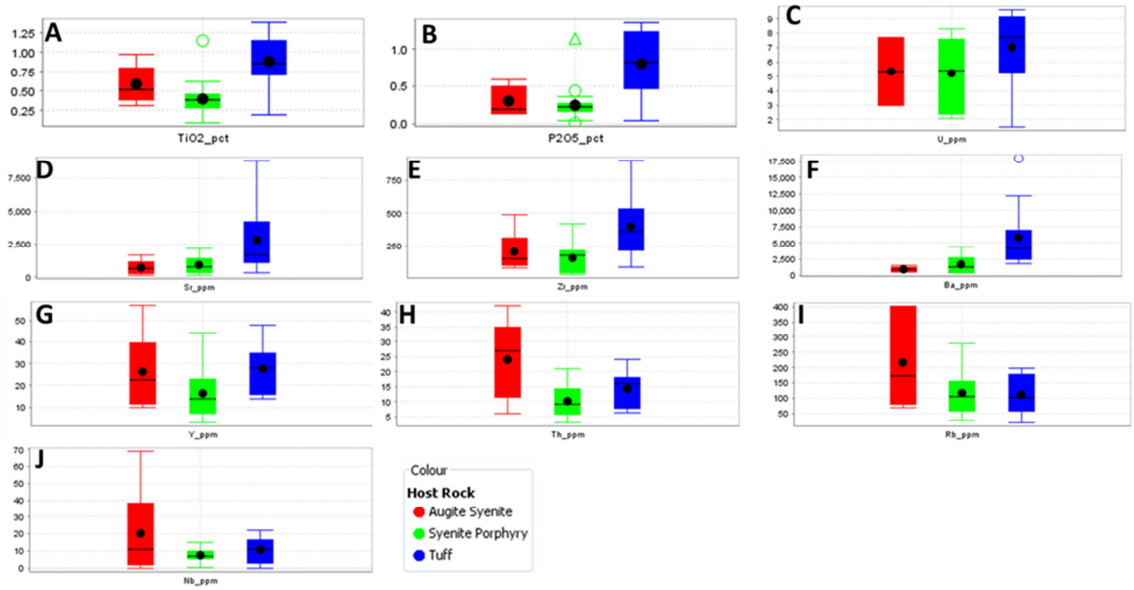

Figure 20 – Select box plots of elements showing variability as a result of different lithologies where (A) TiO_2 (wt %), (B) P_2O_5 (wt %), (C) U (ppm), (D) Sr (ppm), (E) Zr (ppm), (F) Ba (ppm), (G) Y (ppm), (H) Th (ppm), (I) Rb (ppm), and (J) Nb (ppm) for Augite Syenite (Red) , Syenite Porphyry (Green), and Tuff (Blue). For all elements analyzed, these are the only analyses in which results show lithological variability.

The main distinction between augite syenite and syenite porphyry is seen within the total alkali to silica plot (Figure 21). Syenite porphyry tends to have higher silica content than augite syenite and tuff. Beyond what is listed above, there is no significant distinction in the range of trace and major element geochemistry between augite syenite and syenite porphyry. The only distinction is that syenite porphyry shows a smaller range than augite syenite in TiO_2, Fe_2O_3, CaO, P_2O_5, and Cr_2O_3 concentrations.

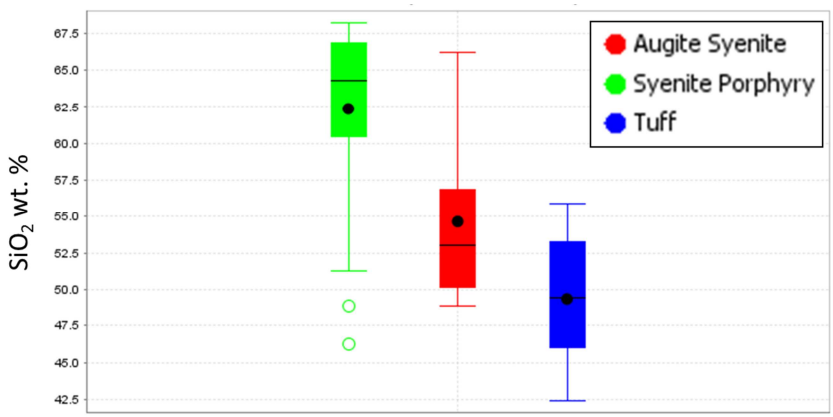

Figure 21 – Box plot showing the total SiO_2 wt.% between tuff (blue), augite syenite (red), and syenite porphyry (green) in fresh samples with minimal alteration and veining. Syenite porphyry tends to be higher in silica content than augite syenite and tuff. Tuff and augite syenite have a range which does overlap, however, tuff generally has lower silica content.

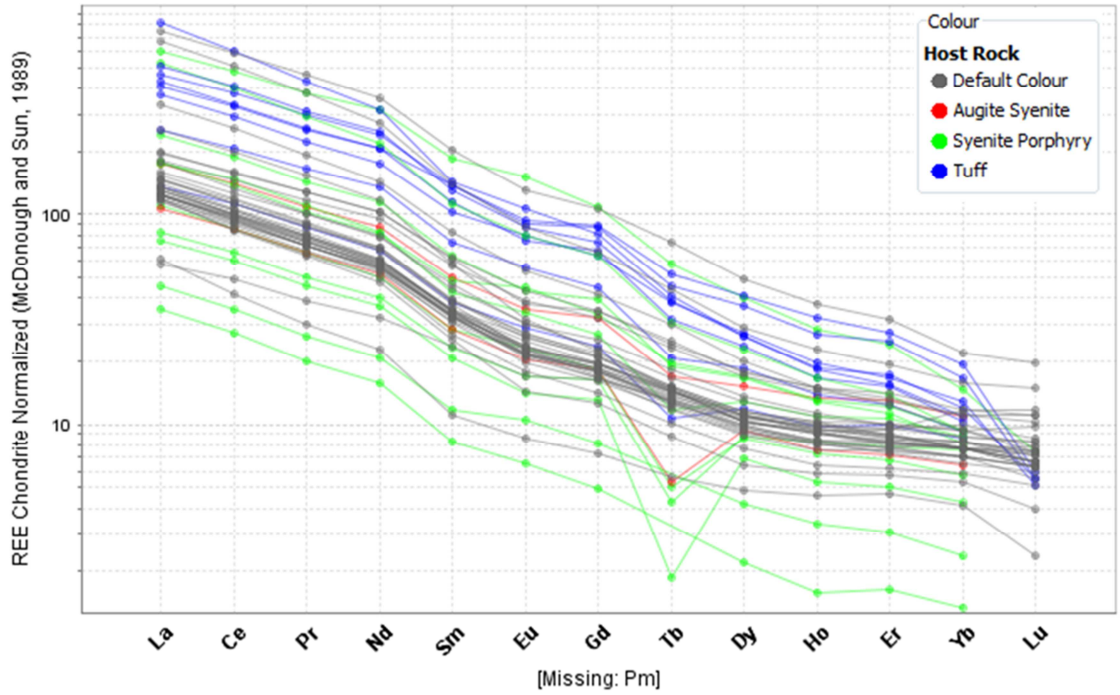

Figure 22 - Chondrite Normalized REE of Augite Syenite (Red), Syenite Porphyry (Green), Tuff (Blue), and Unknown due to strength of alteration and/or mineralization (Grey). More variation is seen in the lithologies than from the mineralization or alteration. However, variation within a lithology is usually seen as an elemental increase with alteration. Variation in the LREE is greater than in the HREE, usually in samples with greater alteration.

4.4.2 Alteration Geochemistry

Alteration has resulted in an increase in K_2O, Fe_2O_3, and CaO and a decrease in Na_2O compared to fresh rock observed between Tables 3 and 4. These are representative of local alteration assemblies which include the addition of sericite, potassium feldspar, hematite, and carbonate. This is known within the mine as bleaching (K-feldspar, sericite, and carbonate), sericitization (sericite), and hematitization (hematite). The decrease in Na_2O represents the replacement of the plagioclase feldspars with these alteration minerals. Other notable differences within the minor and trace elements (Tables 3 and 4) include an increase in Mo and Light Rare Earth Elements (LREEs) concentrations. The LREE are mobile elements, and are early geochemical indicators of an encroaching fluid (Kerrich et Fryer, 1978). The SMC has a higher concentration of SiO_2, Na_2O, SrO, and Mo and lower concentrations of Fe_2O_3, MgO, CaO, Th, As, Zn, Cu, Co, V, and LREE than the Main/'04 Break in its alteration.

In thin section, sericite is seen as a common alteration mineral (Figure 11, and Appendix B). Chemically, sericite has high amounts of potassium and aluminum. Alkali feldspars are also seen as alteration minerals in the groundmass, which also contain appreciable potassium. In Kerrich and Watson (1984), K_2O was determined as a mass gain in the altered samples, and was attributed to the hydrolysis of albite to muscovite with the addition of hydrothermal fluids. For these reasons, variation in K_2O content is interpreted to represent the degree of alteration within a sample.

Within the alteration, represented by an increase in K_2O, there are several trends correlating other elements. The multi-element geochemistry shows the three distinct ore zones previously described in Chapter 3 as the Main/'04 Break, and wide diffuse quartz-molybdenite veining, and cataclasite with narrow veins within the SMC. These are referred to as the Main and '04 Breaks, wide flooding SMC zones, and narrow cataclasite SMC zones respectively. The New South Zone and Barchetta have wide flooding, while Limelight, the #7 Break, and Lower D North display cataclasite with narrow veins. The most notable and pronounced trend is that Na_2O decreases (Figure 23A) as K_2O increases in all types of zones due to plagioclase alteration to sericite and to K-feldspar in the groundmass (Figure 11).

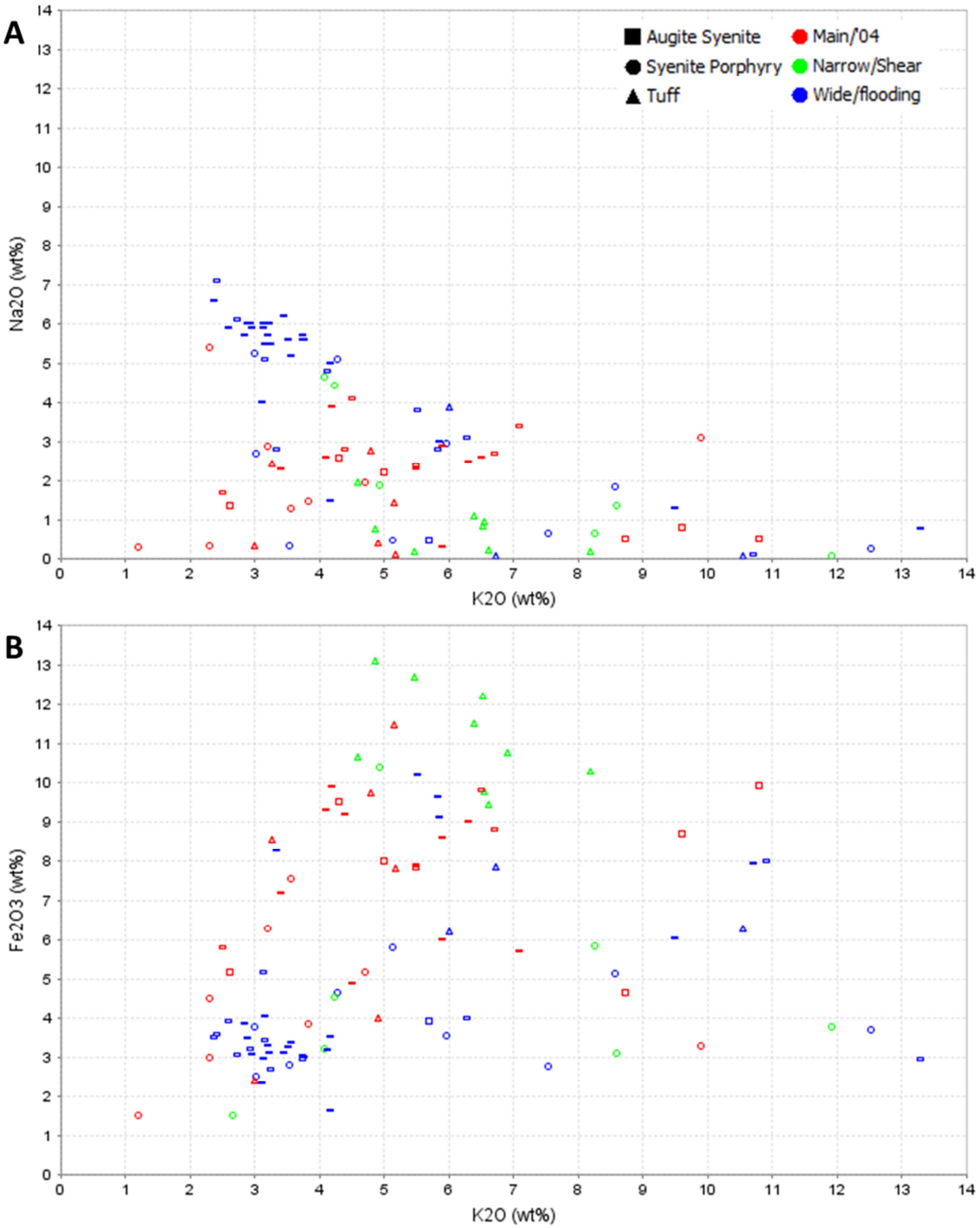
A
Augite Syenite
Syenite Porphyry
Tuff
Main/'04
Narrow/Shear
Wide/flooding
Na2O (wt%)
K2O (wt%)
B
Fe2O3 (wt%)
K2O (wt%)

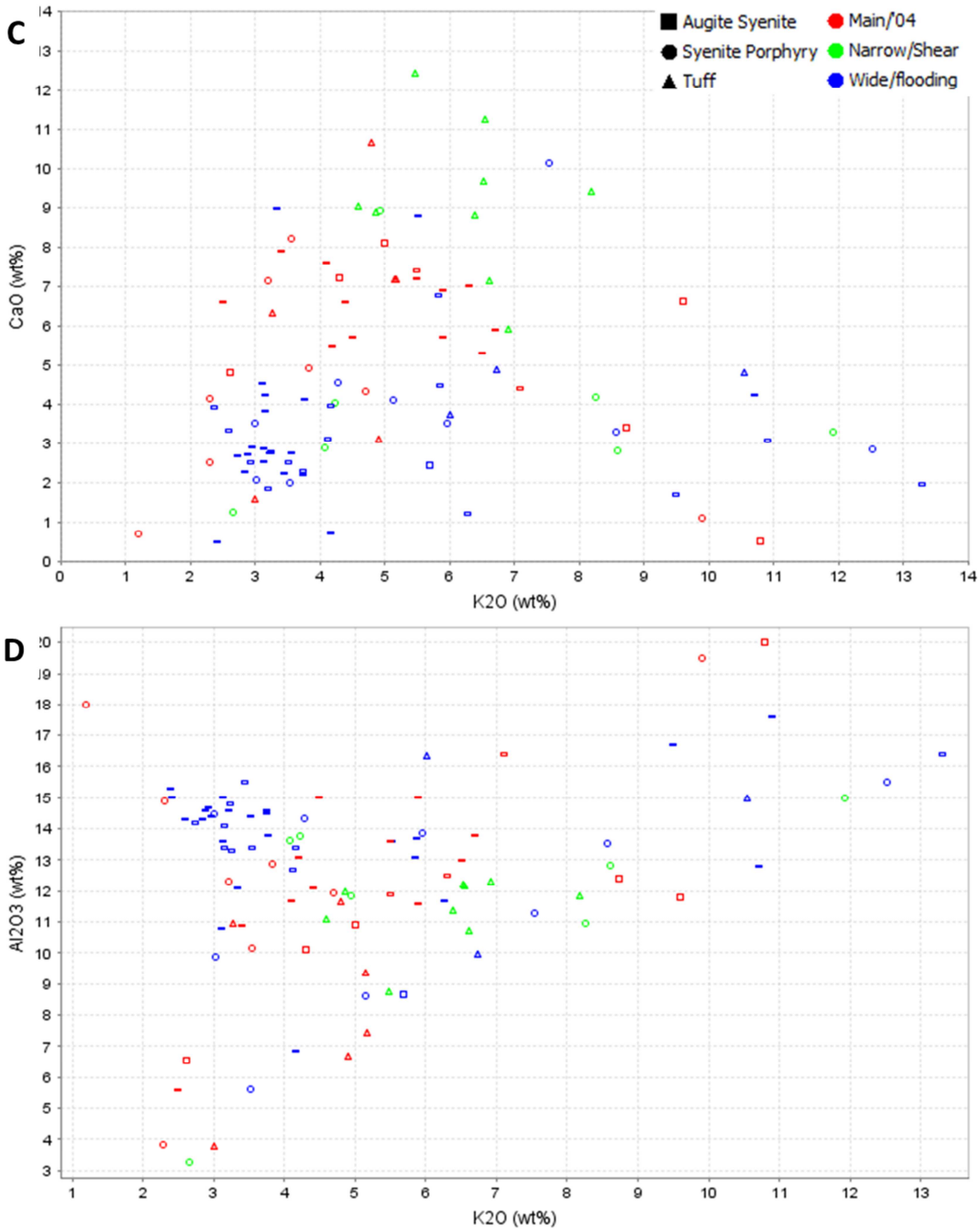

Figure 23 - Relationship between K_2O representing alteration, and (A) Na_2O, (B) Fe_2O_3, (C) CaO, and (D) Al_2O_3 found within samples of varying degrees of alteration within the Main/'04 Breaks (red), the Narrow Shear SMC Zones (green), and the Wide Flooding SMC Zones (Blue). Syenite porphyry (circles) and augite syenite (squares) typically have less Na_2O than tuff (triangles) and there is an inverse correlation between Na_2O and K_2O within lithological parameters. Fe_2O_3 shows a general increase with K_2O. CaO has a low CaO to K_2O ratio in Wide-Flooding SMC zones followed by the Main/'04 Break, and finally high CaO and K_2O in the Narrow Shear SMC Zones. Al_2O_3 shows an increasing trend of Al_2O_3 with K_2O with lithological factors having a greater influence than specific zones.

Alteration increases proportionally within each lithology as Al_2O_3, and decreases proportionally as Na_2O (Figure 23 A, D). Within the Main and '04 Breaks, the following trends (Figures 23A-D) beyond an increase in K_2O and a decrease in Na_2O are observed: Fe_2O_3, CaO, and Al_2O_3 concentrations increase compared to fresh rock. The narrow shear zones of the SMC show an increase in concentration of Al_2O_3, CaO and Fe_2O_3. The wide flooding zones of the SMC are observed to have a drastic decrease in Na_2O, and an increase in Fe_2O_3, Al_2O_3, MgO and CaO.

Alteration minerals observed in Chapter 3 can be related to the geochemistry shown above in Figure 23. The replacement of plagioclase by potassium feldspar is represented by the loss of Na_2O and the addition of K_2O. Sericite is represented by the addition of K_2O, and Al_2O_3 while replacing plagioclase; hematite is observed within the addition of Fe_2O_3; finally, the addition of carbonates should have been observed with the addition of CaO, however, no relationship was seen within these results. The Main/'04 Breaks have K-feldspar, hematite, and sericite alteration, the Narrow Shear SMC Zones have K-feldspar and sericite alteration and the Wide Flooding SMC Zones have strong K-feldspar, hematite, and sericite alteration.

4.4.3 Mineralization Geochemistry

Many of the elements measured in Chapter 4.3 which are higher or lower concentration in the mineralized samples are elements that are known to be mobile (such as large ion lithophiles like K, Rb, Cs, Ba, Pb, Sr, and Eu), and shows differing fluid geochemistry between the zones. Fluid composition varies from wallrock alteration in mobile elements such as Cs, Pb, and Eu (Figure 24A-C). Therefore, the fluid is known to vary beyond the wallrock alteration within some geochemical analyses. The varying geochemistry could suggest remobilization of mineralization within some of the zones (lack of mobile elements), varying distance from the source, or varying host rock.

Figure 24 shows variation as Cs, Pb, and Eu as box plots. A box plot divides the data into four equal parts by using the median and the 25^{th} and 75^{th} percentiles. Within the box plots displayed below, the boxes contain 50% of the data, the median is shown by a line, and the mode by a black circle. In this plot, a fence is the box extended 1.5x the length of

the both towards the minimum and maximum. The fence is shown as ‘whiskers’ protruding from the box. Samples are shown as open circles, and far outliers are shown as open triangles.

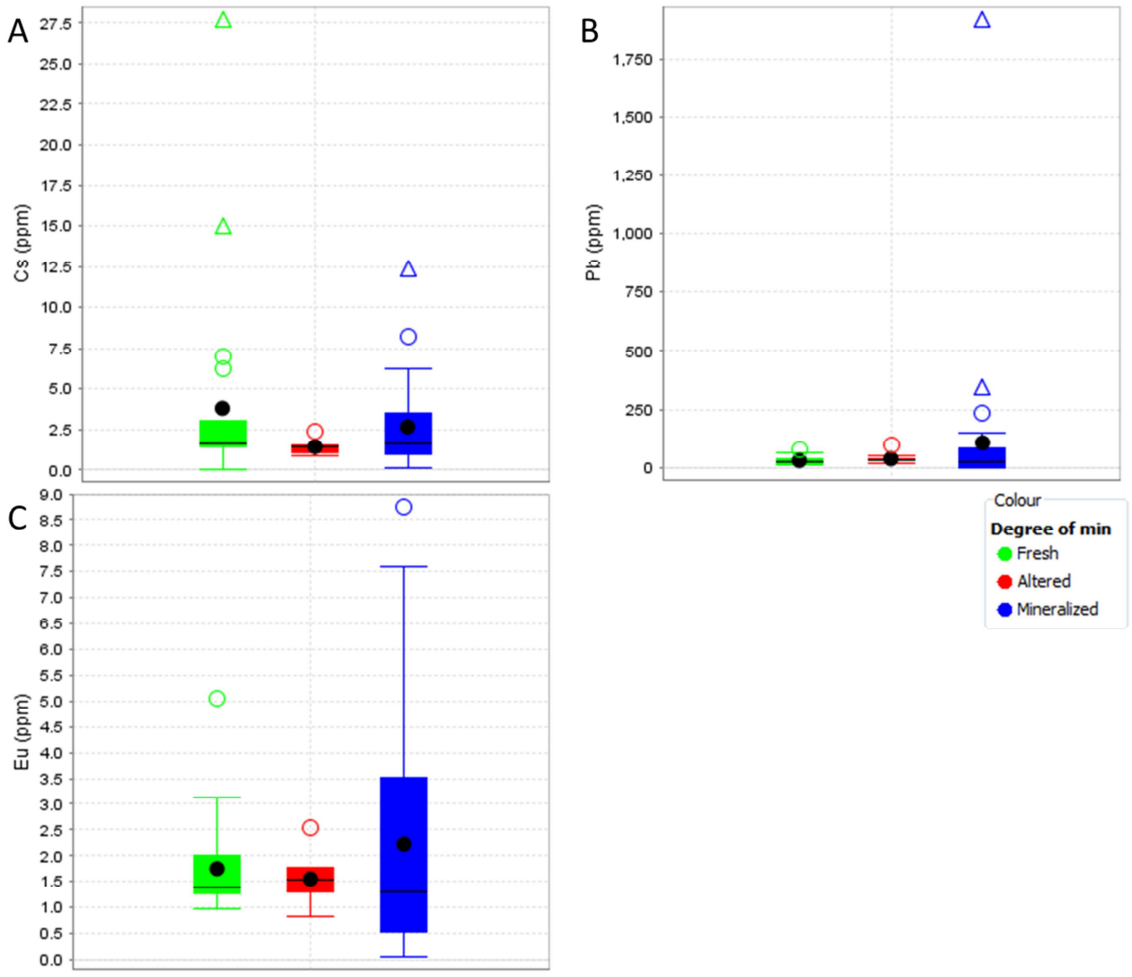

Figure 24 - Box plots showing variation of mobile elements (A) Cs (ppm), (B) Pb (ppm), and Eu (ppm) for all fresh, altered and mineralized samples. There is a significant difference in the concentrations of Cs, Pb, and Eu between the altered and mineralized samples, showing that fluids have different composition than the wallrock alteration.

The geochemistry also shows variability of the alteration fluids within different zones with the higher or lower values of Fe_2O_3, CaO, K_2O, and Na_2O. These alteration elements do not directly correlate with gold mineralization. In mass balance calculations done by Kerrich and Watson (1984), the replacement of albite by sericite is represented by the loss of Na_2O and the addition of K_2O, and Al_2O_3; hematite is observed within the

addition of Fe_2O_3; finally, the addition of carbonates is observed with the addition of CaO. These four major elements define the style of alteration. This is observed in thin section within this project. Higher Fe_2O_3 concentrations have more hematite staining in thin section, higher Al_2O_3 values generally have more sericite replacement, and lower Na_2O values have more plagioclase alteration to sericite and carbonates. Also, there is no correlation seen between S and Fe_2O_3 (Figure 25)

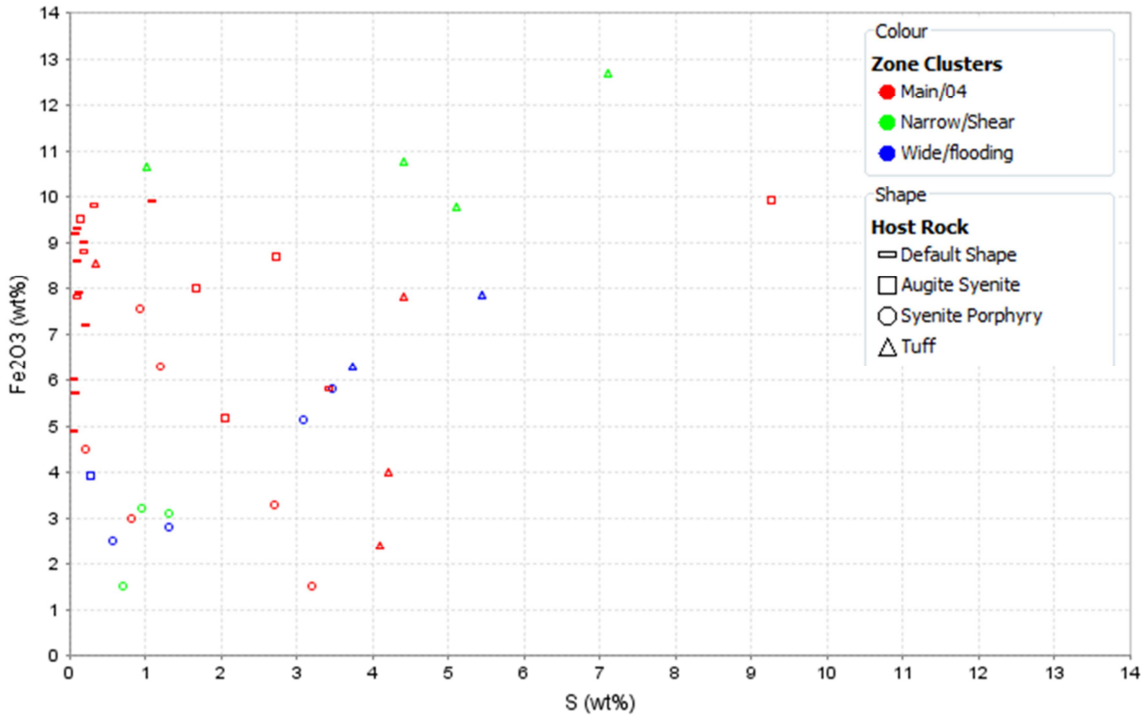

Figure 25 – Fe_2O_3 (wt%) shown plot against S (wt. %) demonstrating a lack of correlation between the two in the Main/'04 Breaks (red), the SMC Narrow Shear Zones (green), and the SMC Wide Flooding Zones (blue). There is also no correlation between the two in lithologies, beyond tuff (triangles) having greater S, which is seen as more primary euhedral pyrite in thin section. Fe_2O_3 values are assumed to be more influenced by hematite alteration than the precipitation of pyrite.

Figure 26 shows a box plot of the concentrations of Au found within mineralized and heavily altered samples. The SMC can have much higher Au concentrations than the Main/'04 Break. Although the differences between the narrow shear SMC zones and the wide flooding SMC zones are more subtle, there is generally a higher gold concentration within the wide flooding SMC zones.

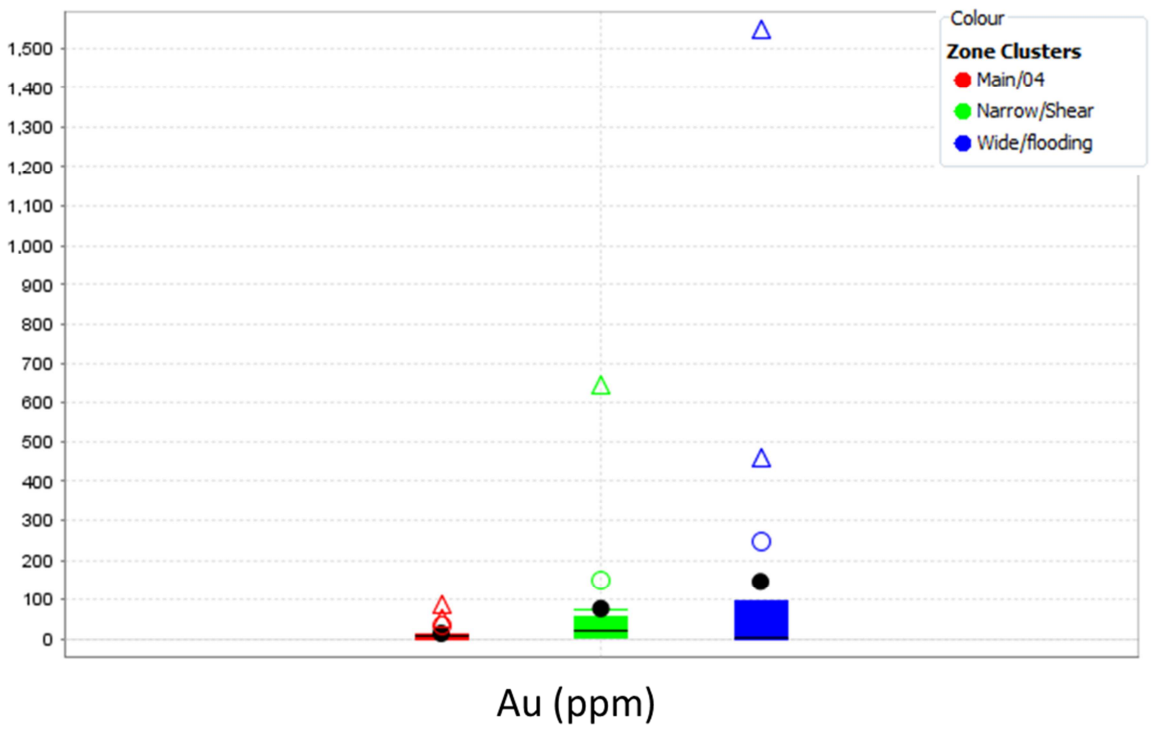

Figure 26 - Box Plot showing the relative abundance of Au within mineralized and heavily (>25%) altered samples. Median is horizontal black line, mode is black circle, outliers are open circles, and far outliers are open triangles.

The wide flooding SMC zones have an abundance of Mo and Pb compared to the Main/'04 Break and the narrow shear SMC zones, and a higher SiO_2 abundance compared to the narrow shear SMC zones (Figure 27). This suggests that the wide flooding SMC zones do have more molybdenite and quartz veining than their counterparts, and most likely have more lead tellurides (altaite). Molybdenum in the form of molybdenite, has been added to a system in mass balance because it is not present as a replacement mineral in thin section, and is only seen in veins and in shear structures (Figure 28).

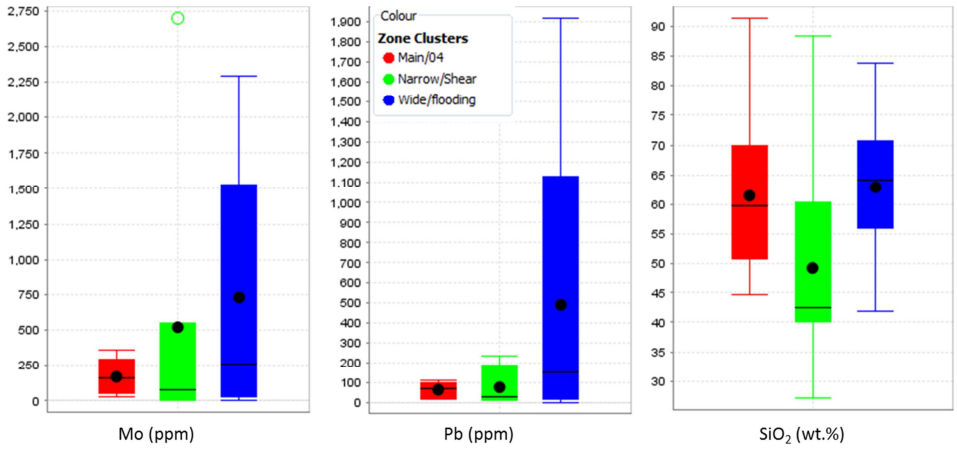

Figure 27 - Box Plots showing the relative abundances between the wide flooding SMC zones (blue), the Main/'04 Break (red), and the narrow shear SMC zones (green) of Mo, Pb, and SiO_2 within mineralized and heavily (>25%) altered samples. Median is horizontal black line, mode is black circle, outliers are open circles, and far outliers are open triangles.

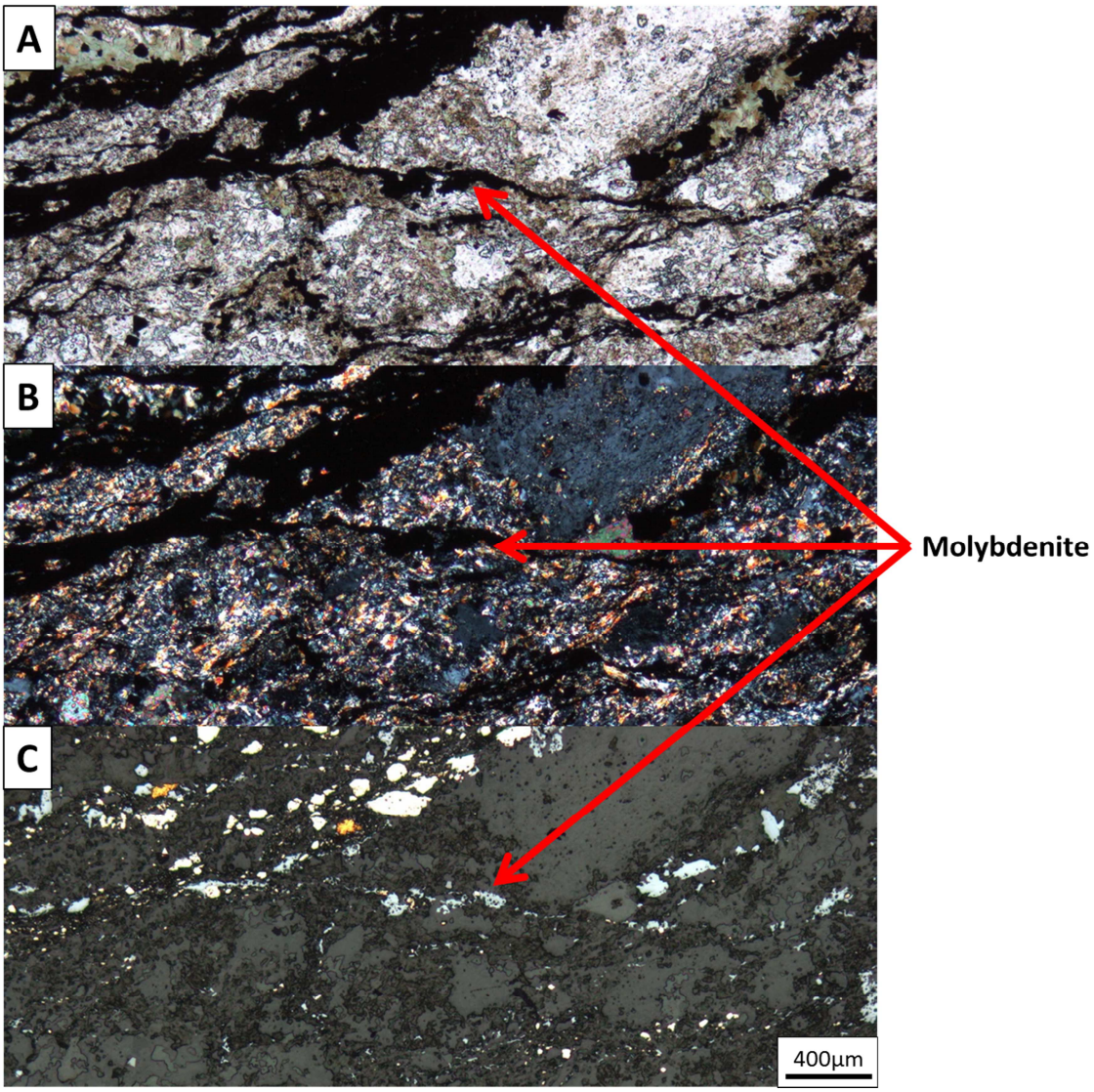

Figure 28 – Photomicrographs of LSKGI091 from the #7 Break showing opaque pyrite, gold, and molybdenite mineralization in shear zone cutting original syenite porphyry host rock, not replacing original mineralogy in (A) plane polarized light, (B) cross polarized light, and (C) reflected light optical microscopy. Scale bar is 400µm. Molybdenite is the grey-blue mineral in reflected light (C) and is black (opaque mineral) in plane (A) and polarized (B) transmitted light as shown by the red arrows.

Within the narrow shear zones, there is more Cu, CaO, Fe_2O_3, and MgO (Figure 29). The CaO, MgO, and Fe_2O_3 denote more carbonate, chlorite, and hematite alteration, respectively (Figure 11). The higher presence of carbonate and chlorite alteration here could mean that there is more reactivation of these shear zones than the wide flooding SMC zones, as the carbonate and chlorite alteration most likely represents later cooler fluids passing through. This would mean that the Main/'04 Breaks also may have had a

more abundant passage of late cool fluids than the wide flooding SMC zones. The higher concentration of Cu denotes the presence of chalcopyrite, which is also observed within optical microscopy and hand sample.

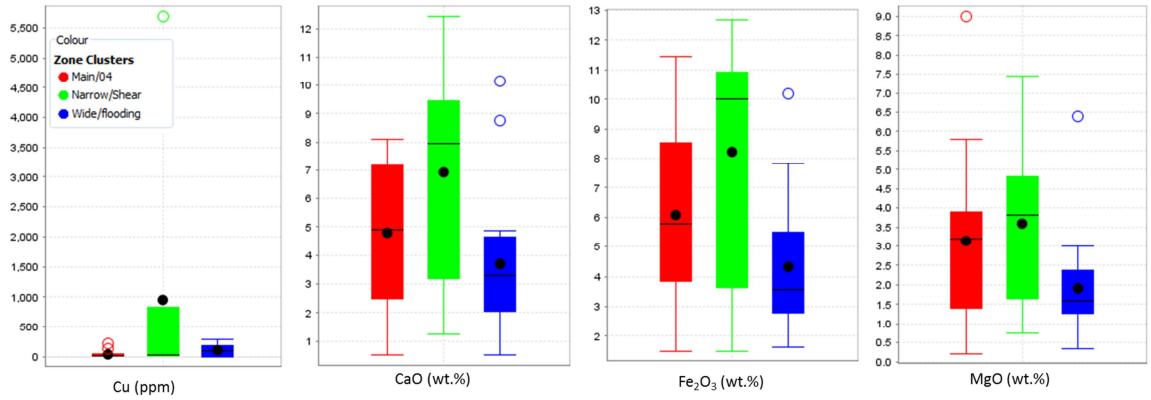

Figure 29 - Box Plots showing the relative abundances between the narrow shear SMC zones (green) and the Main/'04 Break (red), and the wide flooding SMC zones (blue). Cu, CaO, Fe_2O_3, and MgO within mineralized and heavily (>25%) altered samples are considered. Median is horizontal black line, mode is black circle, outliers are open circles, and far outliers are open triangles.

The Main/'04 Breaks have an abundance of Cs and Th compared to the SMC, as well as a depletion of Ga (Figure 30). These are large ion lithophile elements (LILE), which are incompatible elements. Most Archean lode gold deposits have wallrock alteration haloes enriched in LILEs, along with K, CO_2, and sometimes Na and Ca (Groves, 1993). Incompatible elements have difficulty in entering cation sites of minerals, and therefore usually stay longer in the fluid phase. The presence of the LILE as incompatible elements suggests that the alteration fluid is towards the end of the fluid evolution, and more so in the zones in which they have a higher concentration, such as the Main/'04 Breaks.

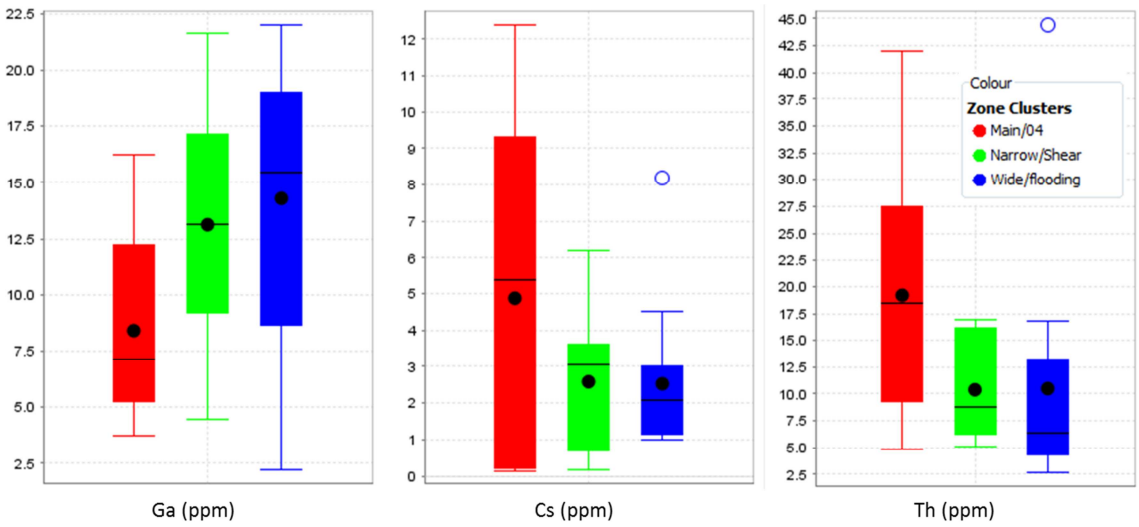

Figure 30 - Box Plots showing the relative abundances between the Main/'04 Break (red), the narrow shear SMC zones (green), and the wide flooding SMC zones (blue) of Ga, Cs, and Th within mineralized and heavily (>25%) altered samples. Median is horizontal black line, mode is black circle, outliers are open circles, and far outliers are open triangles.

Within all zones, there is a positive correlation between Au (representing mineralization) and Pb, and Ag but not Cu (Figure 31A-C). This indicates the presence and correlation of the telluride altaite (PbTe) with gold. It also suggests the presence of electrum, and various gold-silver tellurides (petzite and calaverite). These minerals are in higher abundance when their respective elemental values are higher and can be seen in petrography, XRD, and in EDS SEM. Gold is not necessarily association with chalcopyrite, which is seen in samples with higher Cu values. There are no geochemical signatures that can demonstrate the relative abundances of each tellurides between the SMC and the Main/'04 Breaks.

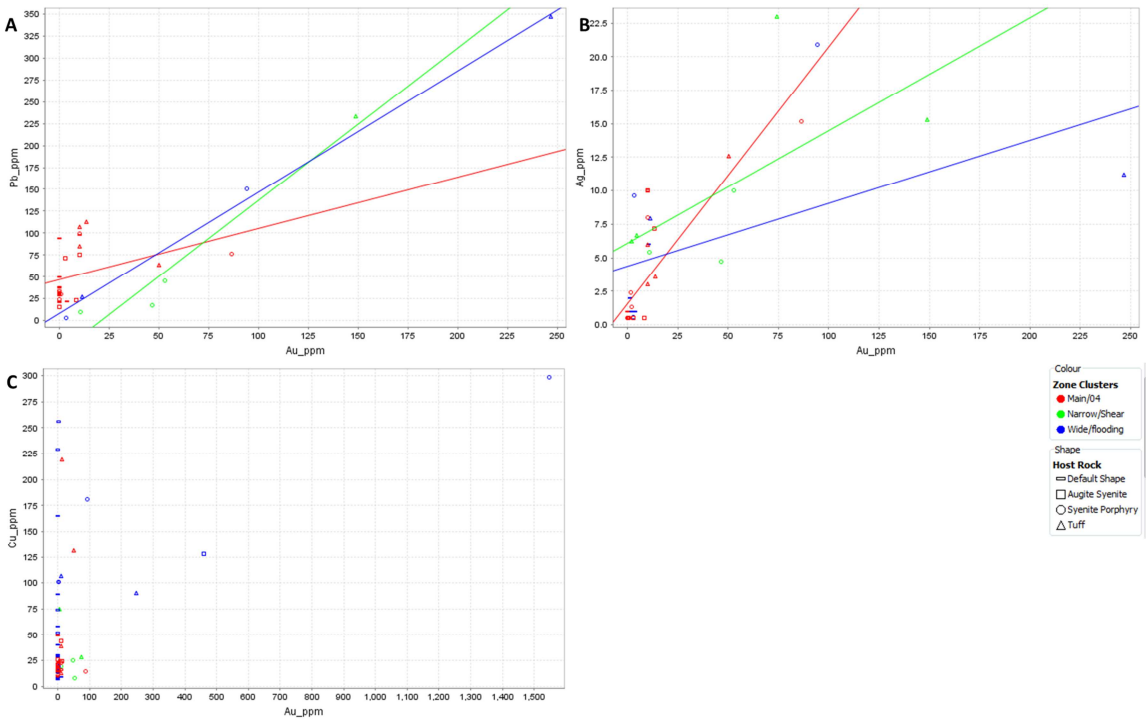

Figure 31 - Correlation between Au Mineralization and (A) Pb, (B) Ag, and (C) Cu in the Main/'04 Breaks (red), SMC Narrow Shear Zones (green), and SMC Wide Flooding Zones (blue) for all samples. No variation was seen due to lithology. One sample (LSKGI154) was excluded in (A) and (B) due to a gold value of 1547ppm, and two samples (LSKGI158 and LSKGI126) were excluded in (C) due to copper values of 5689ppm and 826ppm respectively. (A) has r^2 values of 0.6798 in the Main/'04 Break, 0.4279 in the Narrow Shear SMC and 0.3183 in the wide SMC which demonstrates a weak correlation of Pb with Au. (B) Has r^2 values of 0.1236 for the Main'04 Breaks, 0.9495 for the Narrow Shear SMC, and 0.9966 for the Wide SMC showing a general strong correlation between Au and Ag. Cu and Au show a very weak positive correlation in the Wide Flooding SMC, but are otherwise not related. R^2 and linear regression was calculated using ioGas.

The Main/'04 Breaks and the Narrow SMC Shear Zones show a moderate positive correlation of Au with Mo and As (Figure 32A-B). There is also a presence of Mo within the Wide Flooding SMC Zones, but it is not directly correlated to the strength of mineralization as the R^2 value is too low to be confident in this.

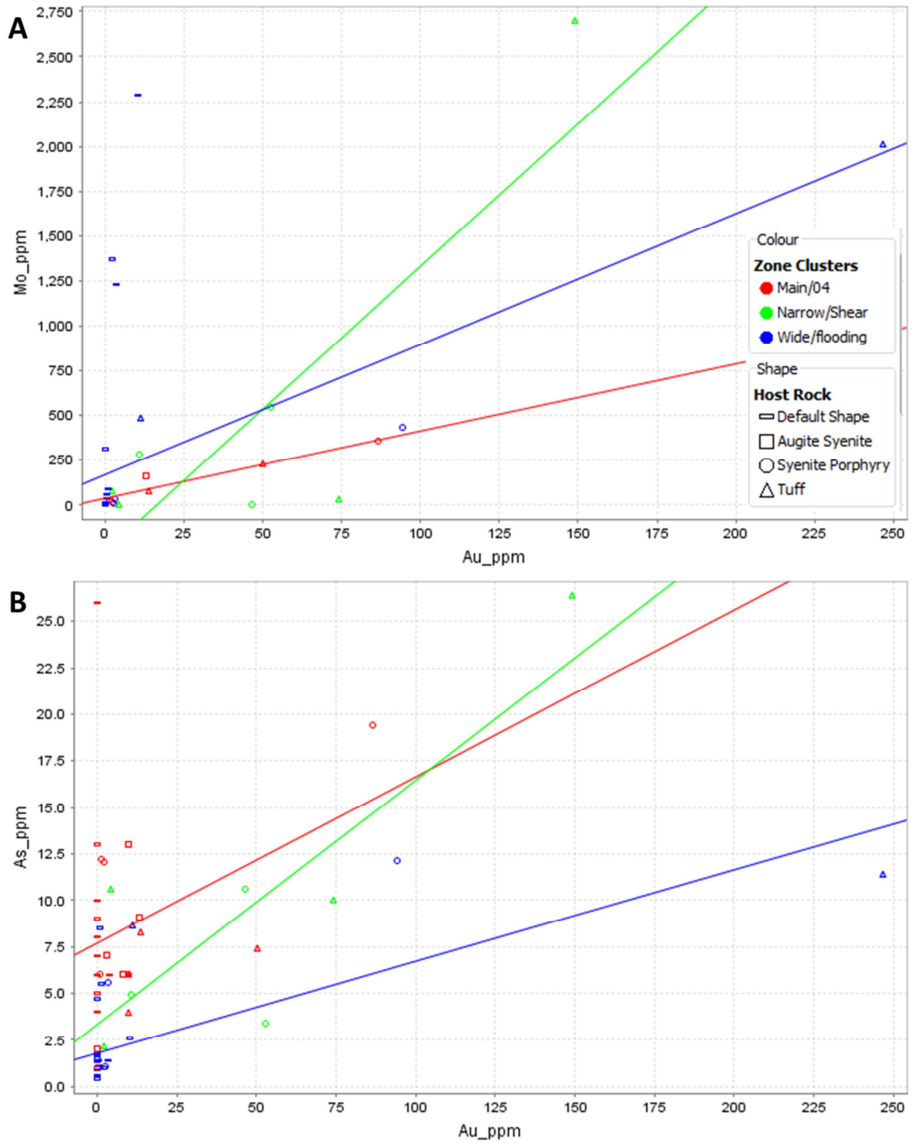

Figure 32 - Correlation between Au mineralization with (A) Mo and (B) As in the Main/'04 Breaks (red), SMC Narrow Shear Zones (green), and SMC Wide Flooding Zones (blue) for all samples. No variation was seen due to lithology. Two samples (LSKGI050 and LSKGI154) were excluded in (A) and (B) due to gold values of 461ppm and 1547ppm respectively. (A) has r^2 values of 0.921 in the Main/'04 Break, 0.718 in the Narrow Shear SMC and 0.314 in the wide SMC which demonstrates a moderate correlation of Mo with Au. (B) Has r^2 values of 0.1042 for the Main'04 Breaks, 0.708 for the Narrow Shear SMC, and 0.4549 for the Wide SMC showing a moderate correlation between Au and As. R^2 and linear regression was calculated using ioGas.

There is a no correlation between Au with SiO_2 in all zones and a moderate correlation between Au and Sb in both the SMC zones but not the Main/'04 Break (Figure 33A-B). This suggests that the gold mineralization is not always dependent on the presence of quartz, normally seen as veining, and considerably so in the narrow cataclasite zones.

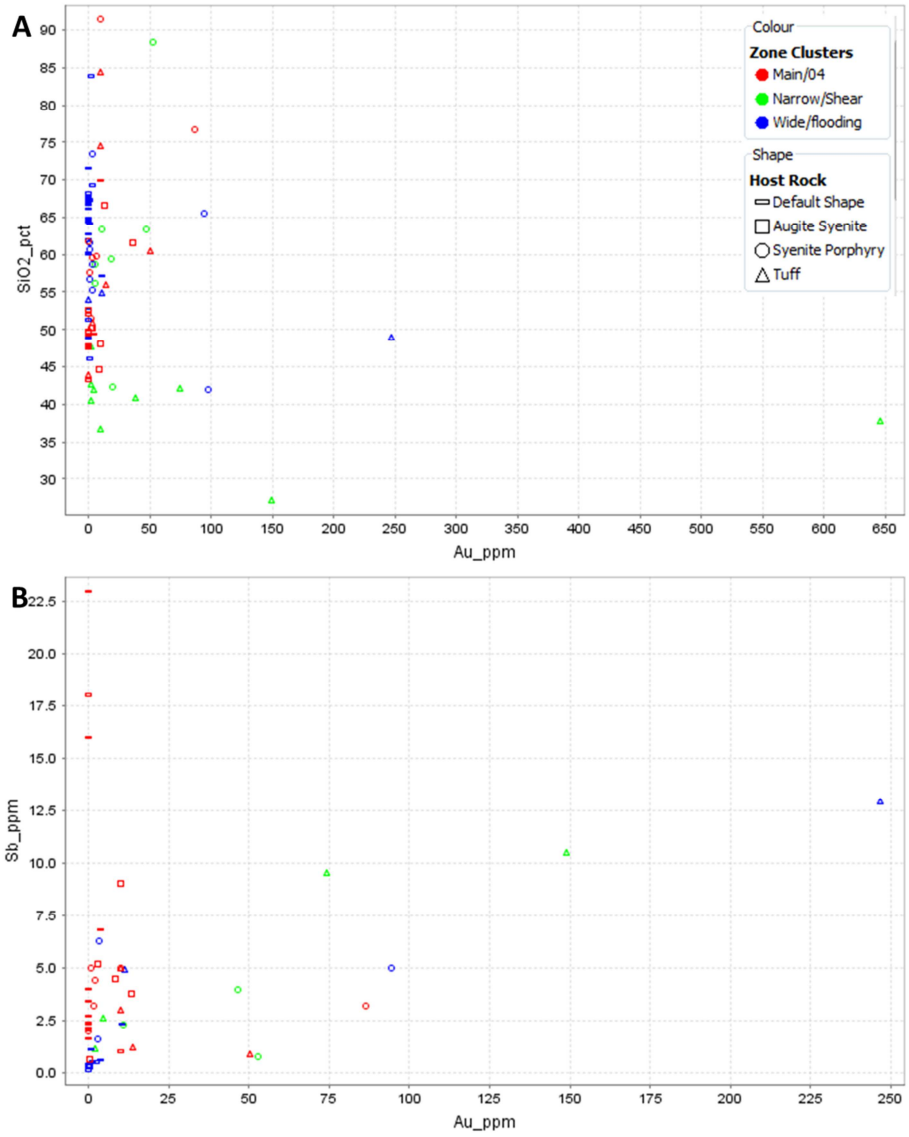

Figure 33 - Correlation of Au Mineralization with (A) SiO_2 and (B) Sb in the Main/'04 Breaks (red), SMC Narrow Shear Zones (green), and SMC Wide Flooding Zones (blue) for all samples. No variation was seen due to lithology. Two samples (LSKGI050 and LSKGI154) were excluded in (A) and (B) due to gold values of 461ppm and 1547ppm respectively. (A) has r^2 values of 0.256 in the Main/'04 Break, 0.0617 in the Narrow Shear SMC and 0.1328 in the wide SMC which demonstrates a no correlation of SiO_2 with Au, especially in the Narrow Shear SMC. (B) has r^2 values of 0.0372 for the Main'04 Breaks, 0.6932 for the Narrow Shear SMC, and 0.767 for the Wide SMC showing a moderate correlation between Au and Sb in the SMC and none in the Main/'04 Breaks. R^2 and linear regression was calculated using ioGas.

Au mineralization has a no correlation with S (Figure 34A). This could suggest that within the strongest mineralization there is less pyrite than directly adjacent to the mineralization in the altered wallrock. There is a moderate negative correlation between

Au and Ga in the Main/'04 Break and within the Wide Flooding Zones of the SMC, but no correlation in the Narrow Shear Zones of the SMC (Figure 34B).

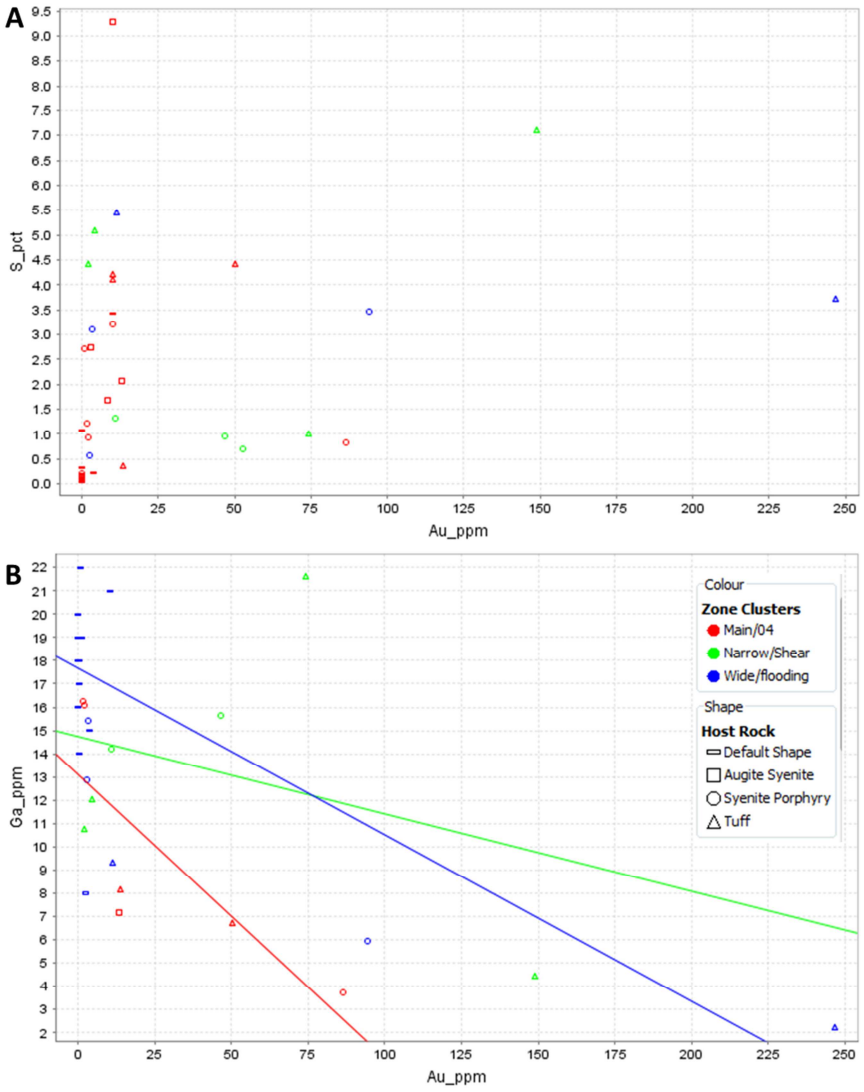

Figure 34 - Correlations of Au Mineralization with (A) S and (B) Ga in the Main/'04 Breaks (red), SMC Narrow Shear Zones (green), and SMC Wide Flooding Zones (blue) for all samples. No variation was seen due to lithology. Two samples (LSKGI050 and LSKGI154) were excluded in (A) and (B) due to gold values of 461ppm and 1547ppm respectively. (A) has r^2 values of 0.0526 in the Main/'04 Break, 0.1062 in the Narrow Shear SMC and 0.0426 in the wide SMC which demonstrates a no correlation of S with Au. (B) has r^2 values of 0.6173 for the Main'04 Breaks, 0.1107 for the Narrow Shear SMC, and 0.5291 for the Wide SMC showing a moderate inverse correlation between Au and Ga in the Wide Flooding SMC and Main/'04 Break, and none in the Narrow Shear SMC. R^2 and linear regression was calculated using ioGas.

4.5 Conclusions

Within the host lithologies, tuff has higher concentrations of incompatible elements (Ti, P, U, Th, Rb, Sr, Y, Zr, Nb, and Ba), and REEs compared to augite syenite and syenite porphyry. As syenite porphyry and augite syenite are thought to be derived from the same parent alkalic igneous suite, they are fairly similar, except syenite porphyry generally has higher silica content.

Alteration geochemistry can be related to the minerals observed within thin section. The replacement of plagioclase by potassium feldspar is represented by the loss of Na_2O and the addition of K_2O. Sericite is represented by the addition of K_2O, and Al_2O_3; hematite is observed within the addition of Fe_2O_3; finally, the addition of carbonates is observed with the addition of CaO. The Main/'04 Breaks have K-feldspar, hematite, and sericite alteration, the Narrow Shear SMC Zones have K-feldspar and sericite alteration and the Wide Flooding SMC Zones have strong K-feldspar, hematite, and sericite alteration.

The SMC has higher Au than the Main/'04 Break, and within the SMC there are higher gold concentration within the wide flooding zones than the narrow cataclastic zones. The higher molybdenite and quartz veining within the wide SMC zones is demonstrated as an abundance of Mo, and SiO_2. Within all zones, there is a positive correlation between Au and Pb, and Ag, but no correlation with Cu. This indicates the presence and correlation of the telluride altaite (PbTe), electrum, and silver tellurides with gold. Chalcopyrite is not correlated with the gold mineralization. The Main/'04 Breaks and the narrow SMC shear zones also have a positive correlation between Au with Mo. As correlates with Au in the Narrow Shear SMC.

Chapter 5

5 Oxygen Isotope Analysis

Isotopes are atoms with the same number of protons and electrons, but a different number of neutrons. The stable isotopes of oxygen are ^{16}O (99.763%), ^{17}O (0.0375%), and ^{18}O (0.1995%) with their respective abundances (Hoefs, 2004) and can be found within the oxygen component of silicate minerals. Stable oxygen isotopes are reported in $\delta^{18}O$ values (‰) and represented the ratio of ^{18}O to ^{16}O, or fractionation, against the Vienna Standard Mean Ocean Water (V-SMOW) (Equation 2).

$$\delta^{18}O = \frac{^{18}O/^{16}O_{sample} - ^{18}O/^{16}O_{V-SMOW}}{^{18}O/^{16}O_{V-SMOW}} \times 10^3 \quad \text{(Eq. 2)}$$

Equilibrium and kinetic factors within a mineralizing system will change the fractionation of the oxygen isotopes when the fluids interact with the host rock. This gives the rock a signature specific of the conditions in which it was mineralized (Hoefs, 2004).

5.1 Whole Rock Analysis

Whole rock oxygen isotopes were analyzed on homogeneous powdered bulk rock samples from unaltered, altered, and mineralized samples. They exhibit $\delta^{18}O$ values ranging between 6.0-11.9‰. A full table of values is available in Appendix E. Values ranged from 6.2-11.9‰ for the SMC and 6.1-11.9‰ for the Main and ’04 Breaks (Figure 35). Although the range for the SMC and the Main/’04 Breaks are very similar in distribution for the bulk rock samples, it is interesting to note that the mode for $\delta^{18}O$ ratios is lower in the SMC than in the Main/’04 Breaks.

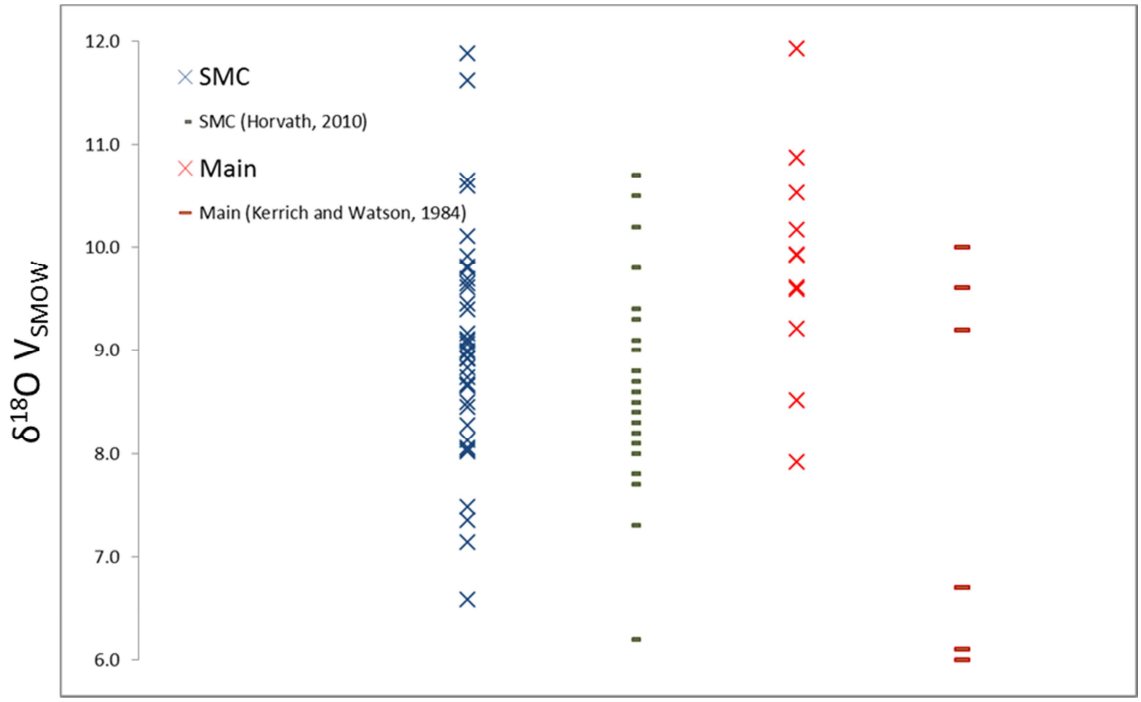

Figure 35 - Bulk Rock $\delta^{18}O_{V\text{-}SMOW}$ for the SMC (blue) and the Main/'04 Breaks (red). Values analyzed by the author are denoted as 'x's while those taken from previous studies (Horvath, 2010; Kerrich and Watson, 1984) are denoted by dashes. Ranges in values overlap between the SMC and the Main/'04 Breaks.

Within individual zones, $\delta^{18}O$ values range from 6.2-10.7‰ for the NSZ, 8.6-9.6‰ for Barchetta, 8.1-9.4‰ for the #7 Break, 7.4-11.9‰ for the Lower D North, 6.6-8.5‰ for Limelight, 8.0-8.3‰ for Lower D, 7.9-11.9‰ for the '04 Break, and 6.0-10.0‰ for the Main Break (Figure 36). Values overlap even when they are broken into individual zones. Lithological constraints are explored in Section 5.3.1.

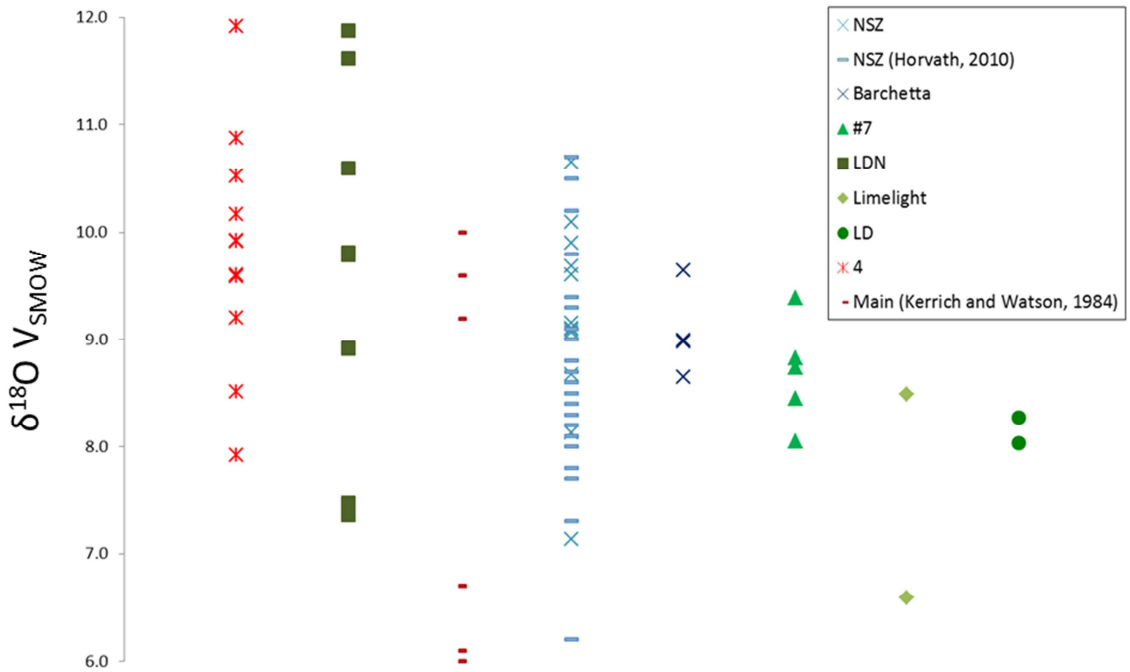

Figure 36 - Bulk rock $\delta^{18}O_{V\text{-}SMOW}$ for wide flooding SMC zones (blue- NSZ, Barchetta), narrow shear SMC zones (green - #7, Lower D North, Limelight, Lower D), and the Main/'04 Breaks (red). Values taken from previous studies (Horvath, 2010; Kerrich and Watson, 1984) are denoted by dashes.

5.2 Quartz-Chlorite Mineral Separates

Mineral separates of quartz and chlorite were chosen from mineralized veins containing quartz and chlorite that exhibited textures indicative of equilibrium. Optical microscopy was performed on all samples from which quartz-chlorite separates were obtained to determine equilibrium between quartz and chlorite (Figure 37). Some samples were rejected due to later shearing and deformation mainly affecting chlorite values (LSKGI111), or chlorite being secondary (LSKGI050, LSKGI158). Chlorite has more variability in its oxygen isotopes due to a few factors: it can have its hydroxyl (-OH) group affixed in various positions in the chlorite molecule and therefore give slightly varying values (Cole and Ripley, 1998), and chlorite generally re-equilibrates and alters faster than quartz leading to more variable results (Cole and Chakraborty, 2001). Because the quartz is taken from a mineralized vein, it is assumed it directly represents the fluid composition. Auriferous and telluride minerals, such as electrum, calaverite, altaite, melonite, sylvanite, and petzite, are texturally related. This is seen in Figure 19, where molybdenite, quartz, electrum, and melonite are seen intergrown.

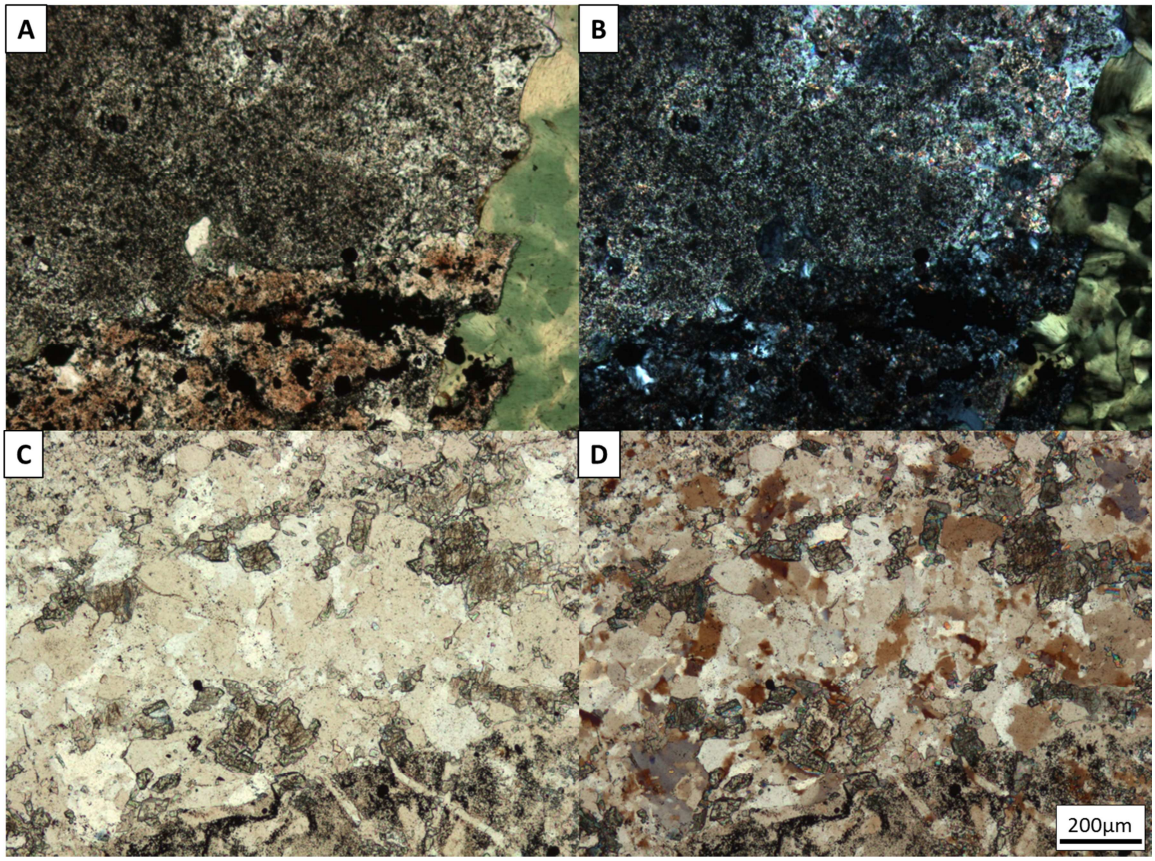

Figure 37 –Photomicrographs of quartz – chlorite veining showing examples of poor equilibrium textures in (A) plane and (B) cross polarized light, and of good equilibrium textures in (C) plane and (B) cross polarized light. (A) and (B) show secondary chlorite overprinting an earlier quartz-carbonate vein in sample LSKGI111. (C) and (D) show intergrown chlorite and quartz vein in sample LSKGI154. Scale bar is 200µm.

Quartz separate $\delta^{18}O$ values at Macassa Mine range from 10.1-14.0‰. Values range from 10.1-12.9‰ for the SMC and 11.0-14.0‰ for the Main/'04 Breaks (Figure 38A). There is overlap between the SMC and Main/'04, but overall there seems to be lower $\delta^{18}O_{qtz}$ in the SMC than the Main/'04 Breaks. Chlorite separates $\delta^{18}O$ values are between -0.4-8.7‰ with values ranging between 0.0-8.7‰ in the SMC and -0.4-7.3‰ in the Main/'04 Breaks (Figure 38B). A comprehensive list of quartz and chlorite separates $\delta^{18}O$ values can be found in Appendix E. The chlorite $\delta^{18}O$ data has significant overlap with very little difference between the SMC and the Main/'04 Breaks.

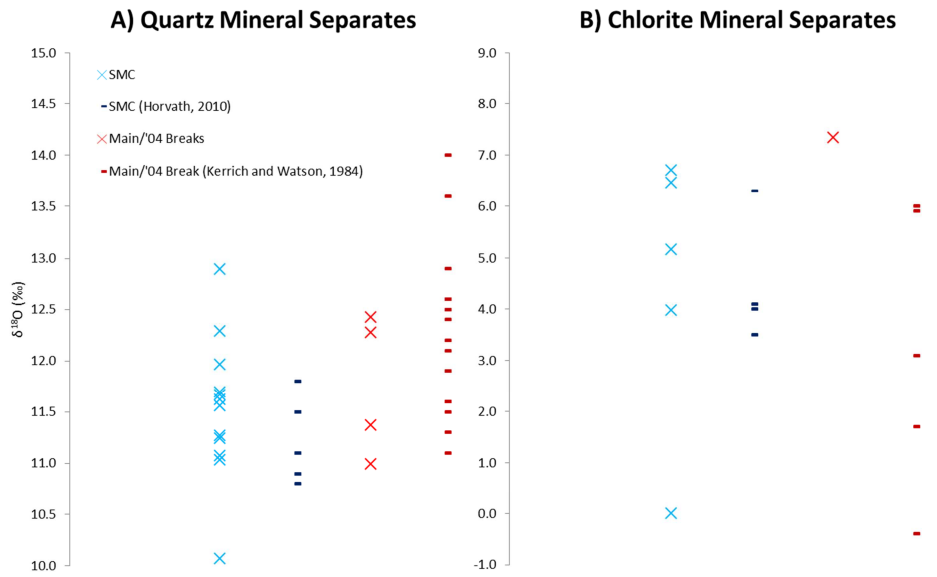

Figure 38 - $\delta^{18}O_{VSMOW}$ values in the SMC (blue) and Main/'04 Breaks (red) for (A) quartz and (B) chlorite mineral separates. Values analyzed by the author are denoted as 'x's while those taken from previous studies (Horvath, 2010; Kerrich and Watson, 1984) are denoted by dashes.

Quartz $\delta^{18}O$ values range from 10.9-12.3‰ in the SMC, 11.7‰ in Barchetta, 11.2‰ in the #7 Break, 10.1-12.9‰ in Lower D North, 11.1‰ in Limelight, 11.0-12.4‰ in the '04 Break, and 11.1-14.0‰ in the Main Break (Figure 39A). Chlorite $\delta^{18}O$ values range from 3.5-8.7‰ in the SMC, 0.0-5.2‰ in Lower D North, 6.7‰ in Limelight, 7.3‰ in the '04 Break, and -0.4-6.0‰ in the Main Break (Figure 39B). Chlorite $\delta^{18}O$ separate values overlap between the different zones.

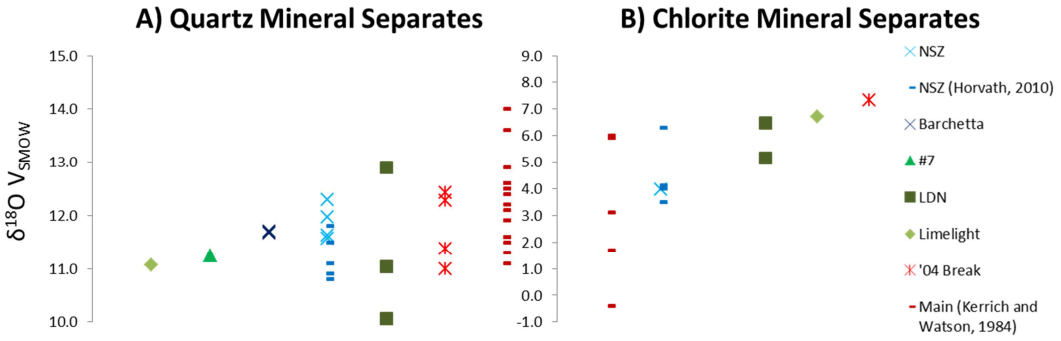

Figure 39 - $\delta^{18}O_{VSMOW}$ of (A) quartz and (B) chlorite mineral separates for wide flooding SMC zones (blue- NSZ, Barchetta), narrow shear SMC zones (green - #7, Lower D North, Limelight, Lower D), and the Main/'04 Breaks (red). Values taken from previous studies (Horvath, 2010; Kerrich and Watson, 1984) are denoted by dashes.

5.3 Discussion

5.3.1 Whole Rock Oxygen Isotopes

The similarity in range of bulk rock oxygen isotope values between the Main/'04 Breaks and the SMC shown in Figures 35 and 36 is most likely related to the similarity in the rock types, while the different modes of the oxygen isotope values represent the possibly of different fluids or temperatures responsible for the mineralization. This is confirmed in Figure 40, which shows that in general, the syenite porphyry has a higher $\delta^{18}O$ values than tuff. There is not enough data within this thesis on the augite syenite to have confirmation, but it seems that it generally shares the same range as the syenite porphyry. Kerrich and Watson (1984) report fresh whole rock values of 6.1-6.7‰ for augite syenite, 6.6-10.0‰ for syenite porphyry and tuffs. The influence of the fluids on mineralization is more strongly represented in the mineral separates. The lower fresh whole rock values recorded by Kerrich and Watson (1984) are enriched by the mineralizing fluids, which include a high amount of quartz. Quartz mineral separate values range from 10.9-12.3‰ in the SMC and 11.0-14.0‰ in the Main/'04 Break. This enriches the bulk rock $\delta^{18}O$ from 6.1-10.0‰ to the values seen in Figure 40. The Main/'04 Breaks have more enriched $\delta^{18}O$ values than the SMC, and therefore the mode is seen to be higher, as the host rock has been influenced by a higher oxygen isotope value.

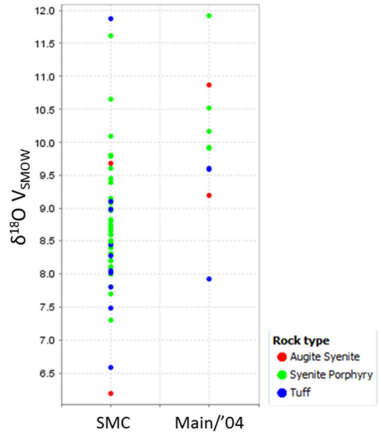

Figure 40 - Bulk Rock $\delta^{18}O_{VSMOW}$ for the SMC and the Main/'04 Breaks showing lithological influence of augite syenite (red), syenite porphyry (green), and tuff (blue). Syenite porphyry tends to be more enriched than the tuff in the SMC and the Main/'04 Break. The wide distribution of $\delta^{18}O_{VSMOW}$ values is seen to be a factor of the host lithology.

Using the bulk rock samples, the $\delta^{18}O$ can be compared to the multi-element analysis. Shown in Figure 41, there is a no correlation between Au and $\delta^{18}O$. However, there is more of a correlation between alteration and $\delta^{18}O$ (Figure 42). There is an increase in total alteration represented by Fe_2O_3, CaO, Al_2O_3, and K_2O with an increase in $\delta^{18}O$. Alteration is seen in thin section to be the replacement of the host rock with hematite, carbonate, sericite, and K-feldspar, which according to mass balance calculations done for alteration in Macassa Mine by Kerrich and Watson (1984) can represent Fe_2O_3, CaO, and K_2O respectively. The stronger the alteration, the more it is depleted it is in $\delta^{18}O$. This confirms that the mineralizing fluid is strongly affecting the host rock. This makes sense as lower $\delta^{18}O$ values are associated within hotter fluid, and temperature of the fluid is a defining factor in the strength and expanse of alteration.

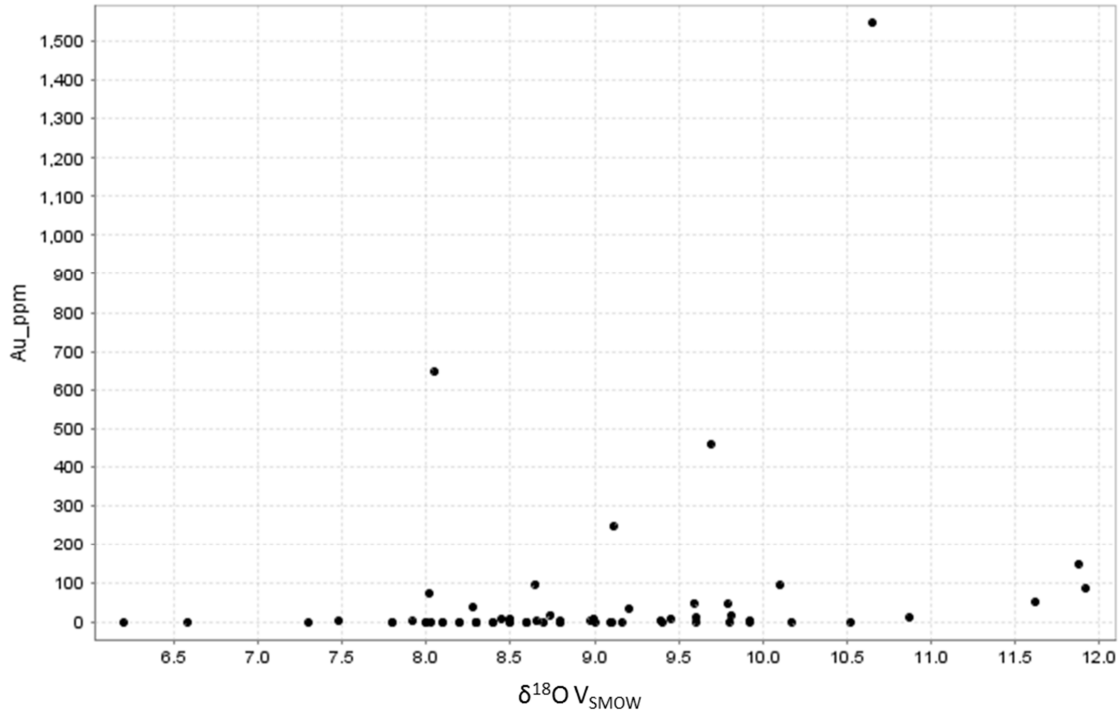

Figure 41 - Whole rock $\delta^{18}O_{VSMOW}$ compared to mineralization, represented by Au, within all samples, including fresh, altered, and mineralized samples from all lithologies. No correlation was seen between Au and $\delta^{18}O_{VSMOW}$ with $r^2 = 0.05601$ on a linear regression analysis.

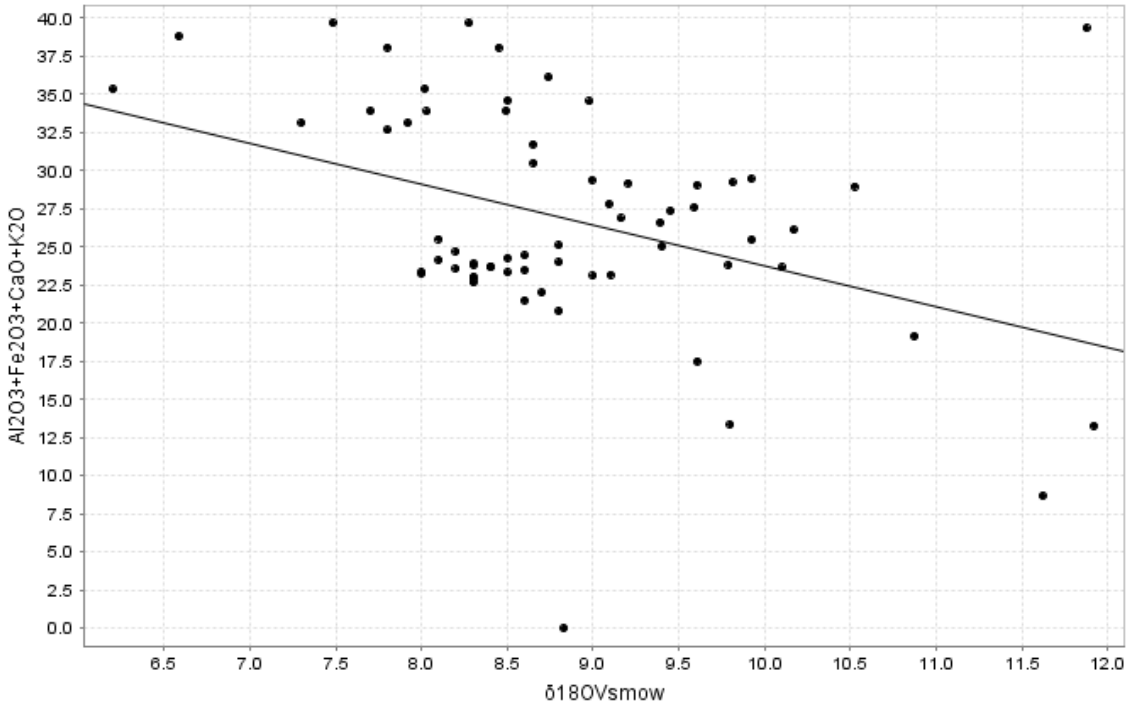

Figure 42 - Whole rock $\delta^{18}O_{VSMOW}$ compared to alteration, represented by the total Al_2O_3, Fe_2O_3, CaO, and K_2O within within all samples, including fresh, altered, and mineralized samples from all lithologies. Line was calculated by ioGas linear regression analysis with an r^2 value of 0.1541. There is a weak negative correlation between alteration and $\delta^{18}O_{VSMOW}$.

Other geochemical relationships with $\delta^{18}O_{VSMOW}$ include a very weak positive correlation with Mo and a weak correlation with SiO_2 (Figure 43A-B). The greater the concentration of quartz and molybdenite, the more enriched in $\delta^{18}O$ the rock is compared to the fresh rock. This entails that the amount of quartz and, to a lesser extent, molybdenite will affect the bulk rock value. The different groupings between the wide flooding SMC, the narrow shear SMC, and the Main/'04 Break could indicate the presence of more than one system. If they were all from the same system, they would show a tighter fit as there would be a more similar concentration of difference minerals like quartz and molybdenite, represented by Si_2O and Mo respectively, within the three. Note that the narrow shear SMC clusters frequently in the same trend as the Main/'04 Breaks.

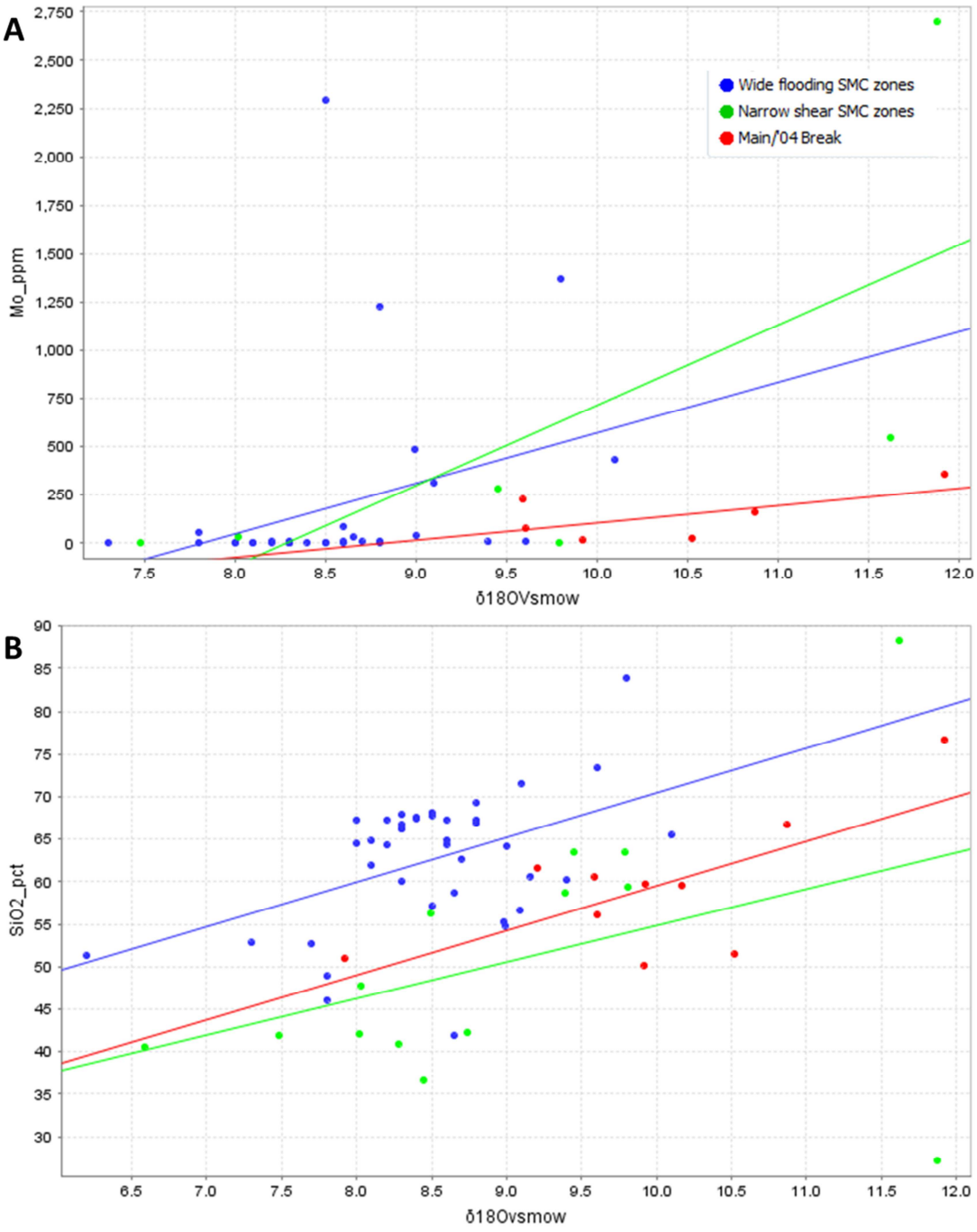

Figure 43 - Whole rock $\delta^{18}O_{VSMOW}$ compared to (A) Mo and (B) SiO_2 within all samples within wide flooding SMC zones (blue), narrow shear SMC zones (green), and the Main/'04 Breaks (red). All samples, including fresh, altered, and mineralized samples from all lithologies were used. R^2 values for Mo calculated by linear regression analysis in ioGas are 0.09535 for wide SMC, 0.5086 for narrow SMC, and 0.3797 for the Main/'04 suggesting Mo and $\delta^{18}O_{VSMOW}$ do not correlate in the wide SMC, and very weakly correlate otherwise. R^2 values for SiO_2 calculated by linear regression analysis in ioGas are 0.2058 for wide SMC, 0.1671 for narrow SMC, and 0.4726 for Main/'04 Break suggesting a very weak correlation between SiO_2 and $\delta^{18}O_{VSMOW}$.

Temperature plays an important role within all isotope fractionation. There is isotopic fractionation occurring in all chemical reactions, and is therefore seen in the precipitation of quartz and chlorite. Isotopic fractionation between the parent and the daughter species generally decreases with increasing temperature, and at very high temperatures the fractionation approaches zero (Taylor et Epstein, 1962). This means that at higher temperatures the variation in O^{18}/O^{16} is less than at lower temperatures. Therefore, $\delta^{18}O$ will be more depleted at higher temperatures than lower temperatures.

A moderate negative trend occurs within the elements Sr and Rb (Figure 44A-B), which are known to be mobile (MacLean and Barrett, 1993), in the narrow shear SMC zones and the Main/'04 Break, but no correlation for the wide flooding SMC. The overall negative correlation indicates that Sr and Rb are present in higher concentrations at lower $\delta^{18}O_{VSMOW}$, and therefore hotter temperatures. Sr appears to be a single trend, and shows the wide flooding SMC zones with lower $\delta^{18}O_{VSMOW}$ and higher Sr, and the Main/'04 Break and narrow shear zones with higher $\delta^{18}O_{VSMOW}$ and lower Sr. It is not known why there is more variability in the Sr in the wide flooding zones of the SMC.

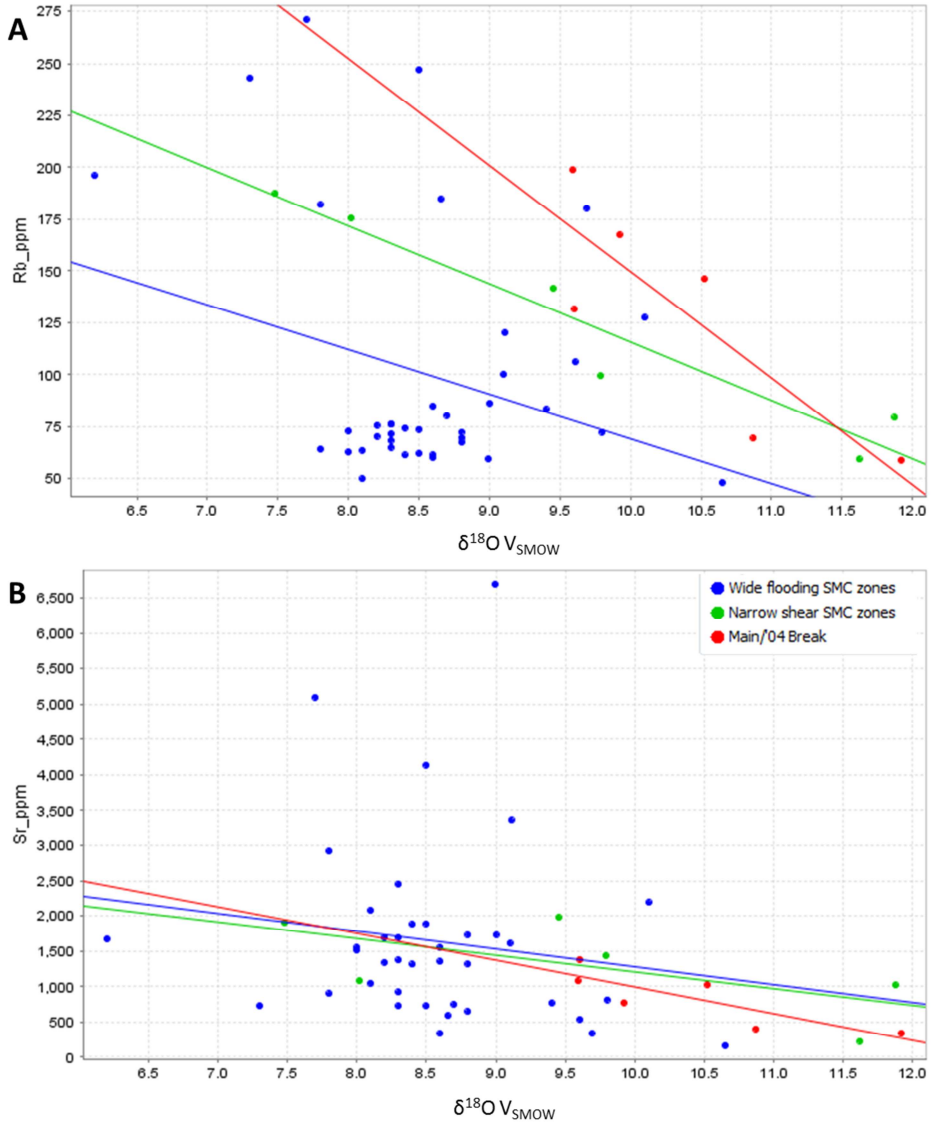

Figure 44 - Whole rock $\delta^{18}O_{VSMOW}$ compared to mobile elements (A) Rb and (B) Sr within all samples within wide flooding SMC zones (blue), narrow shear SMC zones (green), and the Main/'04 Breaks (red). All samples, including fresh, altered, and mineralized samples from all lithologies were used. Linear regression lines and analysis for r^2 values was calculated using ioGas. Rb r^2 values are 0.1208 for the wide SMC, 0.9274 for the narrow SMC, and 0.7146 for the Main/'04 Break. Sr r^2 values are 0.004698 for the wide SMC, 0.4192 for the narrow SMC, and 0.697 for the Main/'04 Breaks.

5.3.2 Mineral Separates Oxygen Isotopes

Quartz mineral separates can be used to represent mineralizing fluid sources. One way in which sources can differ is temperature, which can be represented by differing $\delta^{18}O$ values. As explained in the section above, there is more variation in $^{18}O/^{16}O$ at lower

temperatures during fractionation in a chemical reaction, which will enrich the precipitating mineral in $\delta^{18}O$. Higher temperatures result in a lower $\delta^{18}O_{qtz}$ values than lower temperatures. The SMC $\delta^{18}O_{qtz}$ values are depleted compared to those of the Main/'04 Breaks, which can be explained by the presence of hotter fluids (Figures 38A and 39A). The difference in stable oxygen isotope values within quartz separates from the SMC and the Main/'04 Breaks allows us to hypothesize that there may be different gold mineralization sources between the two systems (Taylor, 1974). The depleted values of the SMC suggest two main possibilities: the first being that there is a higher temperature metamorphic fluid in the SMC than the Main/'04 Breaks, and the second is the possibility of an addition of a magmatic source, in addition to the metamorphic source found within the Main/'04 Breaks (Taylor, 1974; Kerrich and Watson, 1984).

Table 6: Oxygen isotope compositions of quartz and chlorite separates and calculated $\delta^{18}O_{qtz\text{-}chl}$, and fluid temperatures [[1]Clayton et al. (1972)/Wenner and Taylor (1971), and [2]Wenner and Taylor (1971)/ Wenner and Taylor (1971) (Eq. 3 and 4 respectively)]. *Data from Horvath (2010). **Data from Kerrich and Watson (1984). Italicized data were cut due to samples not being in equilibrium.

Sample ID	Lithology	Zone	$\delta^{18}O_{qtz}$ (‰) ±0.2	$\delta^{18}O_{chl}$ (‰) ±0.2	$\delta^{18}O_{qtz\text{-}chl}$ (‰) ±0.2	T (°C)[1]	T (°C)[2]
LSKGI050	*Augite Syenite*	*NSZ*	*11.5*	*7.9*	*3.6*	*616*	*843*
LSKGI111	*Tuff*	*NSZ*	*11.3*	*8.7*	*2.5*	*939*	*1639*
LSKGI126	Tuff	Limelight	11.1	6.7	4.4	497 ±51	646 ±79
LSKGI151	Syenite Porphyry	LDN	10.1	5.2	4.9	437 ±40	556 ±57
LSKGI154	Syenite Porphyry	NSZ	11.6	4.0	7.6	265 ±17	326 ±21
LSKGI158	*Tuff*	*LDN*	*17.3*	*5.0*	*12.3*	*134*	*169*
LSKGI171	Tuff	LDN	11.0	6.5	4.6	473 ±46	609 ±69
304016*	Bimodal Porphyry	NSZ	11.5	4.0	7.5	269 ±18	331 ±22
304022*	Bimodal Porphyry	NSZ	11.5	6.3	5.2	410 ±35	518 ±50
304040*	Syenite Porphyry	NSZ	11.5	4.1	7.4	273 ±18	336 ±23
304046*	Trachyte	NSZ	10.9	3.5	7.4	273 ±18	336 ±23
LSKGI172	Syenite	04 Break	12.3	7.3	4.9	434	553

Sample ID	Lithology	Zone	$\delta^{18}O_{qtz}$ (‰) ±0.2	$\delta^{18}O_{chl}$ (‰) ±0.2	$\delta^{18}O_{qtz\text{-}chl}$ (‰) ±0.2	T (°C)[1]	T (°C)[2]
	Porphyry					±39	±57
A**	Fault gouge: massive selenite, chl, qtz + mag	Main	14.0	1.7	12.3	134 ±7	168 ±9
E**	Quartz fragments and fault gouge (vein)	Main	12.5	3.1	9.4	201 ±12	248 ±14
G-80-60**	High grade vein	Main	12.6	6.0	6.6	313 ±22	387 ±29
G-80-71**	K-spar, actinolite, qtz chl vein	Main	11.9	5.9	6.0	349 ±71	435 ±36
G-82-150**	qtz mag vein	Main	12.1	-0.4	12.6	128 ±7	162 ±8

Hydrothermal temperatures of the mineralizing fluid of different zones were calculated using the quartz-chlorite pairs with two sets of experimentally mineral-water fractionation equations and are reported in Table 6. The first set is between that of Clayton et al. (1972) and Wenner and Taylor (1971) (Equation 3). The second two are both from Wenner and Taylor (1971) (Equation 4). The Clayton et al. (1972) and Wenner and Taylor (1971) quartz-water curves are different, as both sets are experimentally derived. This produces different calculated temperatures, as seen within Table 6. One estimate is not known to be better over the other. Both sets of temperatures are calculated so as to compare to the study done by Kerrich and Watson (1984). Mineral separates of quartz and chlorite were chosen from mineralized veins containing quartz and chlorite that exhibited textures indicative of equilibrium.

$$T(\text{°C}) = \sqrt{\frac{1.82\times10^6}{\delta^{18}O_{Qtz-Chl}-1.3}} - 273.15 \qquad \text{(Eq. 3)}$$

$$T(\text{°C}) = \sqrt{\frac{2.01\times10^6}{\delta^{18}O_{Qtz-Chl}-1.99}} - 273.15 \qquad \text{(Eq. 4)}$$

Temperature errors calculated using the maximum and minimum temperatures that are possible with the $\delta^{18}O_{VSMOW}$ errors for quartz and chlorite and dividing the results by two. For example, LSKGI126 could have $\delta^{18}O_{qtz}$ 11.3‰ and $\delta^{18}O_{chl}$ 6.5‰ to $\delta^{18}O_{qtz}$ 10.9‰ and $\delta^{18}O_{chl}$ 6.9‰, which gives a possible temperature range[1] from 451°C to 552°C, or an error of ±51°C.

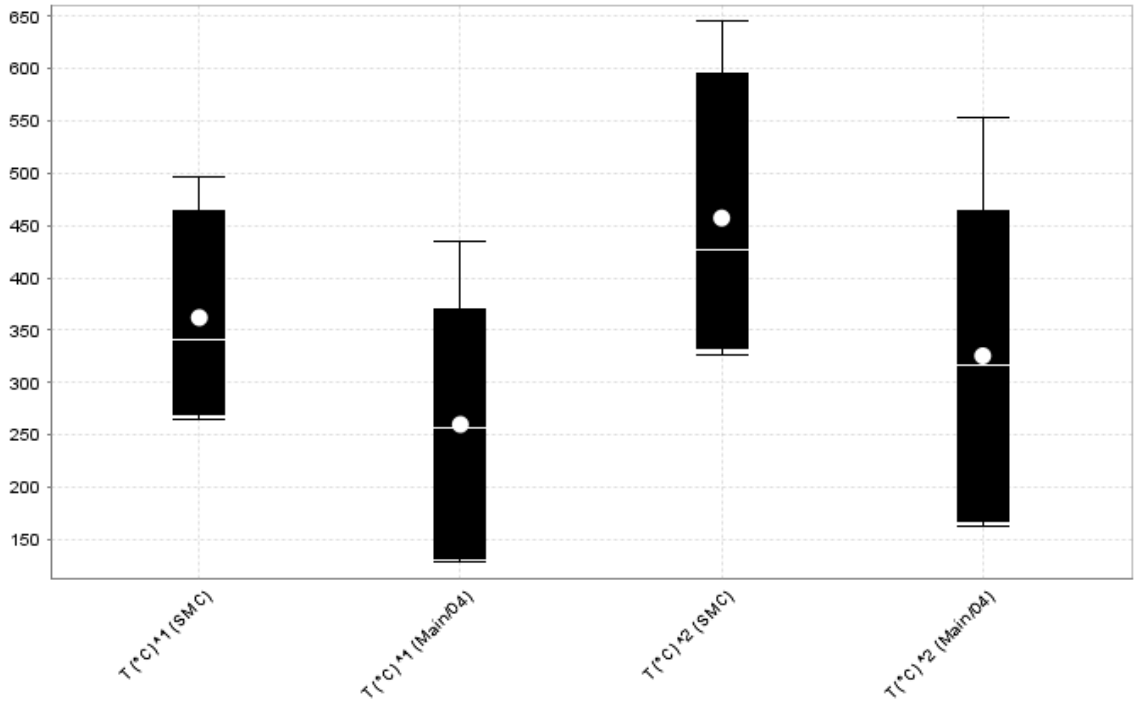

Figure 45 - Box plots of mineralizing fluid temperatures of the SMC and Main/'04 Breaks calculated from oxygen isotope compositions of quartz-chlorite pairs using equations derived by [1]Clayton et al. (1972)/Wenner and Taylor (1971), and [2]Wenner and Taylor (1971)/ Wenner and Taylor (1971). Data from Horvath (2010) and Kerrich and Watson (1984) included in results. This box plot divides the data into four equal parts by using the median and the 25th and 75th percentiles. Within the box plots displayed below, the boxes contain 50% of the data, the median is shown by a line, and the mode by a white circle. In this plot, a fence is the box extended 1.5x the length of the box towards the minimum and maximum. The fence is shown as 'whiskers' protruding from the box. Far outliers are shown as open circles.

Results plotted in Figure 45 show that for both calculated temperatures, the SMC (265°C - 497°C; 326°C - 646°C) has a mineralizing fluid temperature range higher than the Main/'04 Breaks (128°C - 434°C; 162°C – 553°C). Three temperatures (Table 6, italisized) were rejected due to comparitively high $\delta^{18}O_{chl}$ to other samples, and higher

probability of contamination, or from chlorite not appearing in equilibrium in thin section petrography (Figure 37). The chlorite separates show greater variability than the quartz separates (Figures 38, 39). This could be due to re-equilibration of the chlorite. The lower chlorite values from the Main Break by Kerrich and Watson (1984) may represent a later fluid stage or reactivation of the structure. Petrography was not performed on these samples. Disequilibrium may be affecting the temperature calculations, although all quartz-chlorite pairs appeared to be in equilibrium in thin section.

The SMC and the Main/'04 Break have partially overlapping calculated temperatures in both methods. However, the average temperature for the Main/'04 Breaks is cooler than that of the SMC. The temperatures derived indicate the possibility of the mineralizing fluids at Macassa Mine having either a hotter metamorphic fluid or the addition of magmatic component as well as a metamorphic component suggested by Kerrich and Watson (1984). The higher temperatures within the SMC could indicate that the SMC has a hotter metamorphic source or more of a magmatic component than the Main/'04 Breaks.

The SMC has quartz $\delta^{18}O$ values of 10.9-12.3‰ and temperatures 265°C - 646°C while the Main/'04 Breaks have $\delta^{18}O$ values of 11.0-14.0‰ and temperatures from 128°C - 553°C. The difference in stable oxygen isotope values within quartz separates and temperatures between the SMC and the Main/'04 Breaks allows us to hypothesize a variety of possibilities for the source of mineralization. The mineralization fluid source could be the same for the two systems, it could becompletely different between the two systems, or there could be mixing that is occuring between between the mineralizing fluids responsible for the two systems. It is most likely that mixing is occuring, for reasons elaborated on below.

There is a difference in $\delta^{18}O$ and δD with differences between magmatic and metamorphic fluid sources (Taylor, 1974). Since δD values were not considered in this study, only $\delta^{18}O$ will be considered. The range of $\delta^{18}O$ for metamorphic fluids typically falls between 5‰ - 25‰, while the $\delta^{18}O$ values for magmatic fluids are typically between

6‰ - 9‰ (Taylor, 1974; Kerrich and Watson, 1984). Magmatic fluids are observed to generally have lower $\delta^{18}O$ values than metamorphic fluids.

Both the SMC and the Main/'04 Break $\delta^{18}O$ values range in the mid to hot metamorphic fluids (Taylor, 1974). The lower $\delta^{18}O$ values found within the SMC suggest two possibilities: that the fluid within the SMC is a hotter metamorphic fluid, or that that there is potential magmatic influence mixing more within the SMC than the Main/'04 Breaks. The variation in $\delta^{18}O$ values makes it unlikely that the SMC and the Main/'04 Breaks have the same source.

As mentionned in Chapter 4, the SMC can be split into two different types of zones: narrow cataclastic shear zones and the zones with wide diffuse quartz-molybdenite veining. As well as having some differences geochemically, they can also be explored within mineralizing fluids represented by $\delta^{18}O$. Figure 46 illustrates the temperatures found within the Macassa mine split into the SMC narrow shear zones, the SMC wide flooding zones, and the Main/'04 Break. A decreasing continuum of temperatures is observed from the narrow shear zones to the wide veining zones to the Main/'04 Break. The higher temperature in the narrow shear zones than in the wide veining zones is related to their structure. In the formation of the wide zones of the SMC, there would have been more fracturing and shearing than in the narrow shearing zones, allowing more opportunity for the fluid to cool. Therefor, the hotter fluids passing through the SMC would be cooled in the wide veining zones, and would have stayed hotter in the narrow shear zones.

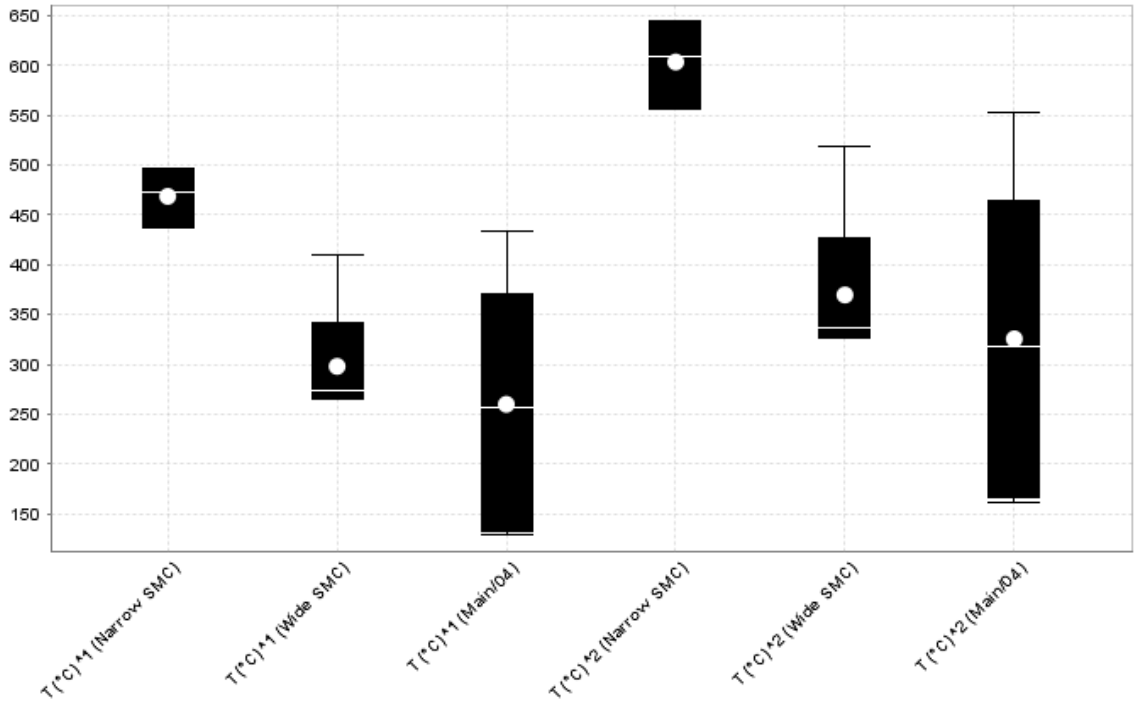

Figure 46 - Box plots of the mineralizing fluid temperatures of the wide flooding SMC, the narrow shear SMC, and Main/'04 Breaks calculated from oxygen isotope compositions of quartz-chlorite pairs using equations derived by [1]Clayton et al. (1972)/Wenner and Taylor (1971), and [2]Wenner and Taylor (1971)/ Wenner and Taylor (1971). Data from Horvath (2010) and Kerrich and Watson (1984) included in results. This box plot divides the data into four equal parts by using the median and the 25th and 75th percentiles. The box plots display the boxes which contain 50% of the data, the median shown by a line, and the mode by a white circle. In this plot, a fence is the box extended 1.5x the length of the box towards the minimum and maximum. The fence is shown as 'whiskers'. Far outliers are open circles.

5.4 Conclusions

Bulk rock oxygen isotope values are similar between the SMC (6.2-11.9‰) and the Main/'04 Break (6.1-11.9‰) due to the similarity in the host lithologies. However, it is possible that the different modes within these values are representative of mineralization. It is observed that the strength of the alteration is proportional to the enrichment in $\delta^{18}O$ values, demonstrating that the mineralizing fluid is affecting the host rock. The influence of the fluids on mineralization is more clearly reflected in the mineral separates.

Different fluid sources can be distinguished using temperature, as it plays an important role within all isotope fractionation. $\delta^{18}O_{qtz}$ values are more depleted than at higher temperatures. The SMC has quartz $\delta^{18}O$ values of 10.9-12.3‰ and temperatures 265°C -

646°C while the Main/'04 Breaks have $\delta^{18}O$ values of 11.0-14.0‰ and temperatures from 128°C - 553°C. As the SMC $\delta^{18}O_{qtz}$ values are depleted compared to those of the Main/'04 Breaks, it is deduced as well as calculated experimentally that the fluid is hotter. Hotter metamorphic fluids or a larger amount of potential magmatic fluids mixing with metamorphic fluid are proposed to have influenced the $\delta^{18}O_{qtz}$ values and calculated temperatures of the SMC. The difference in $\delta^{18}O_{qtz}$ values and temperatures between the SMC and the Main/'04 Breaks is hypothesized to be due to mixing of fluids during the mineralization of the two systems.

Chapter 6

6 Summary and Conclusions

6.1 Summary

The Macassa Mine is located in Kirkland Lake, Ontario, Canada. The Kirkland Lake Mining District is located in Teck Township of the Abitibi Subprovince in the Superior Province. The Abitibi is the largest Archean craton of the Canadian Shield, stretching east-west over 1500 km (Calvert and Ludden, 1999). The Abitibi Greenstone Belt is composed primarily of metamorphosed sedimentary and volcanic rocks, and tonalite-trondhjemite-granodiorite intrusive rocks (Houle, 2008). There are two main east-west trending fault zones that control ore mineralization: the Porcupine-Destor Deformation Zone, and the Larder Lake-Cadillac Deformation Zone (LLCDZ) (Ayer et al., 2005; Jackson and Fyon, 1991). The Macassa Mine is located along a tertiary splay of the LLCDZ. The local geology is underlain by Tisdale and Blake River volcanic assemblages. The Timiskaming rocks lie unconformably in an east-plunging synclinorium over the volcanic units and are comprised of clastic sedimentary rocks and intercalated alkaline volcanic rocks. Finally, Timiskaming aged syenitic intrusions crosscut earlier units (Ayer et al., 2005).

The Kirkland Lake camp is an mesothermal Archean orogenic gold deposit. Orogenic gold deposits are hydrothermal deposits in metamorphic belts (Phillips and Powell, 1993) that have several defining features. These gold deposits are very late to post peak metamorphic timing, located in a metamorphose fore-arc or back-arc, formed in thermal equilibrium with country rocks, and have certain key geochemical incators (Gebre-Mariam et al., 1995; Goldfarb et al., 2005; Goldfarb and Groves, 2015). These orogenic gold deposits have hydrothermally added K, S, CO_2, H_2O, Si, and Au with certain deposits also adding As, B, Bi, Na, Sb, Te, and W. Ore fluids seen in inclusions are supralithostatic H_2O-CO_2-CH_4-N_2-H_2S and low-to-moderate salinity (Goldfarb and Groves, 2015).

The Macassa Mine in the Kirkland Lake gold camp has two main systems of mineralized zones. Both are associated with mineralized faults, known as breaks. The first system is related to the Main/'04 Break and the second is the South Mine Complex (SMC). The Main/'04 Breaks is a semi-brittle reverse-fault system that dips south at 60° to 85° and strikes northeast 060° to 080°. Mineralization occurs in narrow quartz veins in conjunction with a cataclastic fault zone with a thin alteration zone. Gold in the Main/'04 Breaks is associated with pyrite, molybdenite, and tellurides. The SMC is found at depth to the south of the Main/04 Breaks. It dips more shallowly at 25° to 50°, but still strikes northeast 060° to 080°. The SMC is an interconnected network of fault controlled narrow shear zones, quartz-molybdenite veins, and wide alteration halos. Mineralization is found in high-grade zones of finely disseminated pyrite, visible gold and tellurides within the veins and alteration. The SMC is different from the Main/'04 break within the structure, mineralogy, alteration, multi-elemental analysis, and oxygen isotope studies. There are also some differences within the SMC, and two styles of mineralization within the SMC have been proposed within this study: the wide diffuse quartz-molydenite veining zones, and the narrow quartz veins and cataclasite zones.

One of the first differences noted between the SMC and the Main/'04 Break is the difference in structure. Although they both strike 060-080°, the Main/'04 system dips south at 60° to 85° while the SMC dips south only 25° to 50°. The Main/'04 Breaks tend to be narrow strong faults with up to 0.5m of cataclasite on either side. The SMC can have this structure within the western and northern portions, observed within the Limelight, #7 Break, Lower D North, and '08 Break, but the New South Zone and Barchetta Zone in the south-east are observed as wide (up to 3m) quartz-molybdenite weak diffuse veining adjacent to a structure which has been weakly to moderately healed.

Another key difference between the SMC and the Main/'04 Breaks is the mineralogy. The Main/'04 Breaks typically have narrow quartz veins with up to 1-2% molybdenite and minimal pyrite (<5%). Mineralization is observed as visible gold, tellurides (altaite and calaverite), and gold as inclusions and rims within some of the corroded pyrites. The SMC has a variety of mineraliation styles, including the wide diffuse quartz-molybdenite veining, a molybdenite matrix supported breccia, a later quartz veining and brecciation of

the former styles. In narrow cataclasite zones, there is typically quartz veining running parallel to the cataclasite zone. There is a substantial increase in pyrite within all zones compared to the Main/'04 Breaks with 10-15% pyrite in a typical zone. Mineralization is present as visible gold, tellurides (calaverite, petzite, altaite, minor melonite), and as rims and inclusions in the partially reabsorbed pyrites.

The alteration varies between the Main/'04 Break and the two styles of SMC mineralization. The Main/'04 Breaks typically have narrow (<0.5m) strong hematite alteration, showing red colouration in hand sample, as well as K-feldspar, sericite, and minor carbonate alteration. The SMC typically has wide (2-10m) stronger K-feldspar and sericite alteration, showing yellow-beige-green colouration in hand sample, with occassional appearances of carbonate and hematite alteration. Pyrite is strongly associated with the alteration within the SMC, and is not always associated with gold mineralization.

The bulk rock multi-elemental analysis shows lithological influences to the geochemistry which should not be considered when determining the style of mineralization. Tuff is found to have an higher concentration of TiO_2, P_2O_5, U, Th, Rb, Sr, Y, Zr, Nb, Ba, and REEs. Most of these elements are Large Ion Lithophiles (LILs), which are known to be preferential in extrusive phases of plutonic-extrusive complexes (Taylor et al., 1979). Within the framework local syenitic complex, it follows that tuff show these higher concentrations compared to the syenitic porphyry and the augite syenite as tuff is an extrusive component of the syenitic stock.

Bulk rock multi-elemental analysis clearly shows the alteration signature. In general, there is an increase in K_2O, Fe_2O_3, and CaO and a decrease in Na_2O compared to fresh rock when alteration is present. The K_2O increase and the Na_2O decrease is the K-feldspar and sericite alteration replacing the plagioclase feldspars in the host rock, while the Fe_2O_3 represents hematization, and the CaO, carbonitization. There is also an increase in Mo and LREE. These are mobile elements, and are early geochemical indicators of an encroaching fluid. (Gresens, 1967; MacLean and Barrett, 1993)The SMC has a higher concentration of SiO_2, Na_2O, SrO, and Mo and lower concentrations of Fe_2O_3, MgO,

CaO, Th, As, Zn, Cu, Co, V, and LREE than the Main/'04 Break in its alteration, supporting the higher K-feldspar and sericite alteration in the SMC, and a higher hematite and carbonatite alteration in the Main/'04 Breaks. There are higher Al_2O_3 concentrations and lower MgO, CaO, Fe_2O_3 in the narrow cataclastic compared to the wide diffuse quartz-molybdenite veining. Na_2O and K_2O have greater variation within the narrow cataclastic zones.

Many of the elements shown in Chapter 4.3 which have higher or lower concentrations in the mineralized samples are mobile. The variability of the elements shows differing fluid conditions between the zones. A lack of mobile elements in certain zones could suggest remobilization, which would decrease the concentration of these elements within that zone. The low concentration of mobile elements could also suggest varying distance from the source, or varying host rock. There is a higher concentration of gold within the wide SMC zones, then the narrow SMC zones, and finally the Main/'04 Breaks. Compared to other zones, the wide SMC zones have higher concentrations of Mo, Pb, and SiO_2, the narrow SMC zones have higher concentrations of Cu, CaO, Fe_2O_3, MgO, and the Main/'04 Breaks have higher Cs and Th, and lower Ga.

Stable oxygen isotope work has been critical in the study for solidifying the difference between the Main/'04 Break and the SMC as well as giving ideas to the nature of the mineralizing fluid. Whole rock $\delta^{18}O$ values were found to be between 6.0‰ and 11.9‰, and the ranges were statistically similar between the Main/'04 Break and the SMC. However, the average for $\delta^{18}O$ is lower in the SMC than in the Main/'04 Breaks. This suggests that even if the lithological influence is the strongest factor in determining the $\delta^{18}O$ values, there is still a small mineralization influence. When the whole rock $\delta^{18}O$ values were compared to elements representing alteration (Al_2O_3, Fe_2O_3, K_2O, CaO), it was found that there was a negative correlation (Figure 42). This shows that fluids with a more depleted $\delta^{18}O$ generally have stronger alteration. The depletion of the altered rock from the fresh rock confirms that the mineralizing fluid affects the host rock. This correlates to a higher temperature in the altered rock than the fresh rock, as a temperature and $\delta^{18}O$ are inversely correlated.

There is a significant difference in $\delta^{18}O$ values within the quartz separates: 10.1-12.9‰ for SMC and 11.0-14.0‰ for Main/'04 Breaks. Depleted values of the SMC suggest the possibility of a magmatic source, in addition to the mostly metamorphic source proposed within the Main/'04 Breaks (Taylor 1974; Kerrich and Watson, 1984). There was no statistically significant difference in the $\delta^{18}O$ values of the chlorite separates between the SMC (0.00‰ to 8.7‰) and the Main/'04 Breaks (-0.4‰ to 7.3‰). This is mostly likely because chlorite re-equilibrates more easily and this may be an effect of later fluids which were not a part of the mineralizing event. However, when quartz-chlorite pairs are used to calculate temperatures base on experimental equations of Clayton et al. (1972)/Wenner and Taylor (1971), and Wenner and Taylor (1971)/ Wenner and Taylor (1971) it is found that the SMC (265°C to 497°C[1]; 326°C to 646°C[2]) has a mineralizing fluid temperature range higher than the Main/'04 Breaks (128°C to 434°C[1]; 162°C to 553°C[2]). In addition, within the SMC the wide diffuse quartz-molybdenite veining zones (265°C to 410°C[1]; 326°C to 518°C[2]) have a lower mineralizing fluid temperature than the narrow cataclasite zones (437°C to 497°C[1]; 556°C to 646°C[2]). This suggests that the mineralizing fluid temperature of the wide SMC zones was cooler than the narrow SMC zones, although both are still an average hotter than the Main/'04 Breaks. This is due to the width of the linking shear structures in the wide SMC zones that would have allowed for more space for the fluids to cool, than in the narrow shear zones.

Fluid inclusions have been done in abundance on other orogenic gold deposits, especially in the Yilgarn Craton in Western Australia. Most orogenic gold deposits have been found to have supralithostatic $H_2O–CO_2–CH_4–N_2–H_2S$, with low-to-moderate salinity (Goldfarb and Groves, 2015; Ho et al., 1992; Phillips and Powell, 2010). Metal precipitation can be controlled by transient pressure drops (Sibson et al., 1988; Weatherley and Henley, 2013) and so both the ore-forming fluids and phase separation will occur both along the fluid flow path and at the site of gold deposition. Some of the variability that is seen in fluid inclusions could be accounted for these reasons (Goldfarb and Groves, 2015; Ho et al., 1992). The CO_2-rich fluids would provide the neutral pH buffering needed for high gold solubility in gold-hydrosulfide complexes (Phillips and Evans, 2004). Specifically, gold is thought to be carried in mildly alkaline low salinity ore fluids as a reduced sulphur complex such as $Au(HS)_2^-$ or $Au(HS)^0$ (Ho et al., 1992).

According to Ho et al. (1992), this ore fluid composition can be derived from either a deep sourced metamorphic fluid, or a magmatic fluid which is deep enough to separate the CO_2-rich fluid from a saline fluid. Fluid inclusion data and research found within the literature can therefore not provide further details on the source of the mineralization, nor distinguishing the magmatic and metamorphic influences.

6.2 Mineralization Sources

The results of the different components each give pieces of evidence that can lead to the possible sources of mineralization. The differences between the mineralogy, alteration, trace- and major-element geochemistry, structure, and $\delta^{18}O$ values between the Main/'04 Breaks and the SMC that have been demonstrated throughout this study all justify the source of mineralization. At the Macassa Mine, there are three possibilities of fluid source between the Main/'04 Breaks and the SMC: the fluid could be the same, the fluid could be completely different, or the fluid could invoke a difference in degree of mixing between two sources. The fluids contributing to the mineralization seen within this study have the potential to be metamorphic and/or magmatic.

There are several key differences in alteration, mineralogy and geochemistry relevant to determining the source between the Main/'04 Breaks and the SMC (Table 7). First, it is seen that there is a much wider alteration halo in the SMC (3-20m) as opposed to the Main/'04 Breaks (<3m). This suggests that there is a potential difference in temperature because a wider alteration halo is usually associated with a higher temperature fluid. Higher temperature fluids are needed to influence the wallrock at a distance from the conduit structure. As there is no difference in host lithologies, difference in permeability of the host rock is not a contributing factor for the width of alteration. The wider alteration in the SMC suggests a higher temperature fluid than the Main/'04 Breaks.

The Main/'04 Break has a different mineralogy than the SMC. The SMC has 5-7% pyrite, as opposed to 3-5% pyrite seen in the Main/'04 Breaks. There is also more tellurides and gold within the SMC. This was originally observed by Kirkland Lake Gold Inc. in core and in underground samples, as well as when they determined their reserves and resources. Their 2014 resources show the average grade is higher in the SMC (0.54oz./t)

than in the Main/'04 Breaks (0.44oz./t). The grade for the Main/'04 Breaks is similar to that seen historically within the district, with Lakeshore having the highest grade at 0.5oz./t (Kirkland Lake Gold Inc., 2013). The difference in mineralogy suggests that the fluid sources differ between the Main/'04 Breaks and the SMC, as mineralization would have been more similarly allocated if they had come from the same source. The fluids could either be completely different, or there could be a degree of mixing between sources. Textures in the SMC vary slightly from those in the Main/'04 Breaks. There is typically more brecciation and 'flooding' textures in the SMC. 'Flooding' is local terminology for wide diffuse veining which precipitates in a close network of linking parallel shear and fault structures. The brecciation suggests multiple stages of reactivation of faulting in which fluids have traveled through and been deposited under an extensional structural zone. These mineralization textures suggest differing environments in the SMC as opposed to the Main/'04 Breaks.

As previously mentioned, the SMC has more Au than the Main/'04 Breaks. It also has more Pb and Mo. Molybdenite is not typically observed as a metamorphic mineral. Elevated Bi, Te, and Mo in a fluid from orogenic gold deposits have previously been associated with a magmatic source (McCuaig and Kerrich, 1998; Kerrich and Cassidy, 1994). Although this is not always the case, (Goldfarb and Groves, 2015), it is unlikely the high concentrations of Te and Mo in the Macassa Mine have come from the surrounding host rock. The surrounding geology does not have any Mo, except in very distant ultramafic intrusions. The literature is also still unclear if metavolcanic rocks in Precambrian greenstone belts show the leaching of these minerals (Goldfarb and Groves, 2015). There is the possibility that the presence of molybdenum could suggest fluids which have come from a magmatic source at a higher temperature. The geochemistry also varies as more SiO_2 in the wide diffuse veining in the SMC, and more Cu within the narrow shearing zones of the SMC. The Cu may also suggest a magmatic influence. The Main/'04 Breaks generally have higher Cs and Th. Regardless of the possibility of metamorphic and magmatic source, the differing geochemistry suggests that there is influence from more than one source.

Table 7 - Comparison of the differences between the SMC and the Main/'04 Breaks for alteration, mineralogy, mineralization textures, and geochemistry.

	SMC	**Main/'04**
Alteration	3-20m wide	<3m
Mineralogy	5-7% pyrite More tellurides More gold *Differing mineralization textures:* brecciation, flooding	3-5% pyrite
Geochemistry	Au Mo Pb *Wide veining SMC*: SiO_2 *Narrow shearing SMC*: Cu	Cs Th

There are several possible explanations as to the formation of the SMC and the Main/'04 Breaks. However, the most likely model is the formation of the SMC as a linking Riedel shear structure between the Main/'04 Breaks to the north and the Amalgamated Break to the south (Rhys, 2008). Deformation occurring in brittle or cataclastic conditions commonly forms a pattern of faults, which include a set of conjugate shears (synthetic and antithetic Riedel shears), tension gashes, and additional shears (Dresen, 1991; Davis et al, 2000). The Larder Lake – Cadillac Deformation Zone (LLCDZ) would have produced several Riedel structures along its length. Riedel, or conjugate, shears typically form about 15° to the main fault (Tchalenko, 1970), and this is observed both within the Main/'04 Break and the Amalgamated Break with respect to the LLCDZ. As the stress continues, expansion linking structures between the original conjugate shears form.

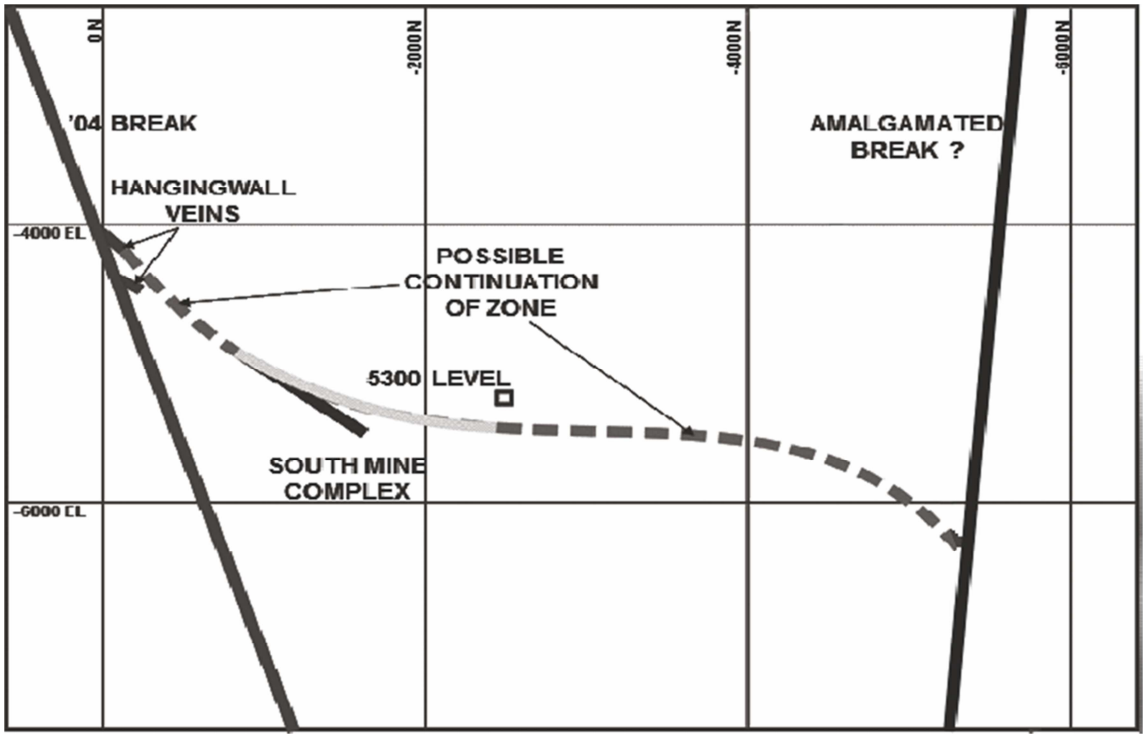

Figure 47 – Inset from Figure 6, showing a schematic of a cross-section looking east. The '04 Break is seen dipping steeply south in the north of the diagram, the SMC is in the center dipping gently to the south, and the Amalgamated Break is seen in the south of the diagram dipping very steeply north. Dashed lines represent the potential unproven continuation of the SMC to the north linking to the '04 Break and to the south linking to the Amalgamated Break at depth as a linking Riedel Shear structure.

The '04 Break and the SMC are likely structurally related (Figure 47) through a Riedel Shear structure (Rhys, 2008). The '04 Break is seen dipping steeply to the south in the north of the schematic. The South Mine Complex (SMC) is south of the '04 Break and dips much more shallowly than the Main/'04 Breaks. This shallow dipping system is atypical of mineralization in the district and is thought to be a Riedel Shear linking structure between the '04 Break to the north, and the Amalgamated Break to the south. This linking structure is most likely the conduit for mineralizing fluids. This would make it unlikely that there were two separate systems, and quite possible that there was a difference in degree of mixing between sources in the SMC and the Main/'04 Breaks.

The variability between the SMC and the Main/'04 Break $\delta^{18}O$ values of quartz separates suggests that there is variability within the fluids. The difference in stable oxygen isotope values within quartz separate allows us to hypothesize that there are different gold

mineralization sources between the two systems (Taylor, 1974). The Riedel shear model can account for a different fluid entering the system from the Amalgamated Break. The depleted values suggest two main possibilities for the SMC: the first being that there is a higher temperature metamorphic fluid, and the second is the possibility of an addition of a magmatic source, in addition to the metamorphic source found within the Main/'04 Breaks.

This study proposes to explain the differences between the SMC and the Main/'04 Breaks as a difference in the degree of mixing occurring between two sources: a metamorphic source, and a potential magmatic source. The evidence for this is as follows.

Firstly, since the Main/'04 Breaks and the SMC are structurally connected, it forms a conduit for a potential magmatic source to come from the south, where there are known to be syenitic plutons (Figure 2). In a Riedel Shear type structure (Figure 47), there are multiple stages of structural activity. As conduits for shearing remain similar in a structural system, there could have been reactivation of the faults that were previously mineralized, and fluids could have mixed. Early metamorphic fluids would have been activated during early stage of the Riedel shear and mineralized the Main/'04 Break when there were no linking structures. As the system progresses, the linking structures open between the two Riedel shears. The Amalgamated Break to the south could have tapped into magmatic fluids from depth to the south and concentrated the gold within the sinks it passed through. The newly opened linking structures would be optimal sinks for gold mineralization. The zones closer to the source would have generally had a stronger magmatic influence.

The wide diffuse veining that is observed within some of the SMC, in particular the NSZ and the Barchetta, could be evidence of some of the stronger deposition of the fluids to the south within the linking structures. This is sometimes observed within hand samples as brecciation of earlier mineralization, and as mineralization in wide diffuse veining. These textures are indicative of the presence of space given by the opening of the linking structure. Since these textures are mostly found within south-eastern portion of the SMC, it follows that the new fluids would be coming from the south.

These south-eastern portions of the SMC, which are hypothesized to be closer to the magmatic source, have higher Mo and Te, which are more likely to have originated from a magmatic source than from a metamorphic source. Finally, the larger alteration haloes in these locations and the depleted oxygen isotope values suggest a hotter temperature in the SMC. A hotter temperature in the SMC is consistent with a possible magmatic component in the SMC.

All of these lines of evidence agree with a magmatic component in the SMC which would have been introduced along the Riedel Shear structure from depth in the south. The difference in fluids within the zones can be attributed to either the mixing of two fluids, magmatic and metamorphic, at the same time, or a metamorphic fluid which has been partially reactivated by magmatic fluids. The scope of this study does not provide sufficient evidence for one possibility over the other.

6.3 Other Orogenic Deposits

Orogenic gold deposits are found worldwide. These include the Yilgarn Craton (Western Australia), the Jiaodong province (China), the Superior and Slave Provinces (Canada), and the Kolar Schist Belt (India) (Groves, 1993). The Superior Province and the Yilgarn Craton are the largest and best preserved Archean cratons for studying greenstone hosted gold (Dubé and Gosselin, 2007). The Macassa Mine is found within the Abitibi Greenstone Belt in the Superior Province.

Orogenic gold deposits are enriched in S, Cu, Mo, Sb, Bi, W, Pb, Zn, Te, Hg, As, and Ag (Goldfarb et al., 2005; Richards, 2009; Tomkins, 2013). Horvath (2010) found higher in Ag, Ba, Sr, Rb, Cu, Mo, As, Bi, Sb, Se, and Te. Kerrich and Watson (1984) measured enriched Te, Mo, W, Ag, Pb, As, and Sb. This study found higher values of Ag, Mo, As, Cu, Pb, and As in the mineralization. Ridley and Diamond (2000) suggest that it is unlikely that orogenic ore-fluid compositions are reflective of the fluid source. Instead, they represent the influence of fluid-rock interactions and depositional processes.

Temperatures for orogenic gold deposits are thought to optimally form between 300-550°C (Tomkins, 2010), but often are within a larger range between 180°C and 700°C

(Phillips and Powell, 2009). Temperatures calculated by Kerrich and Watson (1984) for the Main/'04 Break are between 350°C and 460°C, and by Horvath (2010) for the SMC are between 219°C and 349°C. This study calculated SMC temperatures between 265°C and 646°C. The higher temperatures calculated in this study may be due to chlorite and quartz being in disequilibrium by forming at different times, however, rigorous petrography has been done on samples analyzed for $\delta^{18}O$ in mineral separates and shows textural equilibrium (Section 5.3.2).

Traditionally, the source for orogenic gold was thought to be either from fluids being generated in metamorphic rocks as temperatures increase, or from the release of fluids as felsic-intermediate magmas crystallize. The most prevalent opinion was that metamorphic rocks are the source of the deposits (Goldfarb et al., 2005; Phillips and Powell, 2010; Tomkins, 2013). However, a continuum model has also been suggested (Groves, 1993; Goldfarb et al., 2005; Phillips and Powell, 2009) where the orogenic deposits are from a crustal continuum in temperature-pressure regimes that range over a 20-25km profile (Figure 48). Sources are a combination of metamorphic, magmatic, and mantle-lower crust depending on the position within the continuum (Phillips and Powell, 2009). The mineralization of the orogenic deposits forms at the peak of metamorphism. The entire depth continuum of deposits is not recorded in one single gold camp or greenstone belt (Groves, 1993). The Yilgarn orogenic gold systems in Australia is thought to be a mix of a deeply distally derived reduced fluid with a proximal oxidizing magmatic fluid (Hodkiewicz et al., 2009)

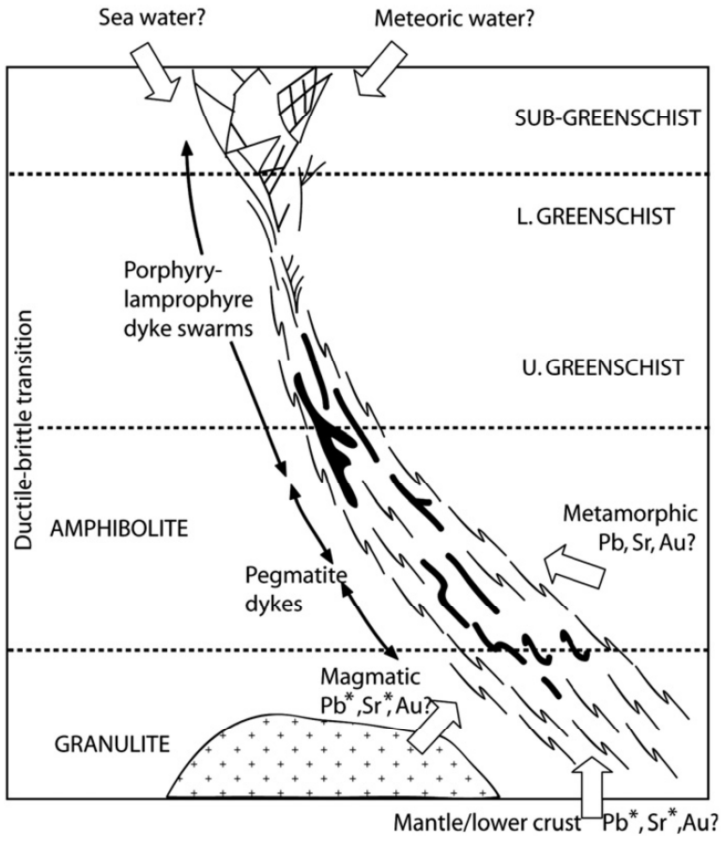

Figure 48 - Diagram of the continuum model. This is over a 20-25 km vertical profile with conditions ranging between granulite to sub-greenschist facies (from Phillips and Powell, 2009, after Groves, 1993). Macassa Mine is in the greenschist facies, although source fluid may have come from further down the profile.

Kerrich and Watson (1984) suggest that the lower $\delta^{18}O$ and δD that were calculated for fluids in the Main/'04 Breaks with quartz-chlorite-magnetite triplets are due in part to a primary magmatic source as well as the traditionally described metamorphic source. The calculated fluids fall within the primary magmatic sources described by Taylor (1974). Horvath (2010) later found that the SMC has lower $\delta^{18}O$ values than those in Main/'04 Breaks found by Kerrich and Watson (1984) and proposed that there was a stronger magmatic influence in the SMC. This study confirms the SMC is more depleted than the Main/'04 Breaks and could either suggest a stronger magmatic influence or a hotter metamorphic influence (Section 6.2).

6.4 Further Work

Further work should be continued in a few areas. Firstly, further data is required to differentiate between a mixing of fluids and a reactivation by magmatic fluids. This can be done by detailing a paragenesis of veining and brecciation, and mapping this paragenesis throughout both systems. Mineral separate triplets on each vein stage should then be done to determine $\delta^{18}O$ and δD values so as to better determine fluid origin and mineralizing fluid temperature. A fluid inclusion study would also be beneficial to compare the fluid composition to those found within other orogenic gold deposits.

Age dating would be extremely beneficial in defining the system. However, as noted by the author, attempts to procure a molybdenite sample unaffected by late reactivation of the system with large enough crystals have so far not been successful. However, if an age was procured from the SMC and the Main/'04 Breaks, it would define the sequence of mineralization. If the Main/'04 Breaks was older than the SMC, and not syn-deposited, this would be another point of evidence for the Riedel Linking Model.

Finally, μXRD and XANES work on pyrites, gold grains, and tellurides was obtained using synchrotron technologies. The time constraints of this study did not allow for the refinement and analysis of this data, but preliminary studies show interesting variations in elemental mapping within mineralized grains, and between the different zones. Further studies should continue the analysis of the μXRD and XANES data.

References

Alexander, E.C., Srinivasan, B, Manuel, O.K. 1969. Xenon in Kirkland Lake Tellurides. Earth and Planetary Science Letters, 5: 478 – 482.

Ayer, J.A., Thurston, P.C., Bateman, R., Dubé, B., Gibson, H.L., Hamilton, M.A., Hathway, B., Hocker, S.M., Houlé, M.G., Hudak, G., Ispolatov, V.O., Lafrance, B., Lesher, C.M., MacDonald, P.J., Péloquin, A.S., Piercey, S.J., Reed, L.E. and Thompson, P.H. 2005. Overview of results from the Greenstone Architecture Project: Discover Abitibi Initiative; Ontario Geological Survey, Open File Report 6154, 146p

Basu, A.R., Goodwin, A.M., Tatsumoto, M. 1984. Sm/Nd study of Achaean alkalic rocks from the Superior Province of the Canadian Shield. Earth Planet Science Letters, 70: 40-46.

Calvert, A. J., Ludden, J. N. 1999. Archean continental assembly in the southeastern Superior Province of Canada. Tectonics, 18: 412-429

Capdevila, R., Goodwin, A.M., Ujike, O., Gorton, M.P. 1982. Trace-element geochemistry of Archean volcanic rocks and crustal growth in southwestern Abitibi Belt, Canada. Geology, 10:418-422.

Card, K.D., 1990. A review of the Superior Province of the Canadian Shield, a product of Archean accretion. Precambrian Research, 48: 99-156.

Card, K.D., Ciesielski, A. 1986. DNAG#1 Subdivisions of the Superior Province of the Canadian Shield. Geoscience Canada, 13 (1): 5-13.

Charlewood, G.H., 1964. Geology of deep development on the main ore zone at Kirkland Lake. Ontario Department of Mines, Geological Circular, 11, 49p.

Clark, G.R., 2013. Kirkland Lake Gold Inc.: Review of Resources and Reserves of Macassa Mine, Kirkland Lake, Ontario. Technical Report.

Clark, G.R., 2014. Kirkland Lake Gold Inc.: Review of Resources and Reserves of Macassa Mine, Kirkland Lake, Ontario. Technical Report.

Clayton, R.N., Mayeda, T.K. 1963. The use of bromine pentafluoride in the extraction of oxygen from oxides and silicates for isotopic analysis. Geochimica et Cosmochimica Acta, 27: 43 – 52.

Clayton, R.N., O'Neil, J.R., Mayeda, T.K. 1972. Oxygen Isotope Exchange between Quartz and Water. Journal of Geophysical Research, 77 (17): 3057 – 3067.

Cole, D.R., Chakraborty, S. 2001. Rates and Mechanisms of Isotopic Exchange. Stable Isotope Geochemistry, Reviews in Mineralogy and Geochemistry, 43.2, 83 - 224

Cole, D.R., Ripley, E.M. 1998. Oxygen isotope fractionation between chlorite and water from 170 to 350°C: A preliminary assessment based on partial exchange and fluid/rock experiments. Geochimica et Geocosmochimica Acta, 63 (3/4): 449 – 457.

Corfu, F., 1993. The Evolution of the Southern Abitibi Greenstone Belt in Light of Precise U-Pb Geochronology. Economic Geology, 88: 1323-1340.

Corfu, F., Jackson, S.L., Sutcliffe, R.H. 1991. U-Pb ages and tectonic significance of late Archean alkalic magmatism and nonmarine sedimentation: Timiskaming Group, southern Abitibi belt, Ontario. Canadian Journal of Earth Sciences, 28: 489-503.

Davis, G.H., Bump, A.P, García, P.E., Ahlgren, S.G. 2000. Conjugate Riedel deformation band shear zones. Journal of Structural Geology, 22: 169-190.

Dimroth, E., Boivin, P., Goulet, N., Laroche, M. 1973. Tectonic and volcanic analytical studies in the Rouyn-Noranda area; Open File Report, Department of Natural Resources, Quebec.

Dimroth, E., Imreh, L., Goulet, N., Rocheleau, M. 1983. Evolution of the south-central segment of the Archean Abitibi Belt, Quebec. Part III: Plutonic and metamorphic evolution and geotectonic model. Canadian Journal of Earth Sciences, 20: 1374-1388.

Dresen, G. 1991. Stress Distribution and the orientation of Riedel shears. Tectonophysics, 188: 239-247.

Dubé, B., and Gosselin, P., 2007, Greenstone-hosted quartz-carbonate vein deposits, in Goodfellow, W.D., ed., Mineral Deposits of Canada: A Synthesis of Major Deposit-Types, District Metallogeny, the Evolution of Geological Provinces, and Exploration Methods: Geological Association of Canada, Mineral Deposits Division, Special Publication No. 5, p. 49-73.

Ewert, W. D., Puritch, E., Burga, D., & Armstrong, T. (2011). Technical report and resources estimate for the Upper Canada gold deposit of the Kirkland Lake gold project Gauthier Township, Kirkland Lake north-eastern Ontario, Canada. Brampton, ON: P&E Mining Consultants Inc (Canada).

Hoefs, J. 2004. Stable Isotope Geochemistry, 5th revision and updated edition. Springer-Verlag, Berlin Heidelberg, New York.

Hoffman, P.F. 1988. United Plates of America, The Birth of a Craton: Early Proterozoic Assembly and Growth of Laurentia. Ann.Rev. Earth Planet. Sci, 16: 543-603.

Gebre-Mariam, M., Hagemann, S.G., Groves, D.I. 1995. A classification scheme for epigenetic Archaean lode-gold deposits. Mineralium Deposita, 30: 408 – 410.

Gibb, R.A. 1983. Model for suturing of Superior and Churchill plates: An example of double indentation tectonics. Geology, 11:413-417.

Goldfarb, R.J., Baker, T., Dubé, B., Groves, D.I., Hart, C.J.R., Gosselin, P. 2005. Distribution, character, and genesis of gold deposits in metamorphic terranes, *in* Hedenquist, J.W., Thompson, J.F.H., Goldfarb, R.J., Richards, J.P., eds., Economic Geology. 100th Anniversary Volume 1905-2005: Littleton, Colorado, Society of Economic Geologists, p. 407-450.

Goldfarb, R.J., Groves, D.I. 2015. Orogenic gold: Common or evolving fluid and metal sources through time. Lithos, 233: 2-26.

Goodwin, A.M. 1977. Archean volcanism in Superior Province, Canadian Shield. Geological Association of Canada Special Paper, 16: 205-241.

Gresens, R.L. 1967. Composition-Volume Relationships of Metasomatism. Chemical Geology, 2: 47-65.

Groves, D.I. 1993. The crustal continuum model for late-Archean lode-gold deposits of the Yilgarn Block, Western Australia. Mineralium Deposita, 28: 366-374.

Guha, J., Lu, H.-Z., Dubé, B. 1991. Fluid Characteristics of Vein and Altered Wall Rock in Archean Mesothermal Gold Deposits. Economic Geology, 86: 667 – 684.

Ho, S.E., Groves, D.I., McNaughton, N.J., Mikucki, E.J. 1992. The source of ore fluids and solutes in Archean lode-gold deposits of Western Australia. Journal of Volcanology and Geothermal Research, 50: 173 – 196.

Hodgson, C.J., Hamilton, J.V. and Guimond, R.P., 1991. Relationship between gold deposits and the tectonic framework of the Abitibi greenstone belt in the Kirkland Lake-Larder Lake area. Ontario Ministry of Northern Development and Mines.

Horvath, S., 2010. Geochemical and Isotopic Examination of the South Mine Complex, Macassa Mine, Abitibi Sub Province. Unpublished M.Sc. Thesis, Western University, Ontario.

Houlé, M.G., Ayer, J.A., Baldwin, G., Berger, B.R., Dinel, E., Fowler, A.D., Moulton, B., Saumur, B.-M., Thurston, P.C. 2008. Field trip guidebook to the stratigraphy and volcanology of supracrustal assemblages hosting base metal and gold mineralization in the Abitibi greenstone belt, Timmins, Ontario. Ontario Geological Survey, Open File Report 6225, 84p.

Hyde, R.S. 1980. Sedimentary facies in the Archean Timiskaming Group and their tectonic implications, Abitibi greenstone belt, northeastern Ontario, Canada. Precambrian Research, 12: 161-195.

Ispolatov, V., Lafrance, B. 2008. Geologic and Structural Setting of Gold Mineralization in the Kirkland Lake-Larder Lake Gold Belt, Ontario. Economic Geology, 103: 1309 – 1340.

Ispolatov, V., Lafrance, B., Dubé, B., Hamilton, M. and Creaser, R. 2005. Geology, Structure, and gold mineralization, Kirkland Lake and Larder Lake areas (Gauthier and Teck Townships): Discover Abitibi Initiative; Ontario Geological Survey, Open File Report 6159, 170 p.

Jackson, S.L. 1991. Structural and stratigraphitic studies in the Kirkland Lake – Larder Lake area. Ontario Geological Survey, Miscellaneous Paper 157: 82-90.

Jackson, S.L., Fyon, J.A., 1991. The Western Abitibi Subprovince in Ontario. In: Geology of Ontario. Edited by: P.C. Thurston, H.R. Williams, R.H. Sutcliffe, and G.M. Scott, Ontario Geological Survey, 4(1): 405-475.

Jolly, W.T., 1978, Metamorphic History of the Archean Abitibi Belt; Metamorphism in the Canadian Shield, Geol. Surv. Canada.

Kerrich, R. 1983. Geochemistry of gold deposits in the Abitibi greenstone belt. Canadian Inst. Mining Metall. Special Paper 27, 75 p.

Kerrich, R. 1986. Fluid Infiltration into Fault Zones: Chemical, Isotopic, and Mechanical Effects. Pageoph, 124 (1,2): 225 – 268.

Kerrich, R. 1988. Detachment zones of Cordilleran metamorphic core complexes: thermal, fluid and metasomatic regimes. Geologische Rundschau, 77 (1): 157-182.

Kerrich, R., Cassidy, K.F. 1994. Temporal relationships of lode gold mineralization to accretion, magmatism, metamorphism and deformation – Archean to present: A review. Ore Geology Reviews, 9: 263 – 310.

Kerrich, R., Fyfe, W.S. 1981. The Gold-Carbonate Association: Source of CO2, and CO2 Fixation Reactions in Archaean Lode Deposits. Chemical Geology, 33: 265 – 294.

Kerrich, R, Fryer, B.J. 1978. Archaean precious-metal hydrothermal systems, Dome Mine, Abitibi Greenstone Belt. II. REE and oxygen isotope relations. Canadian Journal of Earth Science, 16: 440-458.

Kerrich, R. and Watson, G. P. 1984. The Macassa Mine Archean Lode Gold Deposit, Kirkland Lake, Ontario: Geology, Patterns of Alteration, and Hydrothermal Regimes. Economic Geology, 79: 1104-1130.

Kirkland Lake Gold Inc. 2013. Intermediate Gold Production in Ontario High Grade Camp [online]. Available from www.klgold.com. [Accessed 9 January 2014].

Lackey, T.N.L., 1990. Alkaline Tuffs at Kirkland Lake, Ontario. M.Sc. Thesis, Queen's University.

MacLean, W.H., Barrett, T.J. 1993. Lithogeochemical techniques using immobile elements. Journal of Geochemical Exploration, 48: 109-133.

McCuaig, T.C., Kerrich, R. 1998. P-T-t deformation-fluid characteristics of lode gold deposits: evidence from alteration systematics. Ore Geology Reviews, 12: 381 – 453.

Mikuchki, E.J. 1998. Hydrothermal transport and depositional processes in Archean lode-gold systems: A review. Ore Geology Reviews, 13: 307 – 321.

Mining Association of Canada. 2014. Mining Facts [online]. Available from www.mining.ca/resources/mining-facts. [Accessed September 23, 2014].

Mueller, W., Donaldson, J.A.1992. Development of sedimentary basins in the Archean Abitibi belt, Canada : an overview. Canadian Journal of Earth Science, 29: 2249 – 2265.

Percival, J.A. and Card, K.D. 1983. Archean crust as revealed in the Kapuskasin uplift, Superior Province, Canada. Geology, 11: 323-326.

Phillips, G.N., Evans, K.A., 2004. Role of CO_2 in the formation of gold deposits. Nature, 429: 860–863.

Phillips, G.N., Powell, R. 1993. Link between gold provinces. Economic Geology, 88: 1084-1098.

Phillips, G.N., Powell, R. 2010. Formation of gold deposits: a metamorphic devolatilization model. Journal of Metamorphic Geology, 28: 689 – 718.

Poulsen, K.H., Robert, F., Dubé, B. 2000. Geological Classification of Canadian Gold Deposits. Geological Survey of Canada, Bulletin 540, 106 p.

Rhys, D. 2005. Structural Study of the Kirkland Lake Gold System, Ontario, with exploration implications. Unpublished report for Kirkland Lake Gold Inc., 84 pages plus petrographic descriptions.

Rhys, D. 2006. Summary of June-July, 2006 structural work at the Macassa mine. Unpublished report for Kirkland Lake Gold Inc., 20 pages plus petrographic descriptions.

Rhys, D. and Ross, K. 2008. Summary of 2007 structural and petrographic work in the South Mine Complex, Macassa mine. Unpublished report for Kirkland Lake Gold Inc., 25 pages plus petrographic descriptions.

Rhys, D. 2013 Update of Geological Observations and Assessment of Structural Controls on Oreshoots from a Site Visit to the Macassa Mine. Unpublished report for Kirkland Lake Gold Inc., 29 pages plus petrographic descriptions.

Richards, J.P. 2009. Postsubduction porphyry Cu-Au and epithermal Au deposits: Products of remelting of subduction-modified lithosphere. Geology, 37: 247-250.

Ridley, J.R., Diamond, L.W. 2000. Fluid Chemistry of Orogenic Lode Gold Deposits and Implications for Genetic Models. SEG Reviews, 13: 141-162.

Savage, W.S. 1964. Mineral Resources and Mining Properties in the Kirkland Lake-Larder Lake Area. Mineral Resources Circular No. 3, Ontario Department of Mines, 114 pg.

Shelton, K. L., McMenamy, T.A., van Hees, E.H.P., Falck, H. 2004. Deciphering the Complex Fluid History of a Greenstone-Hosted Gold Deposit: Fluid Inclusion and Stable Isotope Studies of the Giant Mine, Yellowknife, Northwest Territories, Canada. Economic Geology, 99: 1643-1663.

Sibson, R.H., Robert, F., Poulsen, K.H., 1988. High-angle reverse faults, fluid pressure cycling, and mesothermal gold–quartz deposits. Geology 16, 551–555.

Spooner, E.T.C. 1993. Magmatic sulphide/volatile interaction as a mechanism for producing chalcophile element enriched, Archean Au-quartz, epithermal Au-Ag and Au skarn hydrothermal ore fluids. Ore Geology Review, 7 (5): 359 – 379.

Still, A.C. 2001. Structural Setting and Controls of Gold Mineralization at the Macassa Mine. M.Sc Thesis, Queen's University.

Taylor, B.E., de Kemp, E., Grunsky, E., Martin, L., Maxwell, G., Rigg, D., Goutier, J., Lauzière, K., Dubé, B. 2014. Three-Dimensional Visualization of the Archean Horne and Quemont Au-Bearing Volcanogenic Massive Sulfide Hydrothermal Systems, Blake River Group, Quebec. Economic Geology, 109: 183 – 203.

Taylor, H.P. 1974. The Application of Oxygen and Hydrogen Isotope Studies to Problems of Hydrothermal Alteration and Ore Deposition. Economic Geology, 69: 843 – 883.

Taylor, H. P. and Epstein, S. 1962. Relationship Between O18/O16 Ratios in Coexisting Minerals of Igneous and Metamorphic Rocks. Geological Society of America Bulletin, 73: 461-480.

Tchalenko, J.S. 1970. Similarities between Shear Zones of Different Magnitudes. Geological Society of America Bulletin, 81: 1625-1640.

Thomson, J.E., 1948. Regional structure of the Kirkland Lake – Larder Lake area. In Structural geology of Canadian ore deposits: Canadian Institution of Mining and Metallurgy, p 627 – 632.

Thomson, J.E., 1950. Geology of the Teck Township and Kenogami Lake Area. Ontario Department of Mines, Annual Report for 1948. **57,** 5:1-53.

Thomson, J.E., Charlewood, G.H., Griffin, K., Hawley, J.E., Hopkins, H., MacIntosh, C.G., Ogrizio, S.P., Perry, O.S., and Ward, W., 1950. Geology of the main ore zone at Kirkland Lake. Ontario Department of Mines, Annual Report for 1948. **57,** 5:54-196.

Thurston, P.C., Chivers, K.M. 1990. Secular Variation in Greenstone Sequence Development Emphasizing Superior Province, Canada. Precambrian Research, 46: 21-58.

Todd, E.W. 1928. Kirkland Lake Gold Area. Ontario Department of Mines. **37, 2:** 1-92.

Tyrell, J.B., Hore, R.E. 1926. The Kirkland Lake Fault. Transactions of the Royal Society of Canada, 3rd Series, **20,** 4:51-63.

Ujike, O. 1985. Geochemistry of Archean alkalic volcanic rocks from the Crystal Lake area, east of Kirkland Lake, Ontario, Canada. Earth Planet Science Letters, 73: 333-344.

Watson, G.P. 1984. Ore Types and Fluid Regimes: Macassa Gold Mine, Kirkland Lake. PhD Thesis, University of Western Ontario. 365pg.

Weatherley, D.K., Henley, R.W., 2013. Flash vaporization during earthquakes evidenced by gold deposits. Nature Geoscience 6, 294–298.

Wenner, D.B., Taylor, H.P. 1971. Temperatures of Serpentinization of Ultramafic Rocks Based on O18/O16 Fractionation between Coexisting Serpentine and Magnetite. Contributions of Mineralogy and Petrology, 32: 165 – 185.

Wilkinson, L., Cruden, A.R., Krogh, T.E. 1999. Timing and kinematics of post-Timiskaming deformation within the Larder Lake – Cadillac deformation zone, southwest Abitibi greenstone belt, Ontario, Canada. Canadian Journal of Earth Sciences, 36: 627 – 647.

Appendices

Appendix A : Sample Overview and Associated Studies

In this appendix, samples are listed with their associated hole or heading, lithology, mineralized zone, extent of mineralization, and if they have been used for optical microscopy, XRD, multi-element analysis, whole rock oxygen isotopes, and chlorite and quartz separates.

Sample	Heading or Hole Number	Lithology	Zone	Mineralization	Thin Section	XRD	Multi-element Analysis	Whole Rock $\delta^{18}O$	$\delta^{18}O_{qtz}$	$\delta^{18}O_{chl}$
LSKGI001	53-2254	Syenite Porphyry	NSZ	None						
LSKGI002	53-2254	Bedded Tuff	NSZ	Alteration		x				
LSKGI003	53-2254	Bedded Tuff	NSZ	Mineralized						
LSKGI004	53-2254	Bedded Tuff	NSZ	None		x				
LSKGI005	53-2254	Syenite Porphyry	NSZ	Weak Alteration						
LSKGI006	53-2254	Syenite Porphyry	NSZ	Weak Alteration						
LSKGI007	53-2254	Syenite Porphyry - Bedded Tuff	NSZ	Mineralized						
LSKGI008	53-2112	Syenite Porphyry	NSZ	None						
LSKGI009	53-2112	Syenite Porphyry	NSZ	Weak Alteration		x				
LSKGI010	53-2112	Syenite Porphyry	NSZ	Alteration	x	x		x		
LSKGI011	53-2112	Syenite Porphyry	NSZ	Mineralized	x	x		x		
LSKGI012	53-2112	Syenite Porphyry	NSZ	Alteration		x				
LSKGI013	53-2112	Syenite Porphyry	NSZ	Weak Alteration		x				
LSKGI014	53-2112	Lapilli Tuff	NSZ	None						
LSKGI015	53-2112	Syenite Porphyry	NSZ	Mineralized		x				
LSKGI016	53-2112	Syenite Porphyry - Bedded Tuff	NSZ	Mineralized		x				
LSKGI017	53-2283	Syenite Porphyry	NSZ	None						
LSKGI018	53-2283	Syenite Porphyry	NSZ	Alteration		x				
LSKGI019	53-2283	Syenite Porphyry	NSZ	Weak Alteration		x				
LSKGI020	53-2283	Syenite Porphyry	NSZ	Mineralized		x				
LSKGI021	53-2283	Syenite Porphyry	NSZ	Alteration						
LSKGI022	53-2283	Bedded Tuff	NSZ	Weak Alteration						
LSKGI023	53-2283	Syenite Porphyry	NSZ	None						
LSKGI024	53-2283	Syenite Porphyry	NSZ	Mineralized	x	x		x		
LSKGI025	53-2260	Syenite Porphyry	NSZ	None						

Sample	Heading or Hole Number	Lithology	Zone	Mineralization	Thin Section	XRD	Multi-element Analysis	Whole Rock $\delta^{18}O$	$\delta^{18}O_{qtz}$	$\delta^{18}O_{chl}$
LSKGI026	53-2260	Syenite Porphyry	NSZ	Weak Alteration		x				
LSKGI027	53-2260	Syenite Porphyry	NSZ	Alteration						
LSKGI028	53-2260	Syenite Porphyry	NSZ	Mineralized						
LSKGI029	53-2260	Type II Porphyry	NSZ	Alteration						
LSKGI030	53-2260	Type II Porphyry	NSZ	Weak Alteration						
LSKGI031	53-2260	Type II Porphyry	NSZ	None						
LSKGI032	53-2260	Syenite Porphyry	NSZ	Mineralized						
LSKGI033	53-2260	Syenite Porphyry - Type II Porphyry	NSZ	Mineralized						
LSKGI034	53-1983	Syenite Porphyry	NSZ	None						
LSKGI035	53-1983	Syenite Porphyry	NSZ	Alteration						
LSKGI036	53-1983	Syenite Porphyry	NSZ	Mineralized						
LSKGI037	53-1983	Syenite Porphyry	NSZ	Alteration						
LSKGI038	53-1983	Syenite Porphyry	NSZ	Mineralized						
LSKGI039	53-1983	Syenite Porphyry	NSZ	Alteration						
LSKGI040	53-1983	Syenite Porphyry	NSZ	None						
LSKGI041	53-1983	Syenite Porphyry	NSZ	Mineralized	x					
LSKGI042	53-1983	Syenite Porphyry	NSZ	Mineralized						
LSKGI043	53-2291	Augite Syenite	NSZ	None						
LSKGI044	53-2291	Augite Syenite	NSZ	Weak Alteration						
LSKGI045	53-2291	Augite Syenite	NSZ	Alteration		x				
LSKGI046	53-2291	Augite Syenite	NSZ	Mineralized	x	x				
LSKGI047	53-2291	Augite Syenite	NSZ	Alteration	x	x				
LSKGI048	53-2291	Augite Syenite	NSZ	Weak Alteration						
LSKGI049	53-2291	Augite Syenite	NSZ	None						
LSKGI050	53-2291	Augite Syenite	NSZ	Mineralized	x	x	x	x	x	x

Sample	Heading or Hole Number	Lithology	Zone	Mineralization	Thin Section	XRD	Multi-element Analysis	Whole Rock $\delta^{18}O$	$\delta^{18}O_{qtz}$	$\delta^{18}O_{chl}$
LSKGI051	53-2329	Tuff	NSZ	None						
LSKGI052	53-2329	Syenite Porphyry	NSZ	Weak Alteration						
LSKGI053	53-2329	Syenite Porphyry	NSZ	Mineralized	x	x	x	x		
LSKGI054	53-2329	Syenite Porphyry	NSZ	Mineralized	x	x	x	x		
LSKGI055	53-2329	Syenite Porphyry	NSZ	Alteration		x				
LSKGI056	53-2329	Syenite Porphyry	NSZ	Weak Alteration						
LSKGI057	53-2329	Syenite Porphyry	NSZ	None			x			
LSKGI058	53-2329	Tuff	NSZ	Mineralized		x				
LSKGI059	53-2336	Augite Syenite	NSZ	None						
LSKGI060	53-2336	Augite Syenite	NSZ	Weak Alteration		x				
LSKGI061	53-2336	Syenite Porphyry	NSZ	Alteration		x				
LSKGI062	53-2336	Syenite Porphyry	NSZ	Mineralized						
LSKGI063	53-2336	Syenite Porphyry	NSZ	Alteration						
LSKGI064	53-2336	Syenite Porphyry	NSZ	Weak Alteration						
LSKGI065	53-2336	Syenite Porphyry	NSZ	None						
LSKGI066	53-2336	Augite Syenite - Syenite Porphyry	NSZ	Mineralized		x				
LSKGI067	53-2336	Syenite Porphyry	NSZ	Mineralized						
LSKGI068	53-2336A	Augite Syenite	NSZ	None						
LSKGI069	53-2336A	Augite Syenite	NSZ	Weak Alteration		x				
LSKGI070	53-2336A	Syenite Porphyry	NSZ	Alteration		x				
LSKGI071	53-2336A	Syenite Porphyry	NSZ	Mineralized		x				
LSKGI072	53-2336A	Syenite Porphyry	NSZ	Mineralized		x				
LSKGI073	53-2336A	Syenite Porphyry	NSZ	Alteration						
LSKGI074	53-2336A	Syenite Porphyry	NSZ	Weak Alteration						
LSKGI075	53-2336A	Syenite Porphyry	NSZ	None						
LSKGI076	53-2336A	Syenite Porphyry	NSZ	Mineralized						

Sample	Heading or Hole Number	Lithology	Zone	Mineralization	Thin Section	XRD	Multi-element Analysis	Whole Rock $\delta^{18}O$	$\delta^{18}O_{qtz}$	$\delta^{18}O_{chl}$
LSKGI077	5315	Syenite Porphyry	#7 HW	Alteration	x	x				
LSKGI078	5315	Syenite Porphyry	#7 HW	Alteration		x				
LSKGI079	5315	Tuff	#7 HW	Mineralized	x	x	x	x		
LSKGI080	5315	Tuff	#7 HW	Mineralized	x	x	x	x		
LSKGI081	5315	Tuff	#7 HW	Alteration		x				
LSKGI082	5609	Syenite Porphyry	Barchetta	Mineralized	x	x	x	x		
LSKGI083	5609	Syenite Porphyry	Barchetta	Mineralized		x				
LSKGI084	5609	Syenite Porphyry	Barchetta	Mineralized		x				
LSKGI085	5609	Syenite Porphyry	Barchetta	Alteration	x	x	x	x		
LSKGI086	5604	Syenite Porphyry	NSZ	Mineralized						
LSKGI087	5604	Tuff	NSZ	Alteration						
LSKGI088	5604	Tuff	NSZ	Weak Alteration						
LSKGI089	5604	Tuff	NSZ	Alteration						
LSKGI090	5604	Syenite Porphyry	NSZ	Mineralized	x					
LSKGI091	5317	Syenite Porphyry	#7	Mineralized	x	x	x	x		
LSKGI092	5317	Syenite Porphyry	#7 HW	Mineralized	x	x				
LSKGI093	5317	Syenite Porphyry	#7	Alteration		x				
LSKGI094	5317	Syenite Porphyry	#7	Alteration	x	x	x	x		
LSKGI095	5317	Tuff	#7	Weak Alteration		x				
LSKGI096	5018	Tuff	04 HW	None		x				
LSKGI097	5018	Tuff	04 HW	Weak Alteration	x	x	x			
LSKGI098	5018	Tuff	04 HW	Mineralized	x	x	x	x	x	
LSKGI099	5018	Tuff	04 HW	None		x				
LSKGI100	5016	Augite Syenite	04	Mineralized	x	x	x	x		
LSKGI101	5016	Augite Syenite	04	Alteration		x				
LSKGI102	5016	Tuff	04	Mineralized		x				

Sample	Heading or Hole Number	Lithology	Zone	Mineralization	Thin Section	XRD	Multi-element Analysis	Whole Rock $\delta^{18}O$	$\delta^{18}O_{qtz}$	$\delta^{18}O_{chl}$
LSKGI103	5016	Tuff	04	Mineralized	x	x	x	x		
LSKGI104	5016	Tuff	04	Weak Alteration		x				
LSKGI105	5106	Syenite Porphyry	LDN FW	Mineralized	x	x	x	x	x	
LSKGI106	5106	Syenite Porphyry	LDN FW	Mineralized	x	x	x	x		
LSKGI107	5106	Syenite Porphyry	LDN FW	Alteration		x				
LSKGI108	5106	Tuff	LDN FW	Weak Alteration		x				
LSKGI109	5311	Tuff	NSZ	Weak Alteration		x				
LSKGI110	5311	Tuff	NSZ	Alteration		x				
LSKGI111	5311	Tuff	NSZ	Mineralized	x	x	x	x	x	x
LSKGI112	5311	Tuff - Syenite Porphyry	NSZ	Alteration		x				
LSKGI113	3827	Syenite Porphyry	04	Mineralized		x				
LSKGI114	3827	Syenite Porphyry	04	Alteration	x	x	x	x		
LSKGI115	3827	Syenite Porphyry	04	Mineralized	x	x	x	x		
LSKGI116	3827	Augite Syenite	04	Alteration		x				
LSKGI117	3827	Syenite Porphyry	04	Alteration		x				
LSKGI118	Lakeshore	Syenite Porphyry	Main	Mineralized	x	x	x	x		
LSKGI119	Lakeshore	Syenite Porphyry	Main	Alteration	x	x				
LSKGI120	Lakeshore	Syenite Porphyry	Main	Alteration		x				
LSKGI121	Lakeshore	Syenite Porphyry	Main	Alteration		x				
LSKGI122	4708	Syenite Porphyry	04	Alteration		x				
LSKGI123	4708	Syenite Porphyry	04	Mineralized	x	x	x	x		
LSKGI124	4708	Syenite Porphyry	04	Alteration		x				
LSKGI125	5320	Tuff	Limelight	Weak Alteration		x				
LSKGI126	5320	Tuff	Limelight	Mineralized	x	x	x		x	x
LSKGI127	5320	Tuff	Limelight	Weak Alteration	x	x	x	x		
LSKGI128	5320	Syenite Porphyry	Limelight	Alteration	x	x	x	x		

Sample	Heading or Hole Number	Lithology	Zone	Mineralization	Thin Section	XRD	Multi-element Analysis	Whole Rock $\delta^{18}O$	$\delta^{18}O_{qtz}$	$\delta^{18}O_{chl}$
LSKGI129	5320	Syenite Porphyry	Limelight	Weak Alteration		x				
LSKGI130	5613	Syenite Porphyry	LDN	None		x				
LSKGI131	5613	Syenite Porphyry	LDN	Mineralized	x	x	x	x		
LSKGI132	5613	Syenite Porphyry	LDN	Alteration	x	x				
LSKGI133	5613	Syenite Porphyry	LDN	Weak Alteration		x				
LSKGI134	5020	Tuff	LD	None		x				
LSKGI135	5020	Tuff	LD	Mineralized	x	x	x	x		
LSKGI136	5020	Tuff	LD	None		x				
LSKGI137	5020	Tuff	LD	Mineralized	x	x	x	x		
LSKGI138	5020	Tuff	LD	None		x				
LSKGI139	Lakeshore	Syenite Porphyry	Main	Alteration		x				
LSKGI140	Lakeshore	Syenite Porphyry	Main	Alteration		x				
LSKGI141	34-621	Syenite Porphyry	4	Mineralized	x					
LSKGI142	34-621	Syenite Porphyry	4	Mineralized	x					
LSKGI151	5412	Syenite Porphyry	LDN	Mineralized	x			x	x	x
LSKGI152	5417	Tuff	#7	Mineralized	x		x	x		
LSKGI153	5313	Syenite Porphyry	LDN FW	Mineralized	x			x		
LSKGI154	5404	Syenite Porphyry	NSZ	Mineralized	x		x	x	x	x
LSKGI155	5404	Syenite Porphyry	NSZ	Mineralized	x			x		
LSKGI156	5033	Tuff	04 HW	Alteration	x			x	x	
LSKGI157	5315	Syenite Porphyry	#7 HW	Mineralized	x		x	x	x	
LSKGI158	5412	Tuff	LDN	Mineralized	x		x	x	x	x
LSKGI159	5404	Tuff	NSZ	Mineralized	x			x	x	
LSKGI160	5402	Syenite Porphyry	NSZ HW	Mineralized	x		x	x	x	
LSKGI161	5033	Tuff	04 HW	Mineralized	x		x	x	x	
LSKGI162	5409 FW Pan	Tuff	Barchetta	Mineralized						

Sample	Heading or Hole Number	Lithology	Zone	Mineralization	Thin Section	XRD	Multi-element Analysis	Whole Rock $\delta^{18}O$	$\delta^{18}O_{qtz}$	$\delta^{18}O_{chl}$
LSKGI163	5409 HW Pan	Tuff	Barchetta	Mineralized						
LSKGI164	5009	Syenite Porphyry	NSZ HW	Mineralized	x		x	x	x	
LSKGI165	5106	Syenite Porphyry	LDN	Mineralized	x			x	x	
LSKGI166	5409	Syenite Porphyry	Barchetta	Mineralized	x			x	x	
LSKGI167	5409	Tuff	Barchetta	Mineralized	x		x	x	x	
LSKGI168	5304	Syenite Porphyry	NSZ	Mineralized	x		x	x		
LSKGI169	5106	Syenite Porphyry	LDN	Mineralized						
LSKGI170	5012	Tuff	LDN (?)	Alteration	x			x		
LSKGI171	5012	Tuff	LDN (?)	Mineralized	x		x	x	x	x
LSKGI172	3422	Syenite Porphyry	4	Mineralized	x		x	x	x	x
LSKGI173	4508	Augite Syenite - Syenite Porphyry	4	Mineralized	x		x	x		

Appendix B : Hand Sample and Thin Section Descriptions

This appendix contains thin section and hand sample descriptions for each of the samples taken from Macassa Mine. Due to the length and large file size, these tables are included on a jump drive provided by the author. If you are accessing this document from outside the University of Western Ontario, please contact the author for any necessary information.

Appendix C : X-Ray Diffraction Results

This appendix contains a consolidated table of all X-Ray Diffraction (XRD) results by element sorted by lithology and mineralized zone. Due to the length and large file size, these tables are included on a jump drive provided by the author. If you are accessing this document from outside the University of Western Ontario, please contact the author for any necessary information.

Appendix D : Multi-Element Data

This appendix contains an extensive list of all trace and major element geochemistry done by Fusion XRF, XRF, ICP-MS, FA-AAS, and LECO of 2013 – 2014 Macassa Mine samples collected by the author. It also includes data by Horvath (2010) and Kerrich and Watson (1984) that is relevant in this study. Due to the length and large file size, these tables are included on a jump drive provided by the author. If you are accessing this document from outside the University of Western Ontario, please contact the author for any necessary information.

Appendix E : Stable Oxygen Isotope Analysis

This appendix gives results from a stable oxygen isotope study of 2013 – 2014 Macassa Mine samples collected by the author. It contains $\delta^{18}O_{VSMOW}$ of whole rock, quartz separates, and chlorite separates as well as calculated temperatures of the mineralizing fluid where quartz-chlorite pairs were found. It also includes data by Horvath (2010) and Kerrich and Watson (1984) that is relevant in this study. Due to the length and large file size, these tables are included on a jump drive provided by the author. If you are accessing this document from outside the University of Western Ontario, please contact the author for any necessary information.

Appendix F : Scanning Electron Microscopy

This appendix gives results from a brief Scanning Electron Microscopy (SEM) back-scattered electron (BSE) imaging and Energy Dispersive X-Ray Spectroscopy (EDS) study done on select samples from 2013 – 2014 Macassa Mine samples collected by the author. It contains BSE images of mineralized grains from twelve select samples. It also contains spectra and results from EDS probe work on these mineralized grains. Due to the length and large file size, these figures and spectra are included on a jump drive provided by the author. If you are accessing this document from outside the University of Western Ontario, please contact the author for any necessary information.

Curriculum Vitae

Name:	Liana Stammers
Post-secondary Education and Degrees:	University of Victoria Victoria, B.C., Canada 2007-2011 H.B.Sc. University of Victoria Victoria, B.C., Canada 2011-2012 P.D.P.P.Ed. (Diploma) Western University London, Ontario, Canada 2013-2016 M.Sc.
Honours and Awards:	The Alan D. Edgar Award in Petrology 2014
Related Work Experience	Exploration Geologist Alexco Resource Corp. 2011, 2012, 2015-2016 Geology Summer Student Kirkland Lake Gold Inc. 2013 Teaching Assistant Western University 2013-2015 Teaching Assistant University of Victoria 2012

Publications:

Stammers, L.K.T. (2011). The Partitioning of Trace Elements into Epidote: Tracing Hydrothermal Fluid Composition at the East Pacific Rise Hydrothermal Systems. University of Victoria Bachelor's Honours, pp. 65.